Polarized ^{3}He Ion Source based on Polarized Electron Capture

Takashi Ohshima

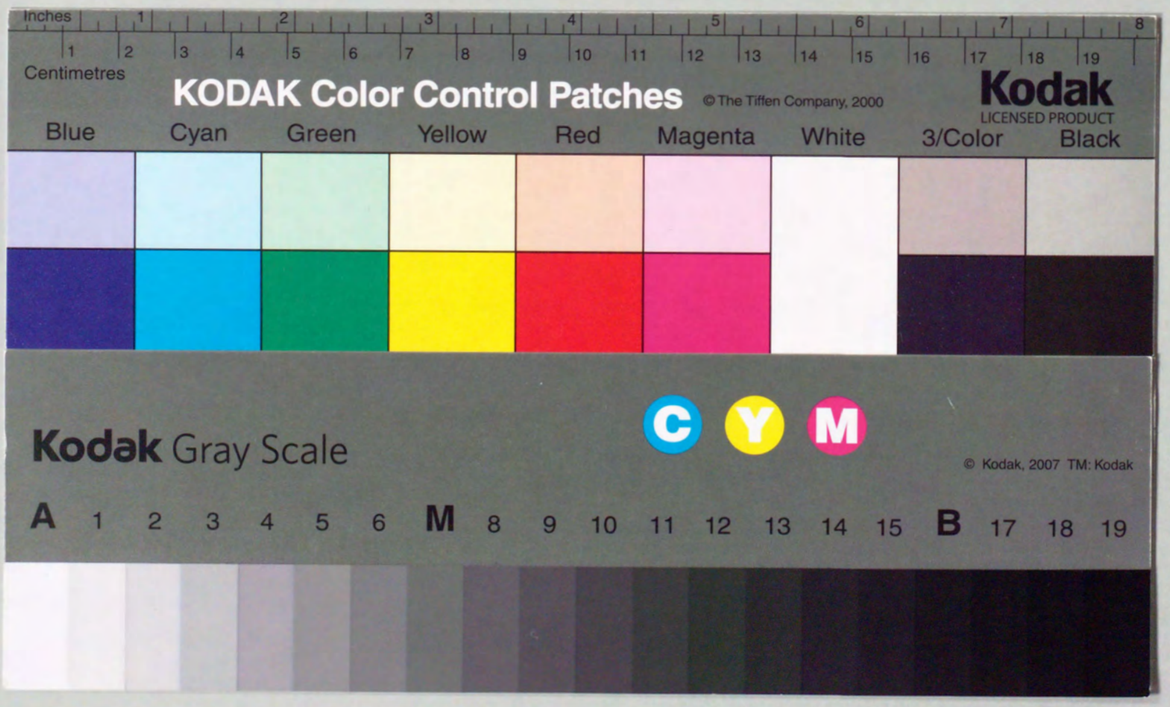

Polarized ^{3}He Ion Source based on Polarized Electron Capture

Takashi Ohshima

Dissertation in Physics

OSAKA UNIVERSITY
GRADUATED SCHOOL OF SCIENCE
TOYONAKA, OSAKA 560, JAPAN

September 1992

Contents

Abstract

We have constructed a polarized ^{3}He ion source based on a polarized electron capture at the Research Center for Nuclear Physics, Osaka University. The $^3He^{2+}$ ions are produced by an Electron Cyclotron Resonance (ECR) ion source. An electron of a sodium atom is polarized by means of optical pumping using a circularly polarized laser light. The $^3He^{2+}$ ion captures an electron from a polarized sodium atom in a magnetic field. Half of the electron polarization of $^3He^+$ is transferred to the nucleus by the hyperfine interaction. A beam foil spectroscopic technique is used to measure the nuclear polarization of the $^3He^+$, in which the circular polarization degree for 389nm photon is measured.

The nuclear polarization was determined to be 0.0415±0.0061 with the ion current of 40nA under the conditions of about 2eμA of 20keV He^{2+} ion extraction from the ECR ion source, and the sodium polarization of 0.30±0.05 with a thickness of 3×10^{13}atoms/cm^2. The reduction (0.259±0.083) of the $^3He^+$ nuclear polarization from the sodium electron polarization was mainly caused by the depolarization due to fine interaction of the excited states in the $^3He^+$ ion formed by an electron capture.

In order to search for the maximum nuclear polarization, the $^3He^+$ nuclear polarization was measured as a function of an incident $^3He^+$ energy. The observed result shows less pronounced dependence on the incident energy in an energy range from 20keV to 28keV.

1. Introduction

Over the past decades polarization phenomena in nuclear physics have provided fruitful information in understanding both the nuclear reaction mechanism and nuclear structure in a wide range of incident energies [BO90]. For this purpose, various types of polarized ion sources have been invented and improved for practical use. In spite of these efforts, the polarized beams have been limited only to p, d, ^{3}He, ^{6,7}Li, and ^{23}Na. Therefore a universal ion source to polarize every nucleus with a spin is desired.

Recently, the production of intense polarized proton beams has become available by a novel technique suggested by Haeberli [HA67], Witteveen [WI79], and Anderson [AN79]. The basic principle of the polarization is to utilize a polarized electron capture by an incident proton from an alkali atom polarized by means of optical pumping. They also suggested the possibility to polarize nuclei heavier than a proton by this technique. This method seems to be very promising for the production of other heavy ions, because owing to the technical developments on the ion sources such as an ECR ion source, and on the high power lasers, one can obtain a large current of a highly stripped ion, and a high degree of an alkali polarization.

Paying attention to this universality, Tanaka proposed in 1985 to construct a polarized heavy ion source by this method [TA85] at the Research Center for Nuclear Physics, Osaka University (RCNP), where the main construction of a ring cyclotron with K = 400 MeV was completed in 1991. Among various proposals of nuclear physics, physics with polarized heavy ion beams is one of the attractive fields in the intermediate energy region. In addition to nuclear physics, the use of the polarized beam is also interesting in the fields of atomic physics, plasma physics and material sciences.

As the first step of our work, we tried to realize the nuclear polarization of the ^{3}He beam ($I^\pi = \frac{1}{2}^+$) by this method since ^{3}He is easily polarized as compared with other heavier nuclei. The construction of the polarized ion source started in 1987.

In this paper we outline a bench test device of the polarized $^3He^+$ ion source based on a polarized electron capture and report the results obtained since 1987. In Chapter 2, a

review of the various methods so far offered to produce the polarized beam is described. In Chapter 3, the basic principles are described for each part of the system; the production of highly stripped ions by an ECR ion source, the production of the polarized sodium atom, the polarization transfer processes following the electron capture, and the measurement of the produced nuclear polarization. In Chapter 4, the experimental setup of each part is described. In Chapter 5, the experimental results and discussion are described, where descriptions on the ion current obtained from the ECR ion source, the achieved sodium polarization, and the results for nuclear polarization measurements are included. In Chapter 6, future prospects are described, where the improvements of the polarized ^{3}He ion source and the feasibility of application of the polarized electron capture method to heavier elements are presented. The conclusion of the present paper is given in Chapter 6.

2 Production of Polarized Beam

The production of the nuclear polarization has been accomplished in various ways. We present here a brief description on each way to produce polarized ions from a historical view point. The definition of the polarization is shown in Appendix.

2-1 Nuclear Reaction

In 1929 Motto [MO29] suggested that an electron scattered by a nucleus was expected to have a preferred orientation of the magnetic moment. As the electron moves to the nucleus, an electromagnetic field B is produced by the nuclear charge which is moving toward the electron on the rest frame of the electron. This magnetic field B is proportional to the orbital momentum of the electron-nucleus system. The interaction of the magnetic moment μ of the electron spin with B is called a spin orbit interaction. The electron feels an additional force which comes from the electron charge and the nuclear charge (Coulomb force). Since spin-up electrons and spin-down electron with a given impact parameter are deflected differently by the spin orbit force and the Coulomb force, the scattered electrons are partially polarized.

If there is a spin orbit force between a projectile nucleus and a target nucleus, the scattered beam will be partially polarized like the above case. The existence of the nuclear spin-orbit force was observed using this mechanism. But the scattered particles do not have a good quality to use as a beam. The intensity of the scattered beam is low. The scattered beam can not easily be focused into a well-formed directional beam. The scattered beam has a considerable energy spread as a result of the relatively thick targets that are required for reason of intensity. The beam energy could not be varied at will without changing the polarization. The background from the primary beam is large. Nevertheless, this method is a way to make a polarized radioactive beam.

Around 1953 a method of producing polarized ions was proposed by Fleichman and Schopper in Hamburg. A few years later a prototype of the polarized ion source came into operation at Erlangen University, Germany. The first operational polarized ion source was constructed at Basel University by Huber et al, in 1960. Since then polarized ion sources

were extensively developed. The quality of the polarized beam was vastly improved by the development of a polarized ion source, i.e., the intensity, the energy spread, and the emittance of polarized beams were greatly improved. The beam energy was changed without perturbing the polarization, and the polarization was easily reversed and thus systematic error of a polarization experiment was reduced.

2-2 Atomic Beam Method

The first polarized ion source was an atomic beam type one. An atomic beam polarized ion source has been widely used for polarizing hydrogen atoms ^{1}H, ^{2}H, and alkali atoms ^{6}Li, ^{7}Li, and ^{23}Na. In case of a hydrogen atom, a thermal hydrogen atomic beam is produced from an RF dissociator by passing through a collimator. The atomic beam is introduced to a Stern-Gerlach magnet (usually 4 or 6-pole magnet is used) where a state with m_J=+1/2 is focused towards the magnetic axis by the force of F=-grad $\mu \cdot \mathbf{B}$. The electron spin polarization is transferred to the nucleus by a method combined with an RF transition and the adiabatic passage [AB58]. After the nuclear polarization is produced, the atom is ionized. The nuclear polarized beam is ionized positively by an electron impact, or is ionized negatively by an electron capture in a sodium cell.

In case of alkali atoms, a thermal atomic beam is produced by a high temperature oven. The ionization of Li or Na atom is done by a surface ionization with high temperature tungsten filament in a strong magnetic field.

Production of polarized ^{3}He is attempted at Laval University [SL85]. They use the metastable state (2^3S_1) of He atom. That is because the total angular momentum of the ground state He atom ($1\,^1S_0$) is zero, there is in no separation of the ground-state beam after passing through the multi-pole magnet. They try to build the ion source in 7.5MV Van de Graaff.

2-3 Lamb Shift Method

Successful results have been obtained for ^{1}H, ^{2}H and ^{3}He with this method. Stripped ions ($^1H^+$, $^2H^+$ or $^3He^{2+}$) are produced by a conventional ionizer and are accelerated. Then the ions pass through a charge exchange cell and capture electrons. A fraction of the beam is formed in a 2s metastable state of a hydrogen atom (^{1}H,^{2}H) or a hydrogen like ion ($^3He^+$). A selective quenching is done by an RF transition in a magnetic field, i.e., the metastable state in M_J=-1/2 decays to the ground state, thus an electron polarized metastable beam is produced. The electron polarization is transferred to the nucleus by a hyperfine interaction using the Sona method [SO67]. Then metastable atoms (ions) are selectively ionized to extract the polarized part of the beam. The polarized ion current is limited by the quenching of the meta-stable particles by space charge effect [CL83].

A polarized ^{3}He beam is produced by Birmingham group using this method. The polarized $^3He^{2+}$ beam was accelerated to 33.4MeV and used for nuclear physics experiments. The extracted current and polarization of the beam were 2nA on target and 0.6, respectively [HA81].

2-4 Optical pumping Method

a) Direct Optical Pumping Method

This method is based on an absorption of circularly polarized photons by the atom. Then an angular momentum of the photon is transferred to the atom, thus the atom is polarized. The detail of this process will be described in section 2. But available strong light sources are in limited wavelength regions. This method is used to polarize Li or Na combined with a Stern-Gerlach magnet to produce alkali atomic beams in one hyperfine state [JA87].

^{3}He (2^3S) atom is polarized by this method at Rice university [MA85]. They used a transition between 2^3S and 2^3P. The corresponding wavelength for this transition is 1.08μm. They accelerated polarized $^3He^+$ ion by the Texas A&M cyclotron between 18.4 and 49.0MeV. They got 100nA $^3He^{2+}$ beam with the polarization of 0.11 on target. The low polarization came from the low intensity of the pumping light, because the light source for optical pumping was not easily available.

b) **Polarized electron capture Method**

It is very difficult for a hydrogen atom to polarized by direct optical pumping method, because the needed light for pumping is in Ultra Violet region. For this reason an indirect optical pumping method is developed. The polarization of alkali atoms (which can be easily optical pumped) is transferred to the hydrogen nuclei. This type of a polarized ion source was proposed by Zavoiskii [ZA57], and later Haeberli [HA67], Anderson [AN79] and Witteveen [WI79]. Successful results are obtained in producing a polarized proton ion [MO89, SC91, YO90, ZE90]. This method is based on a polarized electron capture by a proton from a polarized sodium or a polarized potassium atom. A proton beam produced by an ECR ion source captures a polarized electron from an alkali atom in a strong magnetic field. The electron polarization of the beam is transferred to the nucleus by the Sona method. Then the beam is negatively ionized by an electron capture in another sodium cell.

2-5 Tilting Method

When an ion beam is reflected from a polished metal surface under very small angles or passed through a tilted foil, strong electron orientation of the ion is observed. The electron orientation originates from an anisotropic Coulomb interaction at the surface of the tilted foil or the scattering crystal. The breaking of the axial symmetry with respect to the beam is responsible for this orientation [FA73]. An orbital angular momentum in a well-defined direction is induced, namely in the $\mathbf{n} \times \mathbf{v}$ direction, where $\mathbf{v}$ is the beam velocity and $\mathbf{n}$ is a vector normal to the interaction surface. This orientation is transferred to a nucleus by a hyperfine interaction. In a practical use, the obtained polarization is rather small. The polarization is increased if successive processes of a beam-surface interaction are applied. But it reduces the beam intensity and degrades the beam emittance. The life time of the foils or the crystal surface is less than several hours and this is also a problem to be solved. For the case of tilted surface ultra high vacuum (10^{-10}Torr) is needed. This method is attempted to polarize a radioactive beam obtained from an isotope separator on line [VA92].

In table 2-0-1 the performance of several presently working sources is compared. As for

Laboratory	*Ions available*	*Intensity* (μA)	P_z (%)	*Ref.*
Atomic Beam type				
ETH-Zürich	H^+ D^+	400	85	[SC81]
Saturne	H^+ D^+	580	90	[LE90]
TUNL	H^+ D^+	60	85	
PSI	H^+ D^+	150	85	
Bonn	H^+ D^+	30	80	
Karlsruhe	D^+	60	67	[EH89]
Madison	H^- D^-	3	95	[HA82]
Seattle	H^- D^-	1	93	
Brookhaven	H^-	40	80	[AL90]
INR	H^+	6000	80	[BE90]
RCNP	H^+ D^+	1	85	
Lamb shift type				
Tukuba	H^- D^-	0.4	75	[WA90]
Fukuoka	H^- D^-	1	70	[WA90]
München	H^- D^-	1	83	
Birmingham	$^3He^{2+}$	.002	60	[HA81]
Optical Pumping				
a) Direct Optical Pumping				
Heidelberg	^6Li ^7Li			[JA87]
Rice	^3He	0.1	0.11	[SL85]
b) Polarized Electron Capture				
KEK	H^-	150	65	[MO89]
TRIUMF	H^-	35	61	[BU91]
LAMPF	H^-	20	62	[YO90]
INR	H^+	4000	65	[ZE90]

Table 2-0-1 Performance of presently working polarized ion sources

the ion current, it is not easy to read the table since one has to know how and at which position the given values have been measured.

3. Basic Principle of the Polarized Ion Source

We describe here the basic principle of the polarized ion source based on a polarized electron capture. The block diagram showing the principle of the polarized ion source is presented in Fig.3-0-1.

Firstly $^3He^{2+}$ ions are produced by an ECR ion source. Polarized sodium atom is produced by means of the optical pumping using a circularly polarized light. Then a $^3He^{2+}$ ion captures a polarized electron of a sodium atom. The produced $^3He^+$ is usually in its excited states. If a magnetic field strong enough to decouple the fine interactions (spin-orbit interactions of the atom) is applied, the electron spin polarization of the excited $^3He^+$ ion is kept during the de-excitation to the ground state. Otherwise, the depolarization appears. In our case the needed magnetic field to decouple of fine interactions is much stronger than that we applied in our test bench apparatus. So we treat the depolarization mechanism by fine interactions in a weak magnetic field limit. The electron polarization of the produced $^3He^+$ is transferred to the ^3He nucleus through the hyperfine interaction. The nuclear polarization of $^3He^+$ is finally measured by means of beam foil spectroscopy.

After the polarization is transferred from the electron to the nucleus, the electron should be removed by passing through a gas or a foil stripper to accelerate it up to the maximum energy by a cyclotron.

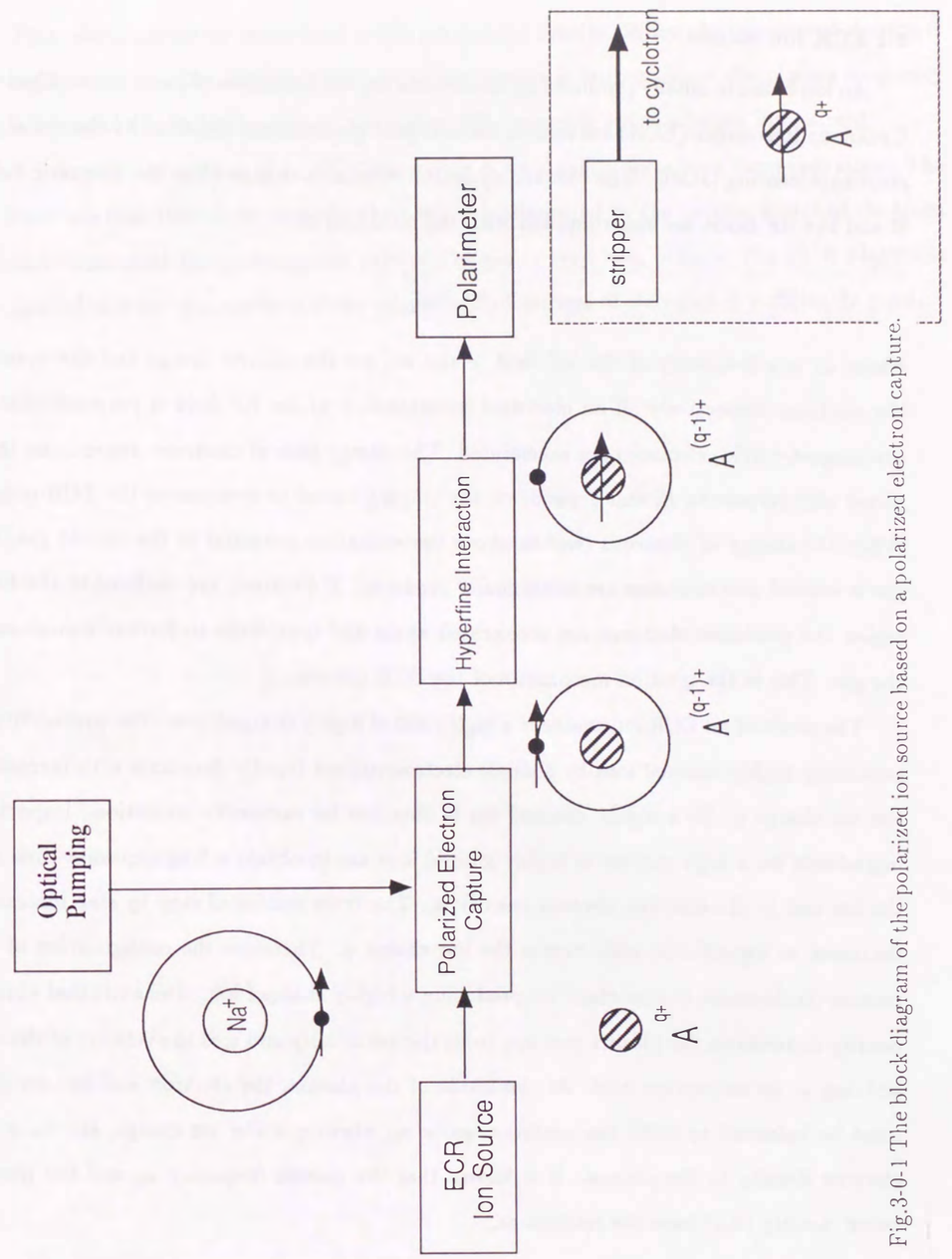

Fig.3-0-1 The block diagram of the polarized ion source based on a polarized electron capture.

3-1 ECR Ion Source

An ion beam is usually produced by an electron impact ionization of gases. In an Electron Cyclotron Resonance (ECR) ion source, the energetic electrons are provided by the cyclotron resonance heating [JO89]. The electron cyclotron resonance occurs when the magnetic fields B and the RF fields are superimposed with the condition of

$$\omega_L = \frac{eB}{m_e},$$

where ω_L is a frequency of the RF field, e and m_e are the electric charge and the mass of the electron, respectively. If an electrical component E of the RF field is perpendicular to the magnetic field, electrons are accelerated. The energy gain of electrons depends on their phase with respect to E, and depends on the staying period of electrons in the ECR region. When the energy of electrons reaches above the ionization potential of the atomic gas, the gas is ionized and electrons are additionally produced. If electrons are confined in the ECR region the produced electrons are accelerated again and contribute to further ionization of the gas. This is the ignition mechanism of the ECR plasma.

The merit of an ECR ion source is a high yield of highly charged ions. The probability of producing highly charged ions by a single electron impact rapidly decreases with increasing the ion charge q. So a highly charged ion is obtained by successive ionization. Important ingredients for a high current of highly ionized ions are to obtain a long exposure time τ of the ion and to increase the electron density n_e. The cross section of step by step ionization decreases as logarithmic scale versus the ion charge q. Therefore the configuration of the plasma confinement is important for producing a highly charged ion. The extracted current density depends on the plasma flow $n_i v_i$ (n_i is the ion density and v_i is the velocity of the ion) arriving at an extraction hole. At the inside of the plasma, the electron and ion densities must be balanced to fulfill the condition $qn_i = n_e$, where q is the ion charge, and n_e is the electron density in the plasma. It is known that the plasma frequency ω_p and the plasma cutoff density (n_{co}) have the relation as,

$$n_{co} = 1.2 \times 10^{-8} \omega_p^2.$$

This relation gives an upper limit of the ion current density. When the ion current density is higher than n_{co}, the stability condition of the plasma is broken. Since the plasma frequency is identical to the RF frequency, the higher RF frequency yields a larger ion current.

Another advantage of an ECR ion source is its stability for a long term operation. The reason is that there is no cathode which might be damaged by the bombardment of electrons and ions. And the consumption rate of the gas is very low, because the ECR plasma is ignited in a low gas pressure if the magnetic confinement of electrons is sufficiently good.

3-2 Polarization of Sodium Atom

a) Optical Pumping

We use an optical pumping method [HA72] to obtain polarized sodium atoms. This method is based on an absorption of a circularly polarized photon by an atom. The maximum value of the atomic polarization by this method is mainly limited by the competition between pumping rate and depolarization rate. The pumping rate is determined by the pumping light intensity. The depolarization rate is mainly determined by two sources. One is a relaxation during the adsorption on a wall surface of the sodium cell. The other is the effect of the radiation trapping. A polarized sodium atom absorbs an unpolarized photon emitted by a neighboring excited sodium atom, which results in the depolarization.

To extract an atomic polarization of sodium atom, a model calculation is carried out. Neglecting the hyperfine coupling of the sodium atom, each of the ground state of the sodium atom $S_{1/2}$ has two magnetic sublevels. The first excited state is $P_{1/2}$, which has also two magnetic sublevels. For the sake of convenience we label the states as shown in Fig.3-2-1: the $S_{1/2}$ $m_J = -1/2$ state is labeled 1, the $S_{1/2}$ $m_J = +1/2$ state is labeled 2, the $P_{1/2}$ $m_J = -1/2$ state is labeled 3, and the $P_{1/2}$ $m_J = +1/2$ state is labeled 4. If a $\sigma-$ circularly polarized light is introduced, the atom in the state 2 absorbs the light and is excited to the state 3. But the atom in state 1 cannot absorb the light. The excited state 3 decays to the state 1 or 2 spontaneously. The atom decaying to the state 2 absorbs the light again. Repeating this process, the atoms are made to populate in the $S_{1/2}$ m_J=$-1/2$ state.

The rate equations for these states become,

$$\frac{dn_1}{dt} = A_{31}n_3 + \frac{n_2 - n_1}{T} - A_{31}R_{31}n_3, \tag{3.2.1}$$

$$\frac{dn_2}{dt} = -\alpha(n_2 - n_3) + A_{32}n_3 - \frac{n_2 - n_1}{T} - A_{32}R_{32}n_3, \tag{3.2.2}$$

$$\alpha = \frac{\lambda^3 A_3}{4h}\frac{h\nu}{\pi c}\frac{I}{h\nu}, \tag{3.2.3}$$

where

I: the light intensity

ν: the frequency of the light

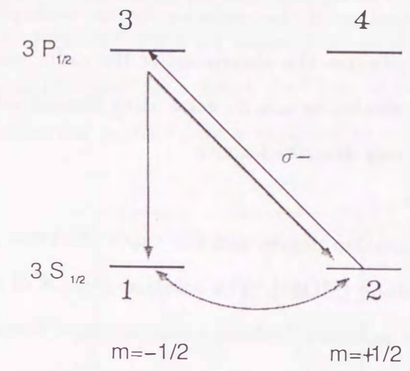

Fig.3-2-1 The ground and the first excited states of a sodium atom

A: Einstein's A coefficient, $A_{31} + A_{32} = A_3$

T: relaxation time between state 1 and state 2

R: effect of the radiation trapping.

The polarization in a steady state is given by taking $\frac{d}{dt} = 0$,

$$P_{Na} = -\frac{n_1 - n_2}{n_1 + n_2} = \frac{-1}{1 + \frac{2}{T(A_{31} - R_{31})}[1 + \frac{A_3 - R_{31} - R_{32}}{\alpha}]} . \tag{3.2.4}$$

To increase the sodium polarization, it is needed to increase the pumping light intensity I and increase the relaxation time T. The effect of the radiation trapping R is significant at a high sodium density. R is expressed as follows;

$$A_{32}R_{32}n_3(\mathbf{r}) = \int d^3\mathbf{r}' d\nu C_{decay}C_{reduce}C_{absorb}$$

$$C_{decay} = n_3(\mathbf{r}', t)A_3\frac{1 + \cos^2\theta}{2}\frac{1}{4\pi|\mathbf{r} - \mathbf{r}'|^2}g(\nu - \nu_{23})$$

$$C_{reduce} = \exp[-\frac{\lambda_{23}^2 A_3}{4\pi}\frac{1 + \cos^2\theta}{2}g(\nu - \nu_{23})\int_0^{|\mathbf{r}-\mathbf{r}'|}(n_2(\rho) - n_3(\rho))d\rho]$$

$$C_{absorb} = \frac{\lambda_{23}^2 A_3}{4\pi} \frac{1+\cos^2\theta}{2} g(\nu - \nu_{23})[n_2(\mathbf{r},t) - n_3(\mathbf{r},t)]$$

where C_{decay} indicates the radiative decays of atoms in state 3 at a position of $\mathbf{r}'$, C_{reduce} indicates the intensity reduction of the radiation by the absorption during a propagation from $\mathbf{r}'$ to $\mathbf{r}$, and C_{absorb} indicates the absorption of the radiation by atoms in state 2 at a position of $\mathbf{r}$. Numerical calculation can be done using Hermit integration [TU86]. R_{31} can be calculated in a similar way described above.

b) Faraday Rotation

We measure the polarization degree and the vapor thickness of the sodium atom using the Faraday Rotation method [MO84]. The rotation angle θ of a linear polarization plane after passing through the polarized sodium vapor is proportional to the sodium thickness NL and the sodium polarization P as expressed in the following way;

$$\theta = (\theta_0(B) + \theta_p P) NL, \tag{3.2.5}$$

where B is a strength of an external magnetic field, θ_0 and θ_p are constants depending on the wavelength of the probe light. The detailed calculations of the values of θ_0 and θ_p are given in Appendix. The sodium vapor thickness is obtained by comparing two rotation angles measured with the magnetic field and without the magnetic field,

$$NL = \frac{\theta(B = B_0, P = 0) - \theta(B = 0, P = 0)}{\theta_0}. \tag{3.2.6}$$

The sodium polarization degree is obtained by comparing two rotation angles measured with the pumping light and without the pumping light,

$$P_{Na} = \frac{\theta(B = B_0, P = P_{Na}) - \theta(B = B_0, P = 0)}{\theta_p NL}. \tag{3.2.7}$$

3-3 Polarization transfer

A large cross section of a polarized electron capture is desired to obtain an intense polarized beam. The cross section of an electron capture by a He^{2+} ion from a Na atom was measured by Dubois et al [DU85]. Fig.3-3-1 shows their results. The cross section of single electron capture is about $10^{-14}cm^2$ for a 20keV He^+ ion. If we use the sodium thickness of $3\times10^{13}atoms/cm^2$, the electron capture rate is expected to be as much as 0.3.

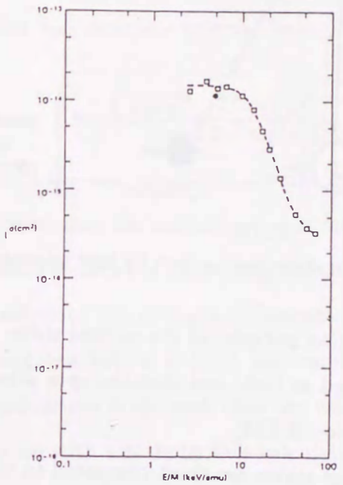

Fig.3-3-1 Single electron transfer cross section for helium ion impact on sodium by Dubois et al, [DU85]

As for a polarization obtained, there are two contributions. One is an electron polarization transfer from a sodium atom to a He^+ ion of the ground state (ϵ_{LS}), and the other is the polarization transfer from the electron to the nucleus (ϵ_{HF}).

a) ϵ_{LS}

In case of a polarized electron capture, formed He^+ ions are mainly in excited states. We assume that this excited He^+ ion is made instantaneously at t=0, where "instantaneous" implies that the excitation time is short compared to other characteristic times (fine interaction

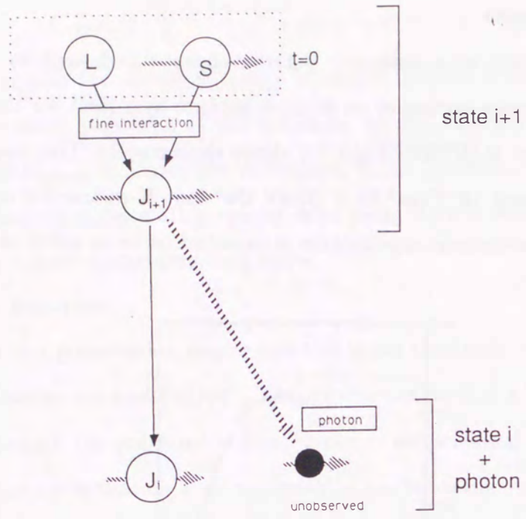

Fig.3-3-2 The depolarization mechanism by fine interactions and E1 transitions

periods or hyperfine interaction periods) of the excited state. This means that the electron polarization will be conserved at t=0, and that the spin orientation during the collision is space fixed during the collision [PE58].

If the life times of excited states are short compared to the fine interaction intervals, or if a magnetic field strong enough to decouple the fine interactions is applied, the electron spin polarization is kept during the de-excitation to the ground state of He^+ ion.

Otherwise, the fine interactions transfer the spin angular momentum into the orbital angular momentum of the electron. A part of the orbital angular momentum in the system is carried away by the photons emitted in the de-excitation processes. Thus a part of the electron spin polarization is lost. Fig.3-3-2 shows this process. Under this assumption we calculate the electron polarization following the photon emission.

We define the efficiency ϵ_{LS} as,

$$\epsilon_{LS} = \frac{P_e(g.s.)}{P_e(0)}, \tag{3.3.1}$$

where $P_e(g.s.)$ is the electron spin polarization of the ground state He^+ ion. $P_e(0)$ is the

electron spin polarization just after the electron capture, which corresponds to the sodium polarization P_{Na}.

Firstly we shall examine lifetimes and fine interaction intervals of hydrogen like ions. For hydrogen like ions with nuclear charge Z, the lifetime τ of the state (n,l) is expressed as [OM83],

$$\tau = \frac{C_{nl} n^3 l^2}{Z^4} \quad nl \gg 1 \quad ,$$

where n,l are principal and angular quantum numbers and C_{nl} is a constant whose value is around $2 \sim 1 \times 10^{-10}$. The fine structure interval $2\pi/\omega_{LS}$ of a state (n,l) has a relation of [BR83],

$$\hbar\omega_{LS} = \frac{e^2}{4\pi\epsilon_0 a}\frac{Z^2}{2n^2}\frac{(Z\alpha)^2}{nl(l+1)} \quad ,$$

where a is Bohr radius, α is the fine structure constant and ϵ_0 is the dielectric constant in vacuum. These relations show that the ratio of $\frac{\tau}{2\pi/\omega_{LS}}$ is approximately 100, i.e., the lifetime of each excited state in cascade decay is much longer than its fine structure period.

The next step is to estimate the strength of magnetic field B_{fine} to decouple the fine interaction. If a strong magnetic field is applied, the coupling of a spin angular momentum and an orbital angular momentum is reduced, thus the value of ϵ_{LS} is nearly 1.0. The value of B_{fine} for hydrogen like ion with a state (n,l) is calculated as,

$$\begin{aligned} B_{fine} &= \frac{\hbar\omega_{LS}}{\mu_e} \\ &= \frac{1}{\mu_e}\frac{e^2}{4\pi\epsilon_0 a}\frac{Z^2}{2n^2}\frac{(Z\alpha)^2}{nl(l+1)} \end{aligned} \quad . \tag{3.3.2}$$

A calculated partial cross section of an electron capture from a sodium atom by a He^{2+} ion [SH87] is shown in Table 3-3-1. The formed He^+ is mainly in the 3d state at an incident energy of 20keV. The dominant de-excitation process of the 3d state is like 3d-2p-1s. In table 3-3-2 the calculated values of B_{fine} for He^+ ion are shown. The fine interaction intervals of the 3d and 2p states are 1S and 180GHz, the life times are 0.97nsec and 0.10nsec, respectively as shown in Table 3-3-2. On the other hand we applied the magnetic field strength of only 3kGauss in our present experimental system. The corresponding Zeeman splitting is only 4.2GHz which is not enough to decouple fine interactions. The depolarization due to fine

Energy (keV)	1s	2s	2p	3s	3p	3d	4s	4p	4d	4f	Total
10.0	0.0011	0.29	0.78	7.47	26.25	70.32	1.51	5.02	10.0	6.13	129.02
21.33	0.0018	0.56	1.14	3.61	14.37	66.84	2.91	6.34	13.43	16.22	126.45
26.67	0.0018	0.42	0.92	3.36	10.83	53.22	4.33	10.03	13.30	14.12	112.14
30.00	0.0047	0.36	0.84	3.18	9.16	50.88	3.80	8.91	14.06	10.38	103.22
40.00	0.0061	0.36	0.72	1.79	5.99	37.42	2.60	7.36	13.05	6.24	78.60
53.33	0.031	0.54	0.84	0.93	3.93	18.81	2.04	6.13	9.33	3.91	52.69
66.67	0.027	0.66	0.62	0.52	2.02	10.77	1.03	3.36	7.01	1.98	35.33
80.00	0.029	0.54	0.49	0.33	1.10	5.71	0.59	2.07	4.38	1.08	23.66
106.67	0.038	0.31	0.34	0.17	0.29	1.88	0.22	0.72	1.72	0.35	11.25
160.00	0.029	0.053	0.16	0.044	0.076	0.29	0.061	0.17	0.29	0.067	2.63
213.33	0.022	0.029	0.093	0.017	0.031	0.075	0.020	0.048	0.075	0.014	0.75
266.67	0.012	0.025	0.051	0.013	0.016	0.026	0.011	0.018	0.027	0.0048	0.35

Table 3-3-1 The partial cross section for the reaction $He^{2+} + Na(3s) \rightarrow He^{+}(nl) + Na^{+}$ in units of $10^{-16}cm^2$ by Shingal et al [SH87].

state	fine structure interval (GHz)	B_{fine} (T)
2p	180	6.4
3p	53	1.9
3d	18	0.65
4p	22	0.80
4d	7.3	0.26
4f	3.7	0.13

Table 3-3-2 The magnetic field B_{fine} to decouple fine interactions of He^{+} ion.

interactions emerges in this case.

In a weak magnetic field limit, the value of ϵ_{LS} is calculated as follows [LI91]. For ions with zero nuclear spin (or the applied magnetic field is strong enough to decouple the hyperfine interactions), the state multipole ${}^{J}\rho$ of the excited state in the $(LS)J$ representation after the electron capture is given as follows,

$$ {}^{J}\rho_Q^K = \sum_{k_L,k_S,q_L,q_S} [(2k_L+1)(2k_S+1)(2J+1)(2J+1)]^{1/2} \begin{Bmatrix} L & S & J \\ L & S & J \\ k_L & k_S & K \end{Bmatrix} \times (-)^{K-Q}\sqrt{2K+1} \begin{pmatrix} k_L & K & k_S \\ q_L & -Q & q_S \end{pmatrix} {}^{L}\rho_{q_L}^{k_L}(0)\ {}^{S}\rho_{q_S}^{k_S}(0) \quad (3.3.3) $$

Here ${}^{L}\rho(0)$ and ${}^{S}\rho(0)$ indicate the state multipoles of the orbital part and of the spin part immediately after the excitation, respectively. The anisotropy of the ground state $(L_0S_0)J_0$ develops from many sequences of orientation and alignment transfers in the transitions from J_{i+1} to J_i. We consider the anisotropy transfer from a state J_{i+1} with a coupling scheme $(J_{i+1}, J_{i+1})k'$ to a state J_i with a coupling scheme $(J_i, J_i)k$. The electric dipole transition (E1) matrix is represented by the coupling scheme $(J_i, J_{i+1})1$. The two states are coupled by the radiative transitions characterized by the dipole transition operator $(\hat{\epsilon}^* \cdot \mathbf{r})(\hat{\epsilon} \cdot \mathbf{r}')$ averaged over directions and polarizations of the photon

$$ \overline{(\hat{\epsilon}^* \cdot \mathbf{r})(\hat{\epsilon} \cdot \mathbf{r}')} = \frac{\mathbf{r} \cdot \mathbf{r}'}{3}. $$

Since this operator is a scalar, the average squared dipole matrix element is characterized by the coupling scheme $(J_i, J_{i+1})1(J_i, J_{i+1})1^{(0)}$. The anisotropy transfer is presented in a recoupling of $(J_iJ_{i+1})1(J_iJ_{i+1})1^{(0)}$ to the coupling $(J_iJ_i)k(J_{i+1}J_{i+1})k'^{(0)}$. Then this gives a following relation;

$$ \begin{aligned} {}^{J_i}\rho_q^k &= \frac{|C_i'(J_{i+1}||\mathbf{r}||J_i)|^2}{\sqrt{(2k+1)(2\times 1+1)}} \sum_{k',k,q',q} ((J_iJ_{i+1})1(J_iJ_{i+1})1^{(0)}|(J_iJ_i)k(J_{i+1}J_{i+1})k'^{(0)})^{J_{i+1}}\rho_{q'}^{k'} \\ &= |C_i'(J_{i+1}||\mathbf{r}||J_i)|^2(-)^{J_{i+1}+J_i+1+k} \begin{Bmatrix} J_{i+1} & J_i & 1 \\ J_i & J_{i+1} & k \end{Bmatrix} {}^{J_{i+1}}\rho_q^k \end{aligned} \quad , \quad (3.3.4) $$

because the recoupling scheme can be expressed as,

$$ \begin{aligned} &((J_iJ_{i+1})1(J_iJ_{i+1})1^{(0)}|(J_iJ_i)k(J_{i+1}J_{i+1})k'^{(0)}) \\ &= [(2k'+1)(2k+1)(2\times 1+1)(2\times 1+1)]^{1/2} \begin{pmatrix} k' & k & 0 \\ q' & q & 0 \end{pmatrix} \begin{Bmatrix} J_{i+1} & J_i & 1 \\ J_{i+1} & J_i & 1 \\ k' & k & 0 \end{Bmatrix} \\ &= (2k+1)\times 3 \times \frac{(-)^{J_{i+1}+J_i+1+k}}{[(2\times 1+1)(2k+1)]^{1/2}} \begin{Bmatrix} J_{i+1} & J_i & 1 \\ J_i & J_{i+1} & k \end{Bmatrix} \delta_{kk'}\delta_{qq'} \end{aligned} . $$

The E1 operator acts on the L component only. From this fact the reduced dipole element can be written in the following

$$ \begin{aligned} C_i'\langle((L_{i+1}S)J_{i+1}||\mathbf{r}||(L_iS)J_i\rangle &= (-)^{L_{i+1}+S+J_i+1} C_i'[(2J_{i+1}+1)(2J_i+1)]^{1/2} \\ &\times \begin{Bmatrix} L_{i+1} & J_{i+1} & S \\ J_i & L_i & 1 \end{Bmatrix} \langle L_{i+1}||\mathbf{r}||L_i\rangle \end{aligned} \quad (3.3.5) $$

Inserting (3.3.5) to (3.3.4), the anisotropy transfer is give by

$$ {}^{J_i}\rho_q^k = C_iB(k, J_i, J_{i+1})^{J_{i+1}}\rho_q^k $$

where

$$C_i = |C_i'\langle L_{i+1}||\mathbf{r}||L_i\rangle|^2$$

$$B(k, J_i, J_{i+1}) = (2J_{i+1}+1)(2J_i+1)(-)^{J_{i+1}+J_i+1+k} \times \begin{Bmatrix} L_{i+1} & J_{i+1} & S \\ J_i & L_i & 1 \end{Bmatrix}^2 \begin{Bmatrix} J_{i+1} & J_i & 1 \\ J_i & J_{i+1} & k \end{Bmatrix}$$

The state multipoles with a rank k for the state $(L_0S_0)J_0$ are computed by summing over all possible transfers. The transformation of the state multipoles are given by the following relation,

$$^{J_1}\rho_q^k = \prod_i C_i \sum_{J_N} D(k, J_0, J_N)\, ^{J_N}\rho_q^k$$

$$D(k, J_0, J_N) = \sum_{J_1, J_2, \ldots, J_{N-1}} B(k, J_0, J_1)B(k, J_1, J_2)\cdots B(k, J_{N-1}, J_N)$$

We choose the quantization axis as the ion beam propagation axis. Because of the axial symmetry, the multipoles with $q \neq 0$ vanish. The electron spin is also along the beam propagation axis in our case. Then the Cartesian polarization P_e of the electron is expressed by using ${}^S\rho_0^k$ as,

$$P_e = \frac{{}^S\rho_0^1}{{}^S\rho_0^0}.$$

Since the value of L in the ground state is 0, the electron spin polarization of the ground state ion $P_e(g.s.)$ is given by

$$\begin{aligned} P_e(g.s.) &= {}^S\rho_0^1(g.s.)/{}^S\rho_0^0(g.s.) \\ &= {}^J\rho_0^1(g.s.)/{}^J\rho_0^0(g.s.) \\ &= \frac{\sum_{J_N} D(1, J_0, J_N)\, ^{J_N}\rho_0^1(0)}{\sum_{J_N} D(0, J_0, J_N)\, ^{J_N}\rho_0^0(0)} \end{aligned}$$

where $\rho(g.s.)$ is the state multipole of the ground state, and $\rho(0)$ is the state multipole just after the electron capture. From the equation (3.3.3) and the property of 9j coefficient, the state multipoles of J are expressed as,

$$^J\rho_0^1 = C_{101}\, ^L\rho_0^0\, ^S\rho_0^1 + C_{121}\, ^L\rho_0^2\, ^S\rho_0^1$$

$$^J\rho_0^0 = C_{000}\, ^L\rho_0^0\, ^S\rho_0^0$$

where C's are constants. Thus the polarization of the ground state He^+ ion is expressed as,

$$\begin{aligned} P_e(g.s.) &= \frac{\sum_{J_N} D(1, J_0, J_N)[C_{101}\, ^L\rho_0^0\, ^S\rho_0^1 + C_{121}\, ^L\rho_0^2\, ^S\rho_0^1]}{\sum_{J_N} D(0, J_0, J_N)[C_{000}\, ^L\rho_0^0\, ^S\rho_0^0]} \\ &= \epsilon_{LS} P_e(0), \end{aligned}$$

where

$$P_e(0) = \frac{{}^S\rho_0^1(0)}{{}^S\rho_0^0(0)}$$

Then we can write ϵ_{LS} as the following form

$$\epsilon_{LS} = Const + Const' \frac{{}^L\rho_0^2}{{}^L\rho_0^0} \tag{3.3.6}$$

The electron spin polarization $P_e(g.s.)$ is proportional to the electron spin polarization just after the electron capture $P_e(0)$.

The value of $\frac{{}^L\rho_0^2}{{}^L\rho_0^0}$ relates to the alignment parameter A_0^{col} defined by Fano [FA73] and this value corresponds to

$$\frac{{}^L\rho_0^2}{{}^L\rho_0^0} = \sqrt{\frac{5L(L+1)}{(2L+3)(2L-1)}}\, A_0^{col}.$$

where

$$A_0^{col} = \frac{\sum_m [3m^2 - L(L+1)]\sigma(m)}{L(L+1)\sum_m \sigma(m)}$$

and $\sigma(m)$ is the capture cross section of the magnetic substate (L,m). For the case of L=2 the value of A_0^{col} can take

$$-1 \leq A_0^{col} \leq 1 \qquad (L=2)$$

For example if the excited states are equally populated $\sigma(m_L) = \frac{1}{2L+1}\,\sigma$, the value of A_0^{col} is 0. If the excited states are formed in $m_L = 0$ state only $\sigma(m_L) = \delta_{m_L 0}\,\sigma$, the value of A_0^{col} is -1. An example of a calculation of ϵ_{LS} is given in Appendix. The result of the calculation of ϵ_{LS} is shown in Table 3-3-3.

As one can see in Table 3-3-1, the formed He^+ is mainly in the 3d state at an incident energy of 20keV. The value of ϵ_{LS} is calculated to be 0.301 at $A_0^{col} = 0$ for the cascading transitions from the 3d state (l=2) to the ground state (l=0).

b) ϵ_{HF}

The second process is a transfer of an electron polarization to a nuclear polarization by the hyperfine interactions. We define the efficiency for the polarization transfer of this process as ϵ_{HF} in the following,

$$\epsilon_{HF} = \frac{P_N}{P_e(g.s.)}, \tag{3.3.7}$$

L	ε_LS		
	Acol max	Acol =0	Acol=-1
1	0.556	0.407	0.111
2	0.502	0.301	0.099
3	0.486	0.257	0.074
4	0.479	0.234	0.059
5	0.475	0.219	0.048
6	0.473	0.209	0.041
7	0.472	0.202	0.036
8	0.471	0.196	0.031
9	0.470	0.192	0.028
10	0.470	0.188	0.025
11	0.469	0.185	0.023
12	0.469	0.183	0.021
13	0.469	0.181	0.020
14	0.469	0.179	0.018
15	0.468	0.178	0.017
16	0.468	0.176	0.016

Table 3-3-3 The calculated values of ϵ_{LS}. The value of L is an orbital quantum number, and *Acol* is an alignment factor of an initially formed excited state.

where P_N is the nuclear spin polarization and $P_e(g.s.)$ is the electron spin polarization of the ground state He^+ ion. In the magnetic field strong enough, the electron spin and nuclear spin are decoupled. As the strength of the magnetic field is reduced, the electron and nuclear spins become to be coupled by a hyperfine interaction. The Hamiltonian is expressed as,

$$H' = a\mathbf{I}\cdot\mathbf{J} - \mu_e g_J \mathbf{J}\cdot\mathbf{B} - \mu_N g_I \mathbf{I}\cdot\mathbf{B},$$

where a is a hyperfine constant, μ_e is the Bohr magneton, μ_N is a nuclear magnetic moment, g_J is a gyromagnetic ratio of the electron, g_I is a gyromagnetic ratio of the nucleus. If the external magnetic field B is applied to z direction as (0,0,B_z), the Hamiltonian is expressed as,

$$H' = a(\frac{I_+J_- + I_-J_+}{2} + I_zJ_z) - \mu_e g_J J_z B_z - \mu_N g_I I_z B_z,$$

where

$$J_\pm = J_x \pm J_y \quad \text{and} \quad I_\pm = I_x \pm I_y.$$

Using a first order perturbation theory the energy of the hyperfine state $E(F, m_F)$ is calculated for ground state $^3He^+$ ion [BE65],

$$E(F,m_F) = -\frac{a}{4} - g_I\mu_N m_F B_z \pm \frac{a}{4}(2I+1)\sqrt{1+\frac{2m_F}{I+1/2}x+x^2}$$

$$x = \frac{B_z}{B_{hf}(I+1/2)}$$

$$B_{hf} = \frac{a}{g_I\mu_N - g_J\mu_e} \tag{3.3.8}$$

and the calculated result is shown in Fig.3-3-3. The value of a for a hydrogen like ion of state (n, J, L) with nuclear spin I is calculated [BR83] as,

$$a = \frac{\mu_0}{4\pi} 4 g_I \mu_e \mu_N \frac{1}{J(J+1)(2L+1)} \frac{Z^3}{a_\mu^3\, n^3},$$

where a_μ is a reduced Bohr radius of the ion. For the case of ground state $^3He^+$ ion, the value of a is 8.666GHz and corresponding B_{hf} is 3.1kGauss, g_I is -4.25512 and g_J is 2.0. We labeled the wave functions as shown in Table 3-3-4. The nuclear polarization, i.e., the expectation value of $\frac{1}{I}\langle i|I_z|i\rangle$ for each state $|i\rangle$ [OH69] is shown in Fig.3-3-4. We assume that initially the system is in a strong magnetic field, the nuclear polarization is zero and the electron polarization is $P_e(g.s.)$. Then the population of the initial system can be expressed using $P_e(g.s.)$ as shown in Table 3-3-5.

Next we consider what happens when the external magnetic field is reduced. If the reduction of magnetic field is adiabatic, each state follows the corresponding energy line. The nuclear polarization of this system (P_N) is given by

$$\begin{aligned} P_N &= \sum_{i=1,4} C_i P_i \\ &= 0.5(1 - \frac{x}{\sqrt{1+x^2}}) P_e(g.s.) \\ &= \epsilon_{HF} P_e(g.s.) \end{aligned}$$

$$\epsilon_{HF} = 0.5(1 - \frac{x}{\sqrt{1+x^2}}) \tag{3.3.9}$$

In a strong magnetic field (x=∞), ϵ_{HF} is zero, i.e., there is no hyperfine interactions and no polarization transfer from the electron to the nucleus occurs. If the field strength is reduced

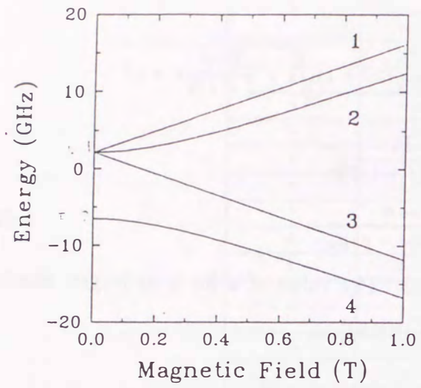

Fig.3-3-3 The hyperfine energy levels of He^+ ion plotted as a function of an external magnetic field.

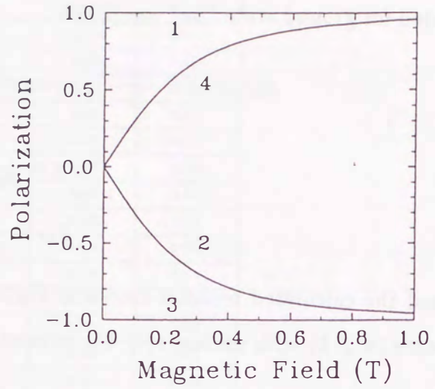

Fig.3-3-4 The nuclear polarization of state i.

wave fuction of state i	$\|I,I_z\rangle\|S,S_z\rangle$ representation
ϕ_1	$\|1/2,+1/2\rangle\|1/2,+1/2\rangle$
ϕ_2	$\frac{x\|1/2,+1/2\rangle\|1/2,-1/2\rangle+(\sqrt{1+x^2}-1)\|1/2,-1/2\rangle\|1/2,+1/2\rangle}{\sqrt{x^2+(\sqrt{1+x^2}-1)^2}}$
ϕ_3	$\|1/2,-1/2\rangle\|1/2,-1/2\rangle$
ϕ_4	$\frac{x\|1/2,+1/2\rangle\|1/2,-1/2\rangle-(\sqrt{1+x^2}-1)\|1/2,-1/2\rangle\|1/2,+1/2\rangle}{\sqrt{x^2+(\sqrt{1+x^2}-1)^2}}$

Table 3-3-4 The wave functions of He^+ hyperfine levels

state i	population C_i
1	$\frac{1}{2}\cdot\frac{1+P_e}{2}$
2	$\frac{1}{2}\cdot\frac{1+P_e}{2}$
3	$\frac{1}{2}\cdot\frac{1-P_e}{2}$
4	$\frac{1}{2}\cdot\frac{1-P_e}{2}$

Table 3-3-5 The population of each state at t=0 with electron polarization of $P_e(0)$.

to zero adiabatically (x=0), we have ϵ_{HF} = 0.5, i.e., half of the electron spin polarization is transferred to the nucleus.

The adiabaticity is fulfilled under the following condition [ME60],

$$T \gg \frac{1}{a}, \tag{3.3.10}$$

$$T = \frac{B_{hf}}{\frac{dB}{dt}} = \frac{B_{hf}}{v_z \frac{dB}{dz}},$$

where T is the time needed to change the magnetic field strength from B_{hf} to zero, a is the hyperfine interval, and v_z is the velocity of the ion beam. For the 20keV $^3He^+$ beam, the velocity v_z of the ion is 10^8 cm/s, and the adiabaticity is fulfilled when $\frac{dB}{dz} \leq 10^5$ Gauss/cm.

In conclusion, the obtained helium nuclear polarization P_N is expressed by the product of three parameters as,

$$P_N = P_{Na}\, \epsilon_{LS}\, \epsilon_{HF}, \tag{3.3.11}$$

where P_{Na} is the sodium polarization defined in equation (3.2.4), ϵ_{LS} is the efficiency defined in equation (3.3.1) and (3.3.6), and ϵ_{HF} is the efficiency to transfer the electron spin polarization to the nuclear polarization defined in equation (3.3.7) and (3.3.9).

3-4 Beam Foil Spectroscopy

To improve the performance of the polarized ion source, it is essential to monitor the nuclear polarization of the ^{3}He beam. We developed a beam foil spectroscopic technique for this purpose [OH92]. The principle is as follows: The polarized $^3He^+$ ion is selected by an energy analyzer and is deflected by 90 degree without changing the spin direction. The analyzed beam passes through a thin carbon foil. The electron capture and loss cross sections are of the order of $10^{-14} \sim 10^{-16}$cm^2. While a 5μg/cm^2 carbon foil has 2.5×10^{17}atoms/cm^2. Thus the electron polarization of the incoming $^3He^+$ ion is lost during the passage of the foil. At the exit of the foil, the ion captures an electron to its excited state from the last layer of the foil [AN79II]. Though the electron polarization is lost during these collisions, the nuclear polarization is kept because the cross section for spin exchange between an electron and a nucleus is of the order of 10^{-21}cm^2. And the depolarization due to hyperfine interactions is not significant, because the period passing through the foil is of the order of 10^{-14}sec, which is shorter than hyperfine periods. After the passage, most of the incident $^3He^+$ is neutralized but in its excited state. As the excited atoms move away from the foil into vacuum, an angular momentum transfer occurs by a hyperfine interaction from the ^{3}He nucleus to the electron orbit, then photons emitted from the excited states become circularly polarized. This circular polarization degree is proportional to the initial ^{3}He nuclear polarization. Thus the nuclear polarization degree is extracted from the circular polarization of the emitted photon from He atom. Fig.3-4-1 is a schematic drawing of this process.

In this method, different from the polarization measurement by nuclear reactions, we do not need to accelerate the ions up to the MeV energy region, and we can monitor the nuclear polarization at the site of the ion source.

The Stokes parameter which expresses the circular polarization degree of light is defined as,

$$S/I = \frac{I(\sigma_+) - I(\sigma_-)}{I(\sigma_+) + I(\sigma_-)},$$

where $I(\sigma_+)$ is the intensity of right handed circularly polarized light, and $I(\sigma_-)$ is the intensity of left handed circularly polarized light. As for a convenience we label $I(\sigma_+)$ as $I(e_{+1})$

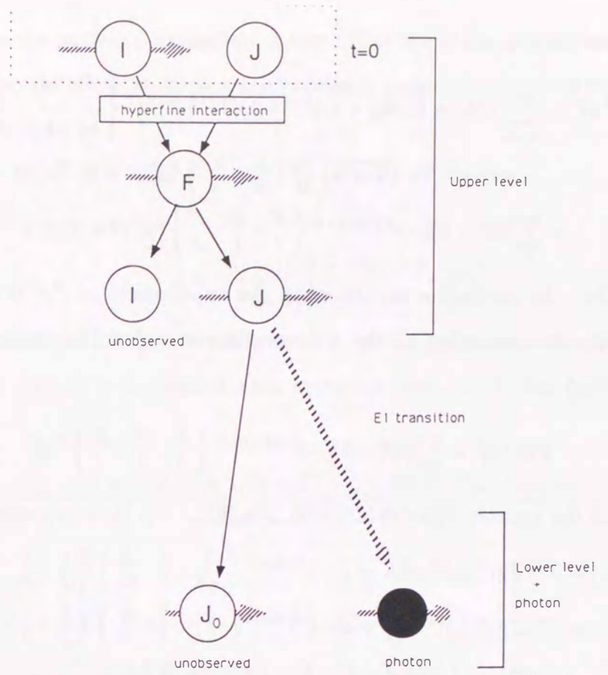

Fig.3-4-1 The process of polarized photon emission from initially nuclear polarized atom.

and $I(\sigma_-)$ as $I(e_{-1})$. For a particular transition from the state (LS)J to (L_0S)J_0, the Stokes parameter is calculated under the following assumptions; (1) the photon measurement is done along the initial spin quantization axis, (2) the time intervals of fine and hyperfine interactions are short compared with the life time of the excited state, (3) we cannot distinguish the fine structure lines, (4) the excitation cross section is proportional to a statistical weight (2J+1), and (5) there is no cascade contributions to the (LS)J state.

The state multipole of the upper state under the hyperfine interaction is characterized by the total angular momentum **F** (=J+I). The multipole ${}^F\rho$ in the F representation is constructed from the production of the state multipoles of the nuclear spin part ${}^I\rho$ and of

the electron spin part ${}^J\rho$ as,

$$
\begin{aligned}
{}^F\rho_0^K &= \sum_{k_I,k_J}[(2k_I+1)(2k_J+1)(2F+1)(2F+1)]^{1/2}\begin{Bmatrix} I & J & F \\ I & J & F \\ k_I & k_J & K \end{Bmatrix} \\
&\quad\times(-)^{K-Q}\sqrt{2K+1}\begin{pmatrix} k_I & K & k_J \\ 0 & 0 & 0 \end{pmatrix}{}^I\rho_0^{k_I}(t=0)\ {}^J\rho_0^{k_J}(t=0) \\
&= \sum_F(2F+1)(-)^{F+J+I+K}\begin{Bmatrix} F & F & K \\ I & I & J \end{Bmatrix}{}^I\rho_0^K(t=0)\otimes\mathbf{1}
\end{aligned}
$$

because just after the excitation the electrons are unpolarized i.e.,${}^J\rho_q^K(t=0) = {}^J\rho_0^0(t=0)$. The state multipole concerning to the E1 transition is ${}^J\rho_q^K$. The state multipole ${}^J\rho_q^K$ is obtained from ${}^F\rho_q^K$ as,

$$
\mathbf{1}\otimes{}^J\rho_0^K = \sum_F(2F+1)(-)^{F+J+I+K}\begin{Bmatrix} F & F & K \\ J & J & I \end{Bmatrix}{}^F\rho_0^K.
$$

The intensity of the emitted light $I_0^K(e_\lambda)$ with a helicity λ is then expressed as [BL81],

$$
\begin{aligned}
I_0^K(e_\lambda) &= |C'\langle J||\mathbf{r}||J_0\rangle|^2\sqrt{2K+1}(-)^{J+J_0+\lambda}\begin{pmatrix} 1 & 1 & K \\ -\lambda & \lambda & 0 \end{pmatrix}\begin{Bmatrix} 1 & 1 & K \\ J & J & J_0 \end{Bmatrix}{}^J\rho_0^K \\
&= |C'\langle J||\mathbf{r}||J_0\rangle|^2\sqrt{2K+1}(-)^{J+J_0+\lambda}\begin{pmatrix} 1 & 1 & K \\ -\lambda & \lambda & 0 \end{pmatrix}\begin{Bmatrix} 1 & 1 & K \\ J & J & J_0 \end{Bmatrix} \\
&\quad\times\sum_F(2F+1)^2\begin{Bmatrix} F & F & K \\ J & J & I \end{Bmatrix}\begin{Bmatrix} F & F & K \\ I & I & J \end{Bmatrix}{}^I\rho_0^K(t=0) \\
&= \sqrt{2K+1}(-)^\lambda\begin{pmatrix} 1 & 1 & K \\ -\lambda & \lambda & 0 \end{pmatrix}B(K,J){}^I\rho_0^K(t=0),
\end{aligned}
$$

where B(K,J) is

$$
\begin{aligned}
B(K,J) =& |C'\langle J||\mathbf{r}||J_0\rangle|^2(-)^{J+J_0}\begin{Bmatrix} 1 & 1 & K \\ J & J & J_0 \end{Bmatrix} \\
&\times\sum_F(2F+1)^2\begin{Bmatrix} F & F & K \\ J & J & I \end{Bmatrix}\begin{Bmatrix} F & F & K \\ I & I & J \end{Bmatrix}.
\end{aligned}
$$

Then the photon intensity is expressed as,

$$
I_0^K(e_\lambda) = \sqrt{2K+1}(-)^\lambda\begin{pmatrix} 1 & 1 & K \\ -\lambda & \lambda & 0 \end{pmatrix}\sum_J(2J+1)B(K,J){}^I\rho_0^K(t=0).
$$

The stokes parameter S/I is expressed as,

$$
\begin{aligned}
S/I &= \frac{I_0^1(e_1)-I_0^1(e_{-1})}{I_0^0(e_1)+I_0^0(e_{-1})} \\
&= \sqrt{\frac{3}{2}}\frac{\sum_J(2J+1)B(K=1,J)}{\sum_J(2J+1)B(K=0,J)}\frac{{}^I\rho_0^1(0)}{{}^I\rho_0^0(0)} \\
&= \sqrt{\frac{3}{2}}\frac{\sum_J(2J+1)B(K=1,J)}{\sum_J(2J+1)B(K=0,J)}P_N(0),
\end{aligned}
\tag{3.4.1}
$$

where $P_N(0)$ is the nuclear polarization at t=0. Thus the Stokes parameter for photons emitted in the direction of the quantized axis is linearly proportional to the nuclear polarization. We can denote it as

$$
S/I = \bar{A}P_N(0)
$$

where

$$
\bar{A} = \sqrt{\frac{3}{2}}\frac{\sum_J(2J+1)B(K=1,J)}{\sum_J(2J+1)B(K=0,J)}.
$$

If we observe the photon intensity with a good time resolution and with the energy resolution not enough to distinguish each hyperfine level, the Stokes parameter is expressed as [AN77],

$$
S/I(t) = \sqrt{\frac{3}{2}}\frac{\sum_J(2J+1)[B(K=1,J)+2\sum_{F_1<F_2}B2(F_1,F_2,J)\cos(\omega_{F_1F_2}t)]}{\sum_J(2J+1)B(K=0,J)}P_N(0), \tag{3.4.2}
$$

where

$$
\begin{aligned}
B2(F_1,F_2,J) =& |C'\langle J||\mathbf{r}||J_0\rangle|^2(-)^{J+J_0}\begin{Bmatrix} 1 & 1 & 1 \\ J & J & J_0 \end{Bmatrix} \\
&\times(-)^{F_1+F_2+2J+2I}(2F_1+1)(2F_2+1)\begin{Bmatrix} F_1 & F_2 & 1 \\ J & J & I \end{Bmatrix}\begin{Bmatrix} F_1 & F_2 & 1 \\ I & I & J \end{Bmatrix},
\end{aligned}
$$

and $\omega_{F_1F_2}$ is the frequency corresponding to the energy difference of the state (JF_1) and the state (JF_2). We can see an intensity modulation as a function of time. This comes from an interference of photons corresponding to transitions from different hyperfine levels. This effect is called Quantum Beat. If the time interval for the measurement is long enough, the oscillating terms are averaged out and we can use equation (3.4.1) instead of equation (3.4.2).

4. Experimental Apparatus

To realize the principle described in the previous chapter, we constructed a bench test device of the polarized ion source. The top view of the polarized ion source is shown in Fig.4-0-1. The polarized ion source consists of a 2.45GHz ECR ion source, a sodium oven in a solenoidal coil, a laser system to polarize sodium atoms, and a polarimeter to measure the nuclear polarization of the $^3He^+$ beam.

The ion beam is extracted from the ECR ion source, then the He^{2+} ion is analyzed by a magnetic analyzer. The sodium vapor is produced in the oven and is polarized by the optical pumping using a circularly polarized laser light. The analyzed He^{2+} ion is focused to the sodium oven where a polarized electron capture of the He^{2+} ion occurs. This electron capture is done in a 3kGauss solenoidal coil. After the magnetic field reduction, the electron spin polarization is transferred to the nucleus. A guiding magnetic field is applied downward the solenoidal coil to avoid the effect of perturbing magnetic field. The fraction of the beam which captures the polarized electron from the sodium atoms is analyzed by an electrostatic analyzer. The nuclear polarization degree is measured by the polarimeter based on the beam foil spectroscopic method.

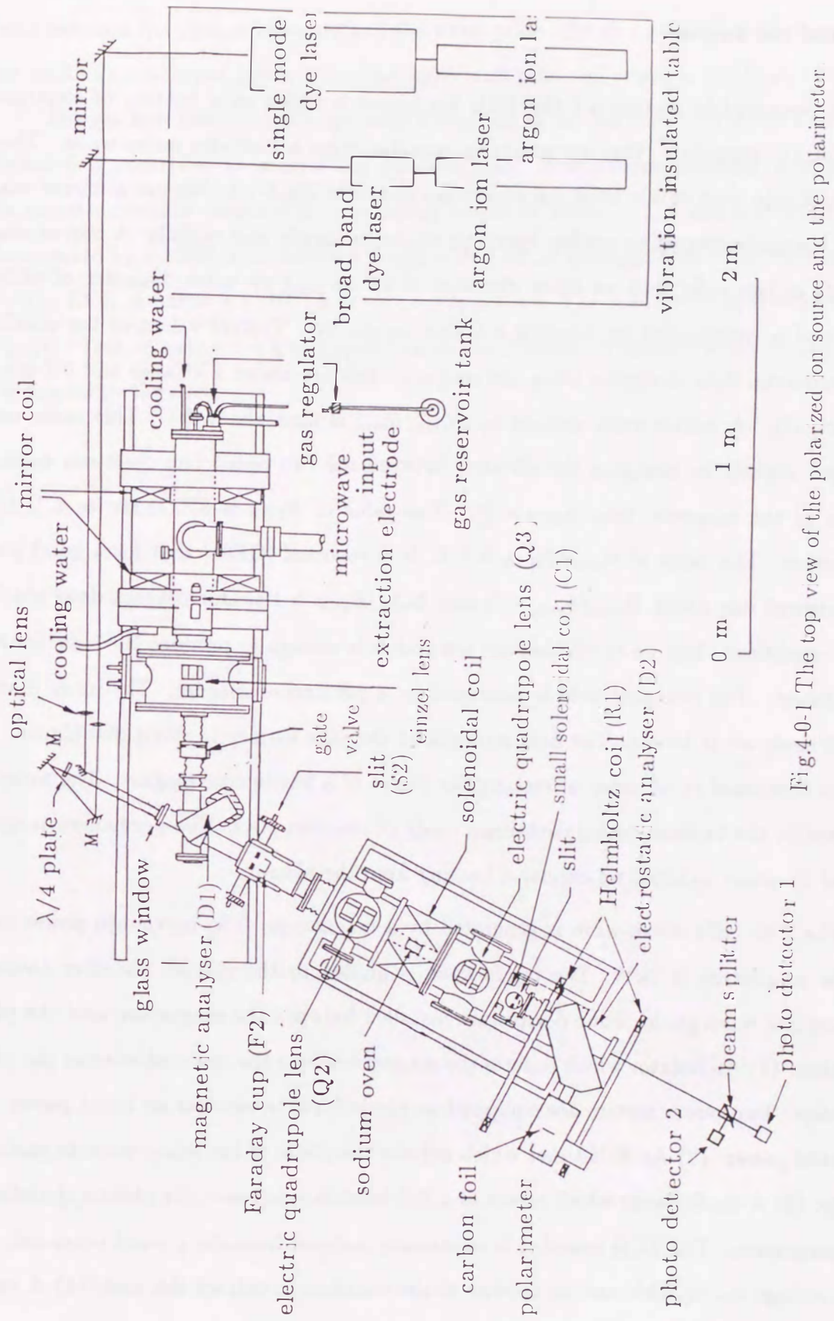

Fig.4-0-1 The top view of the polarized ion source and the polarimeter

4-1 ECR Ion Source

As described in section 3-1 the ECR ion source is based on a heating of electrons by a cyclotron resonance. Our ion source is operated with a 2.45GHz micro-wave. The top view and side view of our ECR ion source are shown in Fig.4-1-1. We use a mirror magnet and a hexapole magnet to confine energetic electrons axially and radially. A mirror magnet consists of two coils with an inner diameter of 25 cm and an outer diameter of 66.5 cm. Each coil is constructed by winding a hollow conductor. Typical values of the maximum and minimum field strengths along the magnetic axis are about 1 kGauss and 0.7 kGauss, respectively. A mirror ratio defined by B_{max}/B_{min} is thus about 1.4. This ratio can be changed slightly by changing the distance between the two coils. The cyclotron resonance occurs at the magnetic field $B_{ECR} = \frac{h\omega}{\mu_e}$. The value of B_{ECR} is 875Gauss for a 2.45GHz microwave. The value of B_{max}/B_{ECR} is 1.1. It is reported [GE91] that for a good plasma confinement one needs $B_{max}/B_{min} \sim 2$ and $B_{max}/B_{ECR} > 1.5$. Our magnet does not fulfill these conditions. But we think that our ion source is enough to produce He^{2+} ion for a test experiment. The hexapole field is produced by a permanent magnet. The inner diameter of the hexapole is 10 cm. The field strength at the pole surface is about 800 Gauss. Each pole is composed of an array of rectangular pieces of a ferrite core magnet. The arrays are inserted in the vacuum sealed containers made of stainless steel. The permanent magnet is cooled by water to avoid an excessive heating from the plasma.

The 2.45 GHz micro-wave is generated by a magnetron. The maximum power output of the magnetron is 5kW. The micro-wave is guided to the plasma chamber through a rectangular wave guide. Four devices are installed between the magnetron and the plasma chamber. (1) An isolator which isolates the magnetron from the reflected wave at the plasma chamber. Two power meters are equipped on the isolator to monitor an input power and a reflected power. (2) An E-H tuner which adjusts the phase of the micro-wave to match the cavity. (3) A chalk flange which serves as a DC insulation between the plasma chamber and the magnetron. The ECR chamber is electrically isolated from the ground potential, and a high voltage up to 20kV can be applied to the chamber to extract the ions. (4) A vacuum

seal between the plasma chamber and the wave guide. For this purpose a fused quartz plate is used. Typical input power is around 700W and reflected power is less than 100W.

The gas flow rate needed is typically 0.2cc/min in our ion source. We use a conventional mass flow controller to control the gas flow rate. The plasma chamber is evacuated by a turbo molecular pump with a pumping speed of $160l$/s. The ion extraction region is evacuated by a $1200l$/s oil diffusion pump with a liquid nitrogen trap. The vacuum pressure of the ECR chamber is 5×10^{-6}Torr without operation. The pressure in operation is typically 2×10^{-5}Torr. A gate valve is equipped to keep the chamber in vacuum when the sodium metal is loaded to the oven.

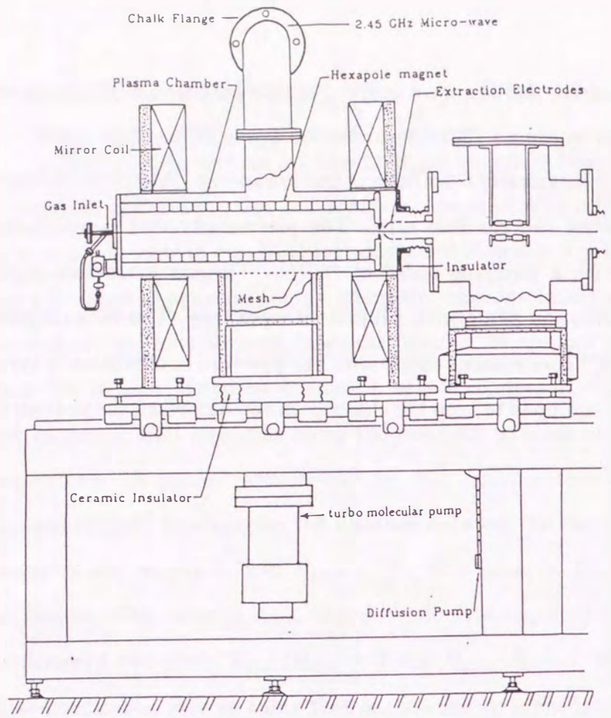

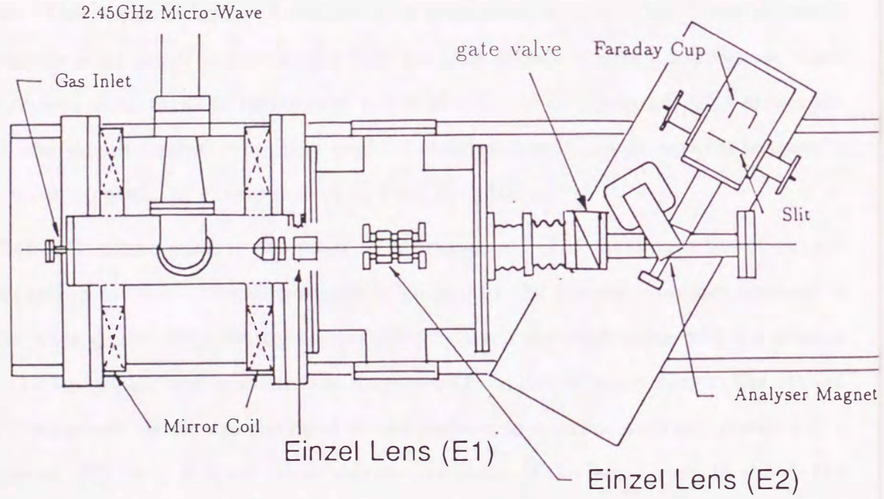

Fig.4-1-1 The side view and the top view of the 2.45GHz ECR ion source

4-2 Sodium Oven

The sodium vapor is produced by a heated oven. In the initial stage of our measurement we used a sodium oven shown in Fig.4-2-1. The oven is made of copper and is wound by a heater. The temperature of the oven is measured by a Platinum 100 Ω thermo resistance. The length of the sodium cell is 6cm. The outer diameter is 3cm. An inner sleeve with a diameter of 1.2cm is inserted into the cell. Various coatings were tested on the surface of this sleeve to examine the depolarization effect. The oven is inserted into a water cooled copper tube. Some fractions of effused sodium vapor are trapped by this tube.

A magnetic field is applied to the collisional region where electron captures occur. This magnetic field is produced by a solenoidal coil. The length of the coil is 36cm and the diameter is 6cm. The maximum field strength produced by this coil is 3 kGauss. A 500 l/s oil diffusion pump with a liquid nitrogen trap is installed upstream from the solenoid, and a 1200 l/s oil diffusion pump with a liquid nitrogen trap is installed downstream from the solenoidal coil for evacuation.

Most of the measurements of the sodium polarization were done with this oven but there is a problem for this oven. During the loading process of the sodium metal into the crucible, the surface of the sodium metal is oxidized. So it is needed to increase the temperature of the crucible up to nearly 300°C to break the surface skin of the sodium oxide. After this procedure, the surface of the inner sleeve is deteriorated by high temperature sodium atoms with a high density. Therefore we constructed a new oven which can control the temperature of the inner sleeve and that of the sodium crucible independently, thus reducing the deterioration of the sleeve surface.

A new oven is shown in Fig.4-2-2. A sodium metal is vaporized in a temperature controlled crucible. The sodium vapor flows through a heated pipe to the collisional region where an electron capture of a He^{2+} ion from a sodium atom takes place. The diameter of the collisional region is 2.0cm, and its length is 12cm. Both ends have a hole with a diameter of 0.6cm. A thin inner sleeve coated with dry film is inserted in the collisional region, and its diameter is 1.9cm. At both the sides of the collisional region, water cooled pipes with a

diameter of 2cm are placed to trap the sodium vapor effused. To measure the temperature of the crucible, we use Platinum 100Ω thermo-resistor. For the temperature measurement of the heated pipe and the inner sleeve, we use thermo-couples. Three power supplies are used for heater wires to control the temperatures independently.

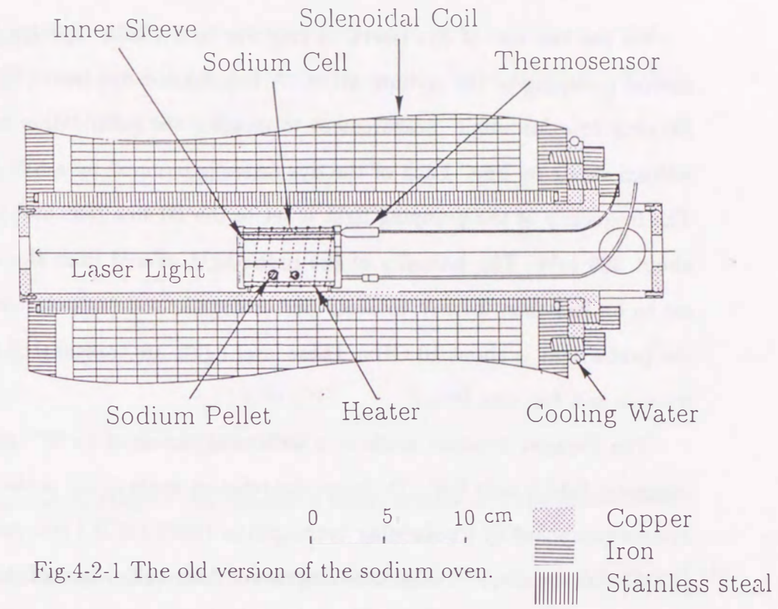

Fig.4-2-1 The old version of the sodium oven.

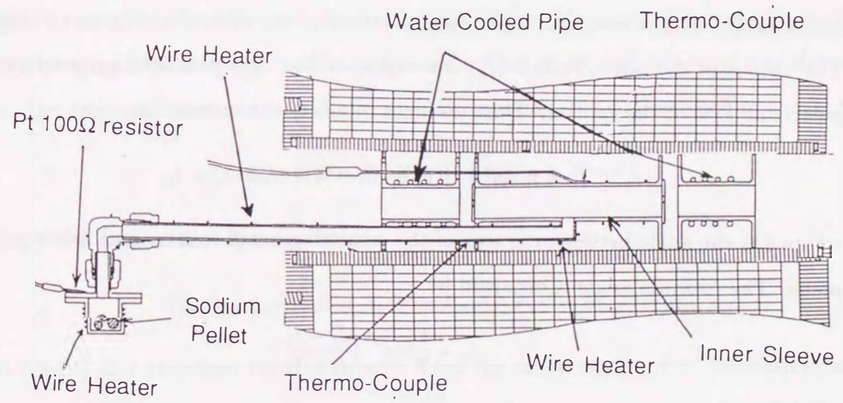

Fig.4-2-2 The new version of the sodium oven.

4-3 Laser System

We use two sets of dye lasers. A ring dye laser (380A, Spectra Physics) is used for the optical pumping of the sodium atom. A broad band dye laser (375B, SP) is used for the Faraday rotation angle measurement to monitor the polarization and the thickness of the sodium vapor on line. Each of the dye lasers is pumped by a 5W argon laser (168B, SP). The frequency of the pumping light is set to the D1 line (589.6nm). Its typical intensity is about 300 mW. The intensity of the probe light offered from the broad band dye laser is set to be less than 0.1mW to avoid perturbing the sodium polarization. The line width of the probe light is about 10 GHz. These laser lights are transmitted to the sodium cell using mirrors and focusing lenses.

The Faraday rotation angle at a sodium thickness of 5×10^{13} atoms/cm^2 with 3kGauss magnetic field is only 0.8°. To detect the rotation angle of the probe light precisely, we use a system composed by a polarizing beam splitter (05FC16PB.3 Newport) and two photodiodes (S2386 Hamamatsu). A schematic diagram of the measurement of the rotation angle is shown in Fig.4-3-1. The specification of each part is tabulated in Table 4-3-1. A typical input light intensity was 10μW. The output of the photodiode was terminated by a 10kΩ resistance, so the output voltage of the photodiode was of the order of 100mV. The output of the photodiode 1 (I_1) is sensitive to the light polarized along the polarizing axis of the splitter. The output of the photodiode 2 (I_2) is sensitive to the light polarized perpendicular to the polarizing axis of the splitter. Then the light intensity is expressed as,

$$I_1 = I_0 \sin^2\theta, \quad I_2 = I_0 \cos^2\theta, \quad I_0 = I_1 + I_2,$$

where θ is the angle between the axis of the polarizing beam splitter and linear polarization plane. The rotation angle is obtained by,

$$\theta_c = \frac{1}{2} Sin^{-1}\left(\frac{I_1 - I_2}{I_1 + I_2}\right). \tag{4.3.1}$$

The output voltages of I_1 and $I_1 - I_2$ are measured by two digital multi-meters (R6450, Advantest and 9300MF, Sanwa) and recorded through a GP-IB interface to the personal computer (PC9801VX, NEC) for on-line calculation of θ. The angle θ is set to $\pi/4$ at

polarizing beam splitter	
extinction ratio	$< 10^{-3}$
transmission	> 0.9
available region	400-700nm
photodiode	
sensitivity	0.4A/W at 589nm
dark current	50pA
temperature dependence	
of dark current	1.12 times/°C
output linearity	1pW-1mW

Table 4-3-1 The specification of the polarizing beam splitter and the photodiode.

a condition that there is no sodium atom, because the sensitivity for the rotation of the polarization plane of the probe light is the largest at this angle setting.

Fig.4-3-2 shows the calculated angle θ_c from the output voltage using the equation (4.3.1) versus the rotation angle of the polarization plane of the incoming light θ. The angle θ is changed by rotating the detector system. One can see a good proportionality of θ_c to θ.

We measured the Faraday rotation angles as a function of the wavelength of the probe laser. The angle $NL\ \theta_0$ was obtained by using the equation (3.2.6) described in chapter 3-2,

$$NL\ \theta_0 = \theta(B = B_0, P = 0) - \theta(B = 0, P = 0).$$

Similarly the angle $NL\ P\ \theta_p$ was obtained by,

$$NL\ P_{Na}\ \theta_p = \theta(B = B_0, P = P_{Na}) - \theta(B = B_0, P = 0).$$

Fig.4-3-3 (a) and (b) show the $NL\ \theta_0$ and $NL\ P\ \theta_p$, respectively. The solid curve is the fitted curve of the calculation (see Appendix). The free parameters are NL and P_{Na}. In this case NL=3.8×10^{13} atoms/cm^2 and P_{Na}=0.32 are obtained. The experimental results reasonably agree with the calculation, which indicates this monitor is a reliable one. In a

usual operation, the wavelength of the probe laser is set to 589.3nm, because the wavelength dependence of Faraday rotation angles is minimum at this point. The frequency of the probe light is monitored by a spectrum analyzer (M410, SP). During an experiment, a fine tuning of the pumping laser frequency is done to maximize the Faraday rotation angle of the probe light, i.e., to maximize the sodium polarization.

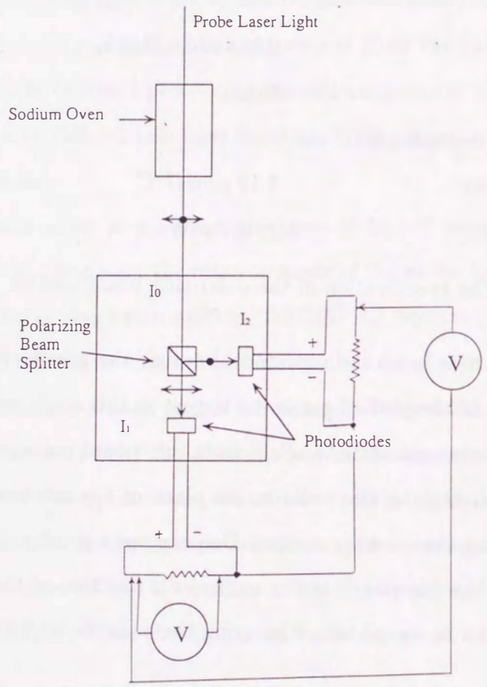

Fig.4-3-1 The detection system of a Faraday rotation angle.

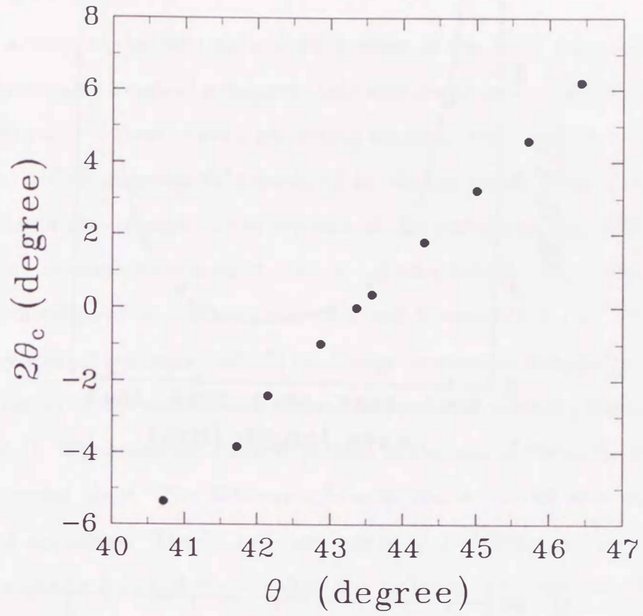

Fig.4-3-2 The calculated angle θ_c from the output voltages of the photodiodes plotted as a function of the angle θ which is the angle between the axis of polarizing beam splitter and the polarization plane of the probe laser light

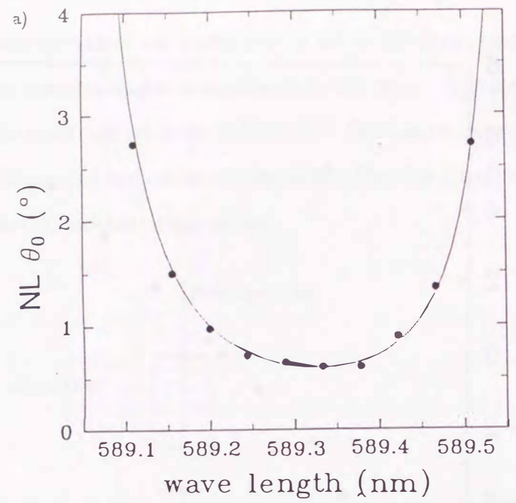

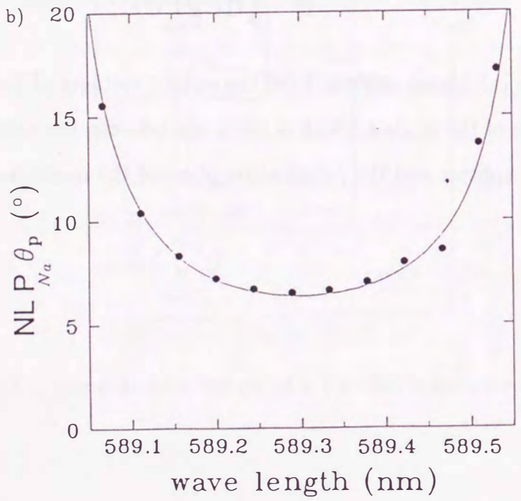

Fig.4-3-3 The measured Faraday rotation angles a) $NL\theta_0$ and b) $NL\ P_{Na}\ \theta_p$ plotted as a function of the wavelength of the probe laser. The solid curve is the fitted curve of the calculation (see Appendix) with NL=3.8×10^{13} atoms/cm^2 and P_{Na}=0.32.

4-4 Guiding Field System

In the system of the electron and the nucleus of the $^3He^+$ ion, the electron spin and nuclear spin strongly couple at a magnetic field with nearly zero. The direction of the electron spin changes easily if there exists a perturbing magnetic field, such as a terrestrial magnetic field and a residual magnetic field produced by electric power lines. Thus the direction of the nuclear spin also changes in the presence of the perturbing magnetic field through the electron spin. To eliminate this effect, a weak magnetic field of a few Gauss is applied parallel to the axial direction of the 3 kGauss solenoidal coil downward the coil. This magnetic field is produced by a small solenoidal coil (C1) and large rectangular Helmholtz coils (R1) covering the whole region of the polarimeter, where the produced nuclear polarization is measured (see Fig.4-0-1). We choose the z axis is parallel to the axis of the solenoidal coil, the x axis is in a horizontal plane. The 3kGauss solenoidal coil is located at z=0mm. The C1 coil is located at z=500mm. The R1 coils are located at z=780mm and z=1200mm. Fig.4-4-1 shows the magnetic field distribution along the 3kGauss solenoidal coil. The ion beam feels a magnetic field reduction from 3kGauss as the ion beam moves away from the solenoidal coil, and the field strength is reduced to 5Gauss at z=400mm. The maximum gradient of the magnetic field is 500Gauss/cm, which satisfies the adiabatic condition of equation (3.3.10). The ratio of $B_{x,y}/B_z$ is less than 0.1 for this region, and this corresponds to the angle between z axis and the magnetic axis is less than 5.7°. The maximum reduction of the expectation value is cos5.7° = 0.995.

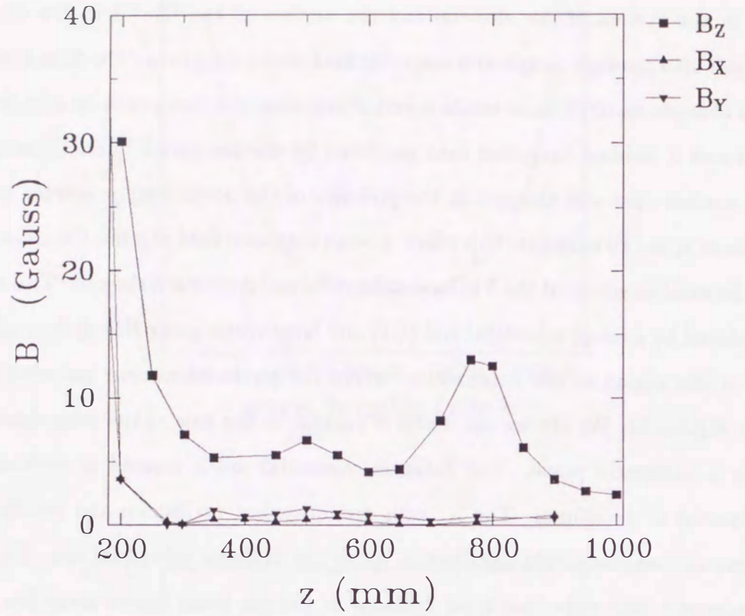

Fig.4-4-1 The measured magnetic field distribution along the axis of the solenoidal coil (the z axis). The x and the y axes are normal to the z axis. C1 coil is located at z=500mm and R1 coils are located at z=780, 1200mm.

4-5 Polarimeter

An outlook of the polarimeter is shown in Fig.4-5-1. The polarized $^3He^+$ ion beam is bent by 90 degree by an electrostatic analyzer. A weak magnetic field is applied the whole region of the polarimeter using rectangular Helmholtz coil to avoid the depolarization caused perturbing magnetic field as described in section 4-3. This section is evacuated by a $500l/s$ turbo molecular pump and by two liquid nitrogen traps. The analyzed $^3He^+$ beam bombards a carbon foil. The thickness of the carbon foil is about 5 $\mu g/cm^2$. The foil surface is set to be perpendicular to the beam axis to avoid an additional polarization production by a tilted foil effect. The position of the foil can be changed upward and downward along the beam axis. The foil is designed to be removed during the tuning of the transportation of the He^+ ion beam. The ion beam passing through the foil is collected by a Faraday cup (F3). A precise measurement of the current is important because we use the current integration for the normalization of the photon counting. For this purpose, we insert two electrodes in front of the cup; one is kept in the ground potential and the other is applied to a potential of about 1 kV. These electrodes play a role of electron repellers which suppress secondary electrons emitted from the Faraday cup.

The photons emitted from the foil-excited He atoms are detected by using a photon detector system. These photons are focused on the head of the photomultiplier by two lenses. The circularly polarized photons are converted to the linearly polarized photons by a 1/4 wave length plate. Then the linearly polarized photons are analyzed by a polarizer filter. The photons that pass through a wavelength filter are finally counted by a photomultiplier. The specification of each component of the photon detector system is tabulated in Table 4-5-1.

The photomultiplier is operated in a photon counting condition. An output of the anode is terminated by 110kΩ resistor. The output signals of the photomultiplier are amplified and converted to logic signals by a single channel analyzer. The number of the logic signals is recorded in a scaler. The photon counts are accumulated alternatively under the condition that the sodium atoms are polarized (N_{pol}) or that the sodium atoms are not polarized

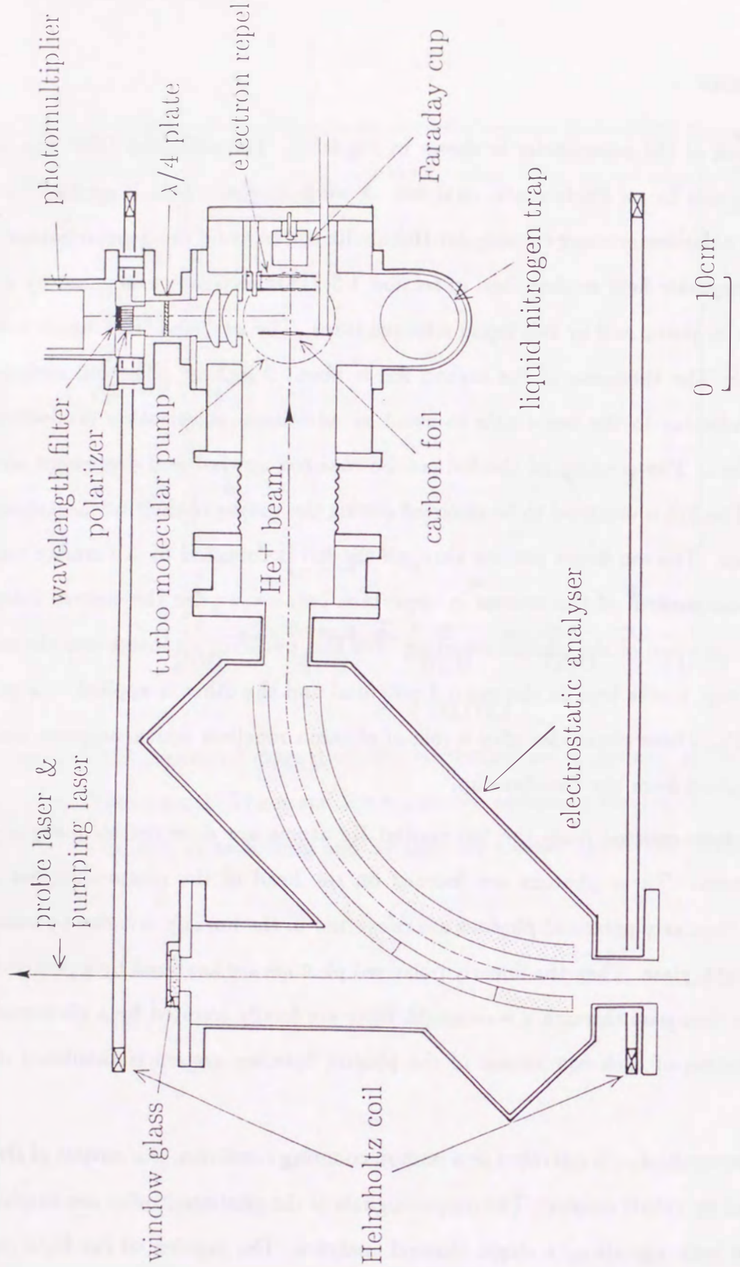

Fig.4-5-1 The outlook of the polarimeter.

lens (Sigma Optics)	
focal length	70mm
diameter	50mm
material	BK7
transmission	91.8% at 389nm
1/4 wavelength plate (Sigma Optics)	
aimed wavelength	389.0nm
transmission	99%
polarizer (Polaroid H22)	
extinction ratio	10^{-4}
transmission	6.12% at 389nm
wavelength filter (Vacuum Corporation of Japan MIF-W)	
centroid of transmission	391.5nm
Full Width at Half Maximum	20nm
transmission	41.5%
photomultiplier (Hamamatsu R464)	
quantum efficiency	23% at 389nm
effective area	5mm×8mm
typical bias voltage	-700V

Table 4-5-1 The specification of components of the polarimeter.

(N_{unpol}). The degree of the circular polarization AP is calculated as follows,

$$AP = r - 1,$$

$$r = \frac{N_{pol}}{N_{unpol}},$$

where N is the photon number counted by the detector. The condition of the sodium polarization is changed by each 10sec to reduce a systematic error. The electronic circuit diagram for the data taking system is shown in Fig.4-5-2.

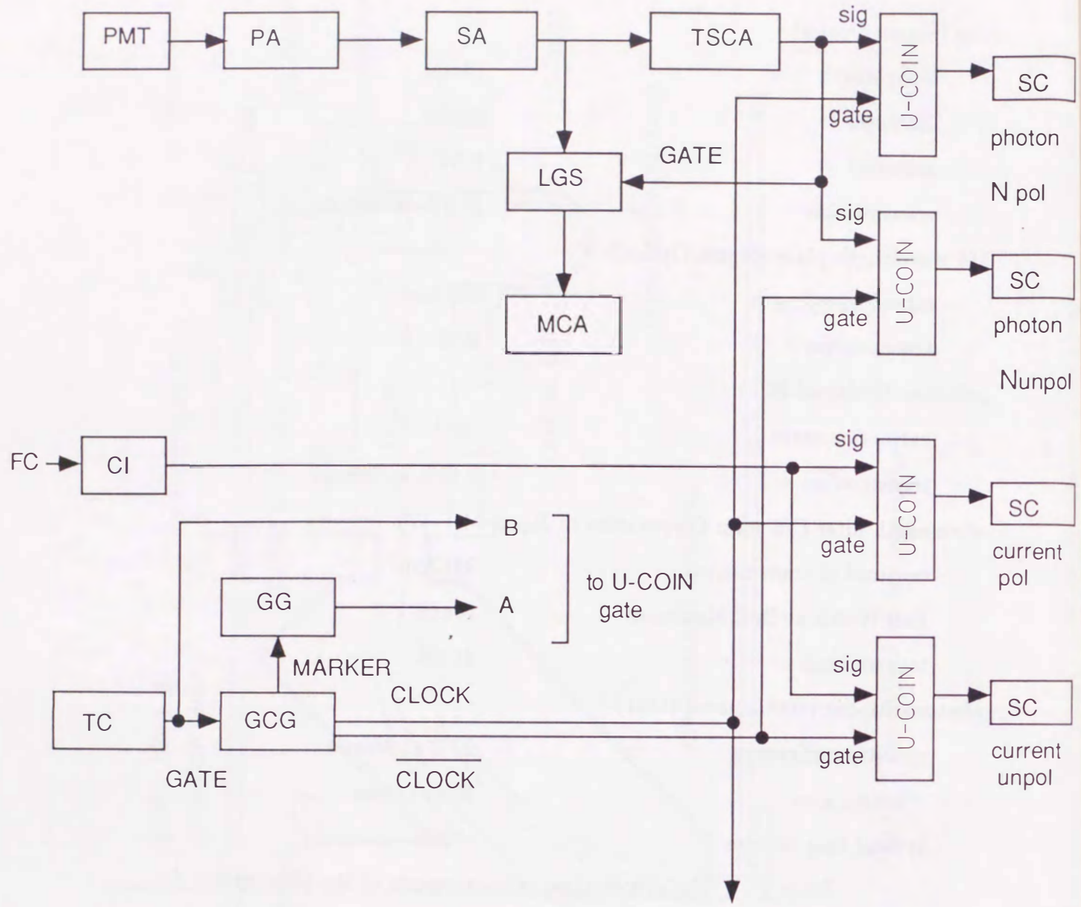

TC : timer counter
GCG : gate and clock generator
GG : gate generator
PMT : photomultiplier
PA : preamplifier
SA : spectroscopic amplifier
TSCA : timing single channel analyzer
LGS : linear gate and stretcher
MCA : multichannel analyzer
U-COIN : universal coincidence
CI : current integrator
SC : scaler

Fig.4-5-2 The electric circuit diagram for data taking.

The pulse height spectrum of the photomultiplier is shown in Fig.4-5-3. The lower discrimination of the single channel analyzer was set at the dip of the spectrum (indicated by the arrow in the figure).

The detection efficiency of the polarimeter along the beam axis was measured as a function of the position of the light source (photodiode was used) which was moved on the beam axis. The result is shown in Fig.4-5-4. The FWHM of this detector system is about 5mm.

The dark current of the photomultiplier without the He^+ ion beam was 0.3cps. But the counting rate was increased when the He^+ ion beam was introduced even at a condition that the carbon foil was removed, . The background counting rate with the He^+ ion beam was measured as a function of the vacuum pressure of the Polarimeter chamber. Fig.4-5-5 shows the result. This background component comes from the neutral He atom produced by the collisions of He^+ ions and the residual gas atoms. The background counting rate was 0.1counts/nC at the pressure less than 10^{-6}Torr. A typical counting rate with the carbon foil (true events) is 50counts/nC. This shows the signal to noise ratio of 2×10^{-3} at the pressure of the polarimeter section less than 10^{-6}Torr.

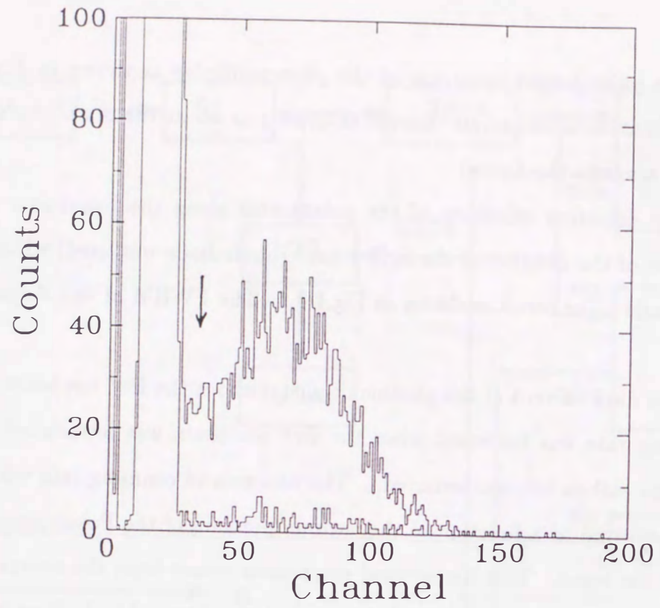

Fig.4-5-3 The pulse height spectrum of the output signal of the photomultiplier. The lower discrimination of a single channel analyzer is set at the position indicated by the arrow.

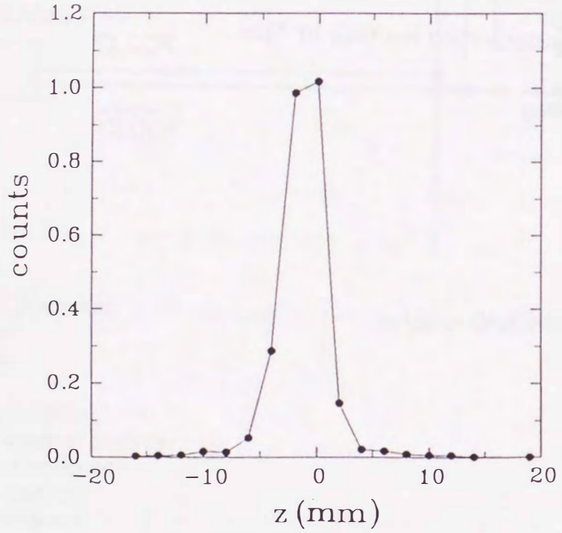

Fig.4-5-4 The detection efficiency of photons plotted as a function of the position of the light source along the beam line.

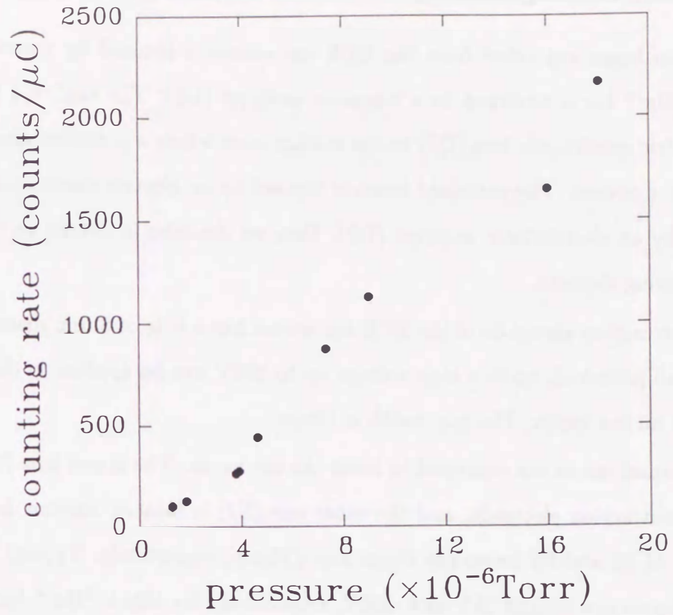

Fig.4-5-5 The background counting rate plotted as a function of the vacuum pressure of the polarimeter chamber. The vertical axis is a photon counts per Coulomb.

4-6 Ion Beam Focusing Elements

The ion beam extracted from the ECR ion source is focused by einzel lenses(E1,E2). Then the He^{2+} ion is analyzed by a magnetic analyzer (D1). The analyzed beam is focused by an electric quadrupole lens (Q2) to the sodium oven where a polarized electron capture of the He^{2+} ion occurs. The polarized beam is focused by an electric quadrupole lens (Q3) and analyzed by an electrostatic analyzer (D2). Here we describe in details on each component of ion focusing element.

The extraction electrode of the ECR ion source has a hole of 8 mm diameter and is kept in a ground potential, while a high voltage up to 20kV can be applied to the ECR chamber to extract an ion beam. The gap width is 10mm.

Two einzel lenses are equipped to focus the ion beam. The einzel lens E1 is located just after the extraction electrode, and the other one (E2) is located 300mm downstream. The diameters of E1 and E2 lenses are 70mm and 120mm, respectively. Typical voltages applied to these lenses are around 2kV and -500V, respectively for 10keV $^3He^{2+}$ beam.

The ion beam is deflected by a magnet (D1). The deflection angle of D1 is 60 degree, and a radius of the ion trajectory is 135mm. The analyzed ion current is measured by a Faraday cup (F2) after a slit (S2). The slit width is usually set to 10mm. The Faraday cup can be removed form the beam path using an air cylinder unit.

The electric quadrupole doublet lenses (Q2,Q3) are used to focus the beam. The aperture of the lens is 30mm and length of the lens unit is 120mm. The electrode is made of a brass pipe with a length of 45mm and a diameter of 30mm. Typical voltage applied to Q2 is around 500V for a 20keV He^{2+} ion, and the voltage applied to Q3 is around 1kV for a 20keV He^{+} ion.

This analyzer (D2) consists of two spherical electrodes made of stainless steal. The radius of the ion trajectory is 250mm. The gap width is 20mm. The applied potentials for these electrodes are set as follows, $V_+ = -1.17V_-$ because the centroid of the trajectory is set to be zero potential. Typical applied potentials are +2.25kV and -2.63kV for the 20keV $^3He^{+}$ ion beam. This analyzer has a double focusing property and focal length is 700mm. Outer side

of the electrodes has a hole through which the laser light and neutral He atoms pass.

5. Experimental Results and Discussion

5-1 Performance of the ECR Ion Source

The performance of the 2.45GHz ECR ion source was checked using a ^{3}He gas. Fig.5-1-1 shows the extracted ion current as a function of the excitation current of the D1 magnet. Ions such as H^+, H_2^+, carbon, nitrogen, and oxygen ions with low charge states were extracted in addition to the He^{2+} and He^+ ions. These components other than He ions are expected to come from a small leakage of an air and a back diffused oil vapor from vacuum pumps. The largest peak in Fig.5-1-1 corresponds to the He^+ ion. The ion current of He^{2+} is about 1~2% of He^+ ion current. We think the low current of He^{2+} come from a low frequency of the electron cyclotron resonance, and from imperfect confinement of energetic electrons because of a low value of B_{max}/B_{ECR}.

In Fig.5-1-2, the $^3He^{2+}$ and $^3He^+$ ion currents are plotted as a function of the ^{3}He gas flow rate. The extraction voltage was 10kV. When a current peak is obtained for the He^{2+} ion, the gas flow rate was less than that of He^+. This may be because the recombination probability between He^{2+} ions and He atoms is considerably large when the vacuum pressure is high.

We measured the $^3He^{2+}$ ion current by varying the extraction voltage, and we could extract more than a few eμA of the $^3He^{2+}$ ion with the energy range of 16 to 28keV.

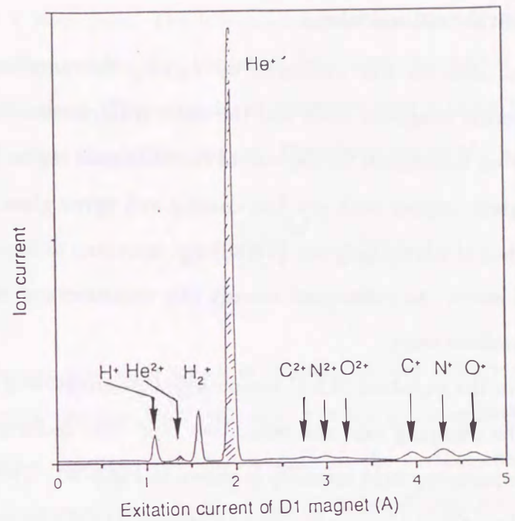

Fig.5-1-1 The mass spectrum of the extracted ion beam from the 2.45GHz ECR ion source. The extraction voltage was 7kV.

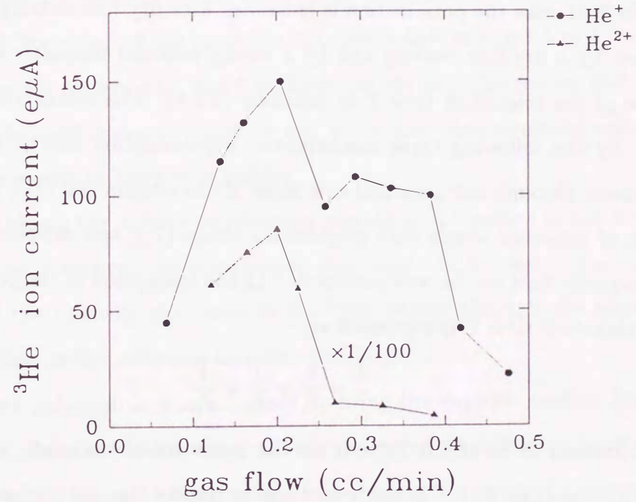

Fig.5-1-2 The $^3He^{2+}$ and $^3He^+$ ion currents plotted as a function of the gas flow rate of ^{3}He.

5-2 Polarization of the Sodium Atom

The sodium polarization was measured by varying the pumping light intensity, the strength of the external magnetic field, and the sodium thickness. To enhance the sodium polarization, we tested 4 materials for the wall of the collisional region [TA90]. The materials are copper, pyrex glass, copper with dry-film coating and pyrex glass with dry-film coating. The dry-film is a kind of silicon polymer [SW88] and is known to have a low relaxation rate for polarized alkali atom. As mentioned already this measurement was carried out mainly with the old type sodium oven.

As it is shown in the equation (3.2.4) the obtained polarization is determined by a competition between the pumping rate and relaxation rate. The sodium polarization observed as a function of the pumping light intensity is shown in Fig.5-2-1. The polarization increases as the pumping light intensity increases. This corresponds to the increase of the value of α in equation (3.2.4). The sodium polarization is shown in Fig.5-2-2 as a function of the external magnetic field. The polarization increases as the strength of the external magnetic field increases. In both case the polarization is enhanced with dry-film coating. The polarization enhancement by a dry-film coating and by a strong external magnetic field correspond to the increase of the relaxation time T in equation (3.2.4). The relaxation time T is mainly determined by the following three mechanisms: depolarization due to the effusion of the polarized atoms through entrance and exit holes of the sodium cell (T_e); depolarization due to collisions of polarized atoms with neighboring atoms (T_c); and depolarization induced by the local magnetic field on the wall surface during the adsorption of the polarized atom (T_w). Thus the relaxation time T is expressed as,

$$\frac{1}{T} = \frac{1}{T_e} + \frac{1}{T_c} + \frac{1}{T_w}.$$

T_e is estimated to be about 300μsec for the geometry of the oven. T_c is negligible at a vapor density less than 5×10^{12}atoms/cm^3 because the Na-Na spin exchange cross section is reported to be $1.6\pm0.5\times10^{-14}$cm^2 [SW88].

The depolarization on the wall surface is caused by the following processes. When an alkali atom strikes the wall, the atom is adsorbed on the wall surface by the Van der Waals

attraction force for a brief time. The interaction potential for adsorption on the surface is not homogeneous. This results that the atom feels time dependent magnetic field as the atom moves on the surface. This modulated magnetic field acts on the valence electron of the alkali atom and causes the depolarization. The relaxation by the wall surface is expressed as [LE88],

$$\frac{1}{T_w(B)} = \frac{2}{3}\frac{\tau_s\gamma^2b^2}{\tau_s+\tau_v}\frac{\tau_c}{1+\omega^2\tau_c^2},$$
$$\gamma = \frac{g\mu_e}{\hbar}, \qquad \omega = \frac{eB}{m_e},$$

where τ_s is the average time that an atom remains on the surface at each collision, τ_v is the average flight time between wall collisions, g is the gyromagnetic ratio of the electron spin, μ_e is the Bohr magneton, b is the strength of the surface magnetic field producing the relaxation, τ_c is the correlation time of the modulated magnetic field, ω is the Larmor precession frequency of the electron spin, and B is the external magnetic field. The data are fitted by treating the value b as a free parameter under the approximation $\tau_s \sim \tau_c$ and using the values $\tau_c = 0.84\times10^{-10}$ sec for a pyrex glass and 0.19×10^{-10}sec for a copper wall [BO66, SW88]. We obtained the modulated magnetic field strength b of 1.5kGauss for pyrex wall, 2.0kGauss for copper wall, and 0.4kGauss for the dry-film-coated walls both on pyrex and copper. The solid curves in Fig.5-2-1 and 5-2-2 show the calculated value. These values agree with the results of Levy et al [LE88].

Fig. 5-2-3 shows the sodium polarization plotted as a function of the sodium thickness. As the thickness increases, the polarization decreases. It is because the pumping light is absorbed and the intensity decreases as the light passes through the sodium vapor, and because the effect of the radiation trapping gets large.

The sodium polarization was enhanced by using the dry-film coating because of its low relaxation rate. But the coating was gradually destroyed when the ion beam was introduced to the sodium cell. This may be due to the bombardment of the wall by electrons or ions. The degradation of the coating was improved by a new type sodium oven. The main differences between the old oven and the new one are the temperature of the inner sleeve and the radius of the inner sleeve. The temperature is reduced from 240°C to 180°C in operation. The

diameter is enlarged from 16mm to 19mm. With this new oven the sodium polarization was kept from 0.4 to 0.2 during a month.

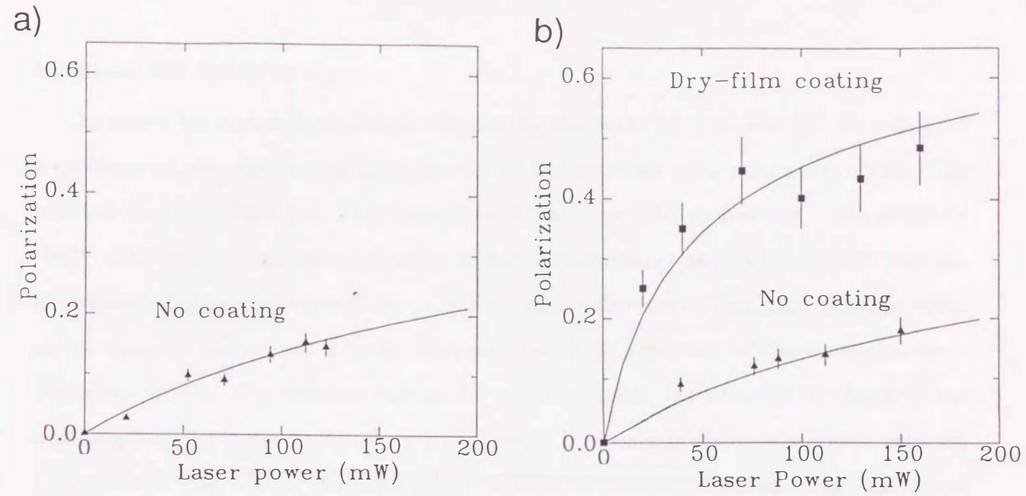

Fig.5-2-1 The sodium polarization plotted as a function of the pumping light intensity with a) a copper wall and a dry-film coated copper wall, and b) a pyrex wall and a dry-film coated pyrex wall. The external magnetic field was 3kGauss and the sodium thickness was 3×10^{13}atoms/cm^2. Solid curves are results of theoretical calculations.

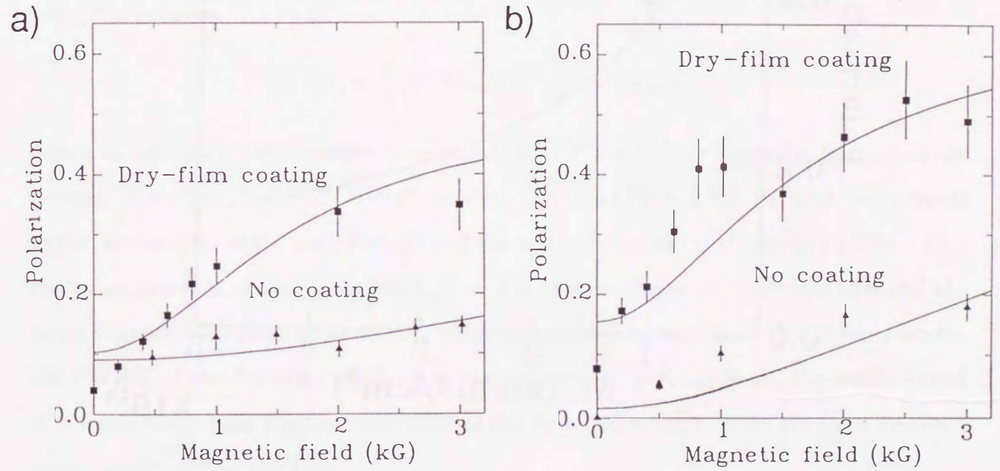

Fig.5-2-2 The sodium polarization plotted as a function of the external magnetic field with a) a copper wall and a dry-film coated copper wall, and b) a pyrex wall and a dry-film coated pyrex wall. The pumping light intensity was 180mW and the sodium thickness was 3×10^{13}atoms/cm^2. Solid curves are results of theoretical calculations.

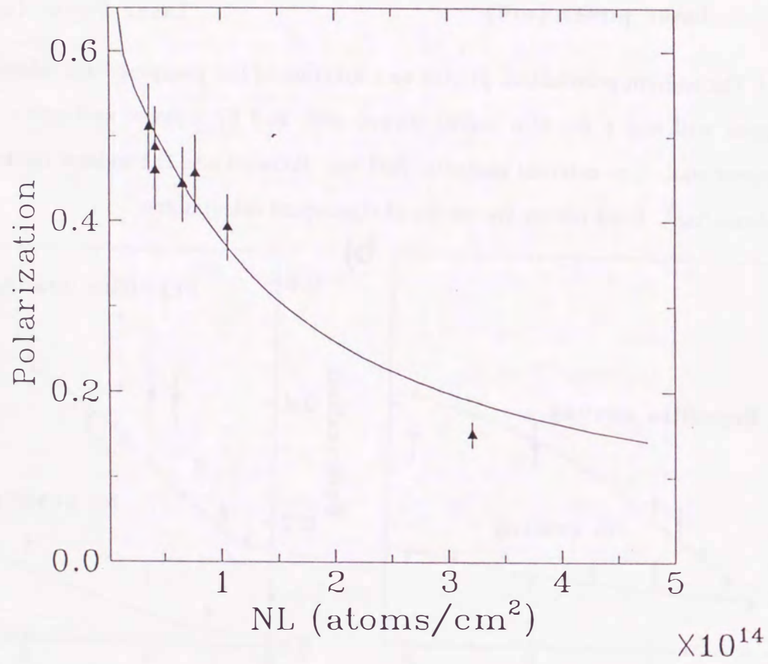

Fig.5-2-3 The sodium polarization plotted as a function of the sodium thickness with dry-film coated wall. The external magnetic field was 3kGauss and the pumping light intensity was 180mW. A solid curve is a result of theoretical calculations.

5-3 Beam Foil Spectroscopy

To search for a photon candidate adequate for the beam foil spectroscopy, we measured a spectrum of photons emitted from the excited helium atom using a monochrometer. The result is shown in Fig.5-3-1. This measurement was done with an incident beam of 20keV $^3He^{2+}$, and with the ion current of about 100nA. At this energy nearly 90% of He^{2+} ions are neutralized after passing through the carbon foil with a thickness of $5\mu g/cm^2$. The slit width of the monochrometer was 0.5mm. The corresponding resolution of the monochrometer was about 0.5nm. The counting rate of the photomultiplier was recorded by changing the wavelength of the monochrometer by a 1nm step. The peaks in the spectrum are assigned to transitions from 5^3D, 4^3D 3^3P states and so on of the neutral ^3He atom. Fig.5-3-2 shows the Grotorian diagram [BA75] of a neutral He atom (He I). The most intense peak is found at 389nm, which corresponds to the transition from the $3^3P_{J=0,1,2}$ state to the $2^3S_{J=1}$ state of the neutral helium atom. The life time of the 3^3P state is 100ns.

The analyzing power A for the transition from the 3^3P state to the 2^3S state is calculated using the equation (2.4.2) as,

$$A(t) = \frac{2}{27}(1 - \cos\omega_1 t) + \frac{2}{15}(1 - \cos\omega_2 t),$$

where ω_1 and ω_2 is the hyperfine intervals of the 3^3P state. The hyperfine interval $\omega_1/2\pi$ between the state (J=1,F=3/2) and the state (J=1,F=1/2) is 2.85GHz, and the interval $\omega_2/2\pi$ between the state (J=2,F=5/2) and the state (J=2,F=3/2) is 539MHz [TI73]. This analyzing power is shown in Fig.5-3-3. Here the z axis is chosen as the beam axis and the beam velocity is assumed to be 10^6m/s which corresponds to the 20keV ^3He beam. Because the FWHM of the detection efficiency of the polarimeter is about 5mm, the oscillation of A is much faster than the time resolution of the detection system. Thus the time averaged value can be used in this case,

$$\bar{A} = 0.207.$$

Because of its large yield and rather large analyzing power $\bar{A}$, we decided to use 389nm photon for the detection of the nuclear polarization of $^3He^+$ beam.

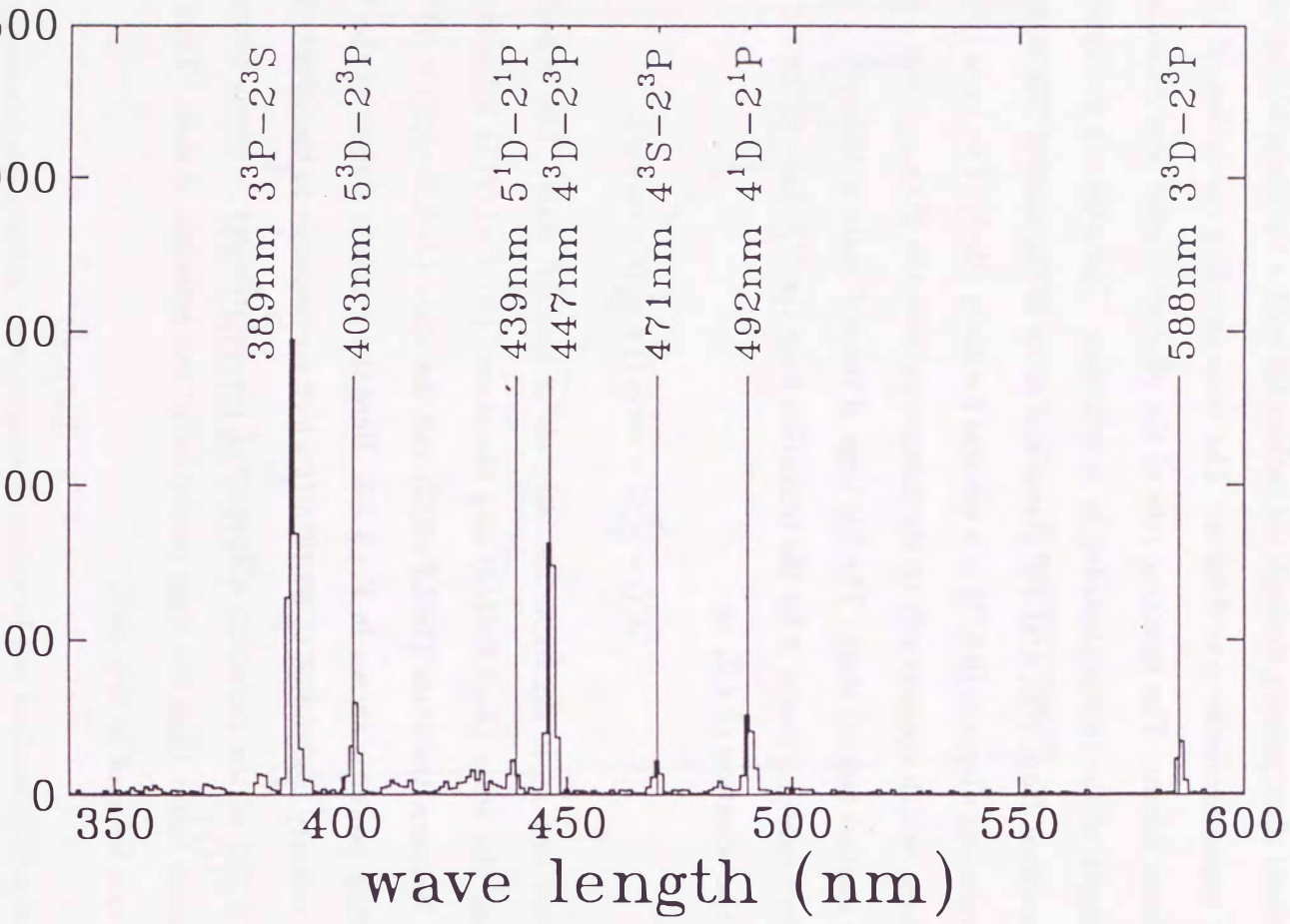

Fig.5-3-1 The observed spectrum from an incidence of 20keV He^+ beam on a $5\mu g/cm^2$ carbon foil.

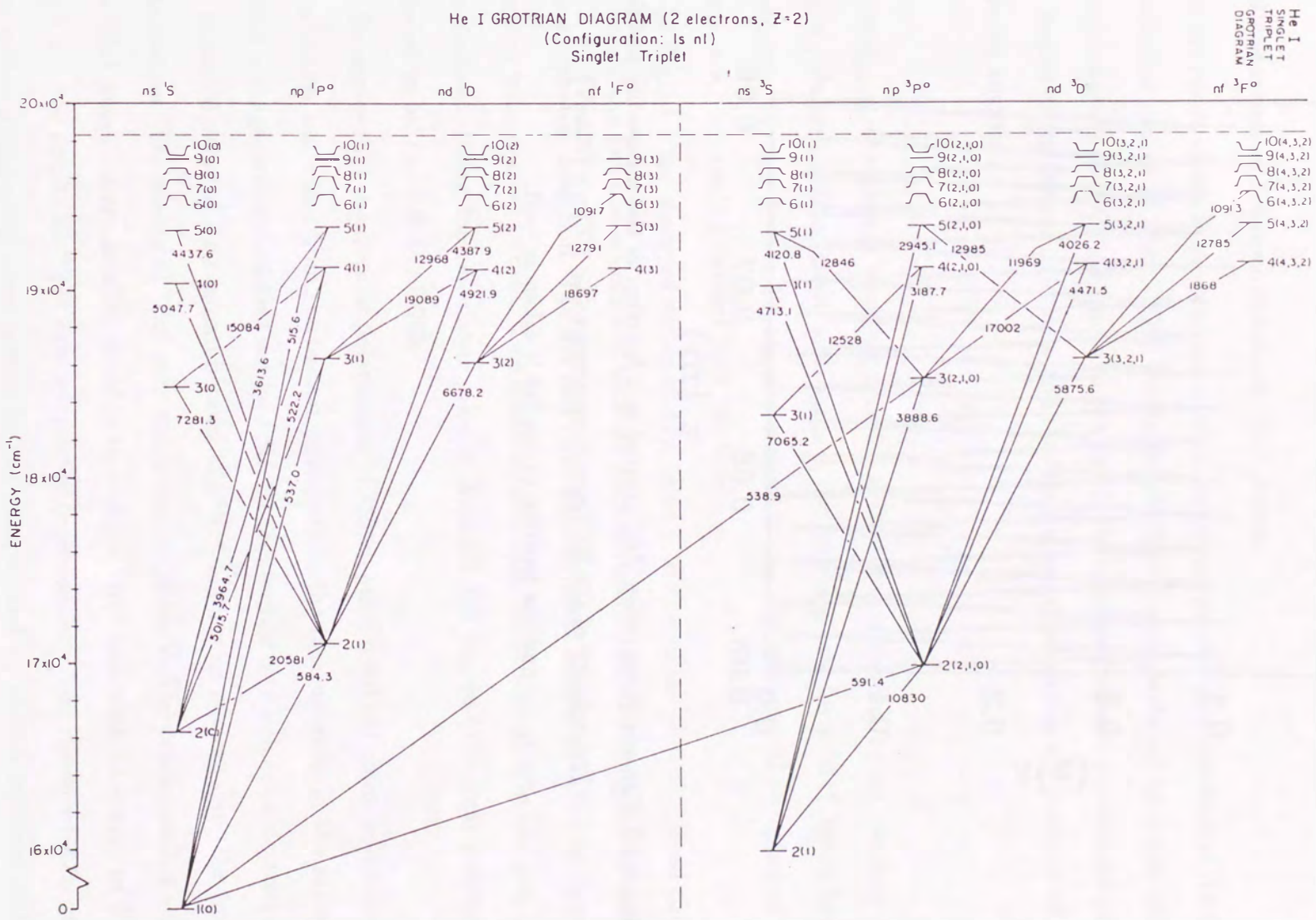

Fig.5-3-2 The Grotorian diagram of a neutral He atom [BA75].

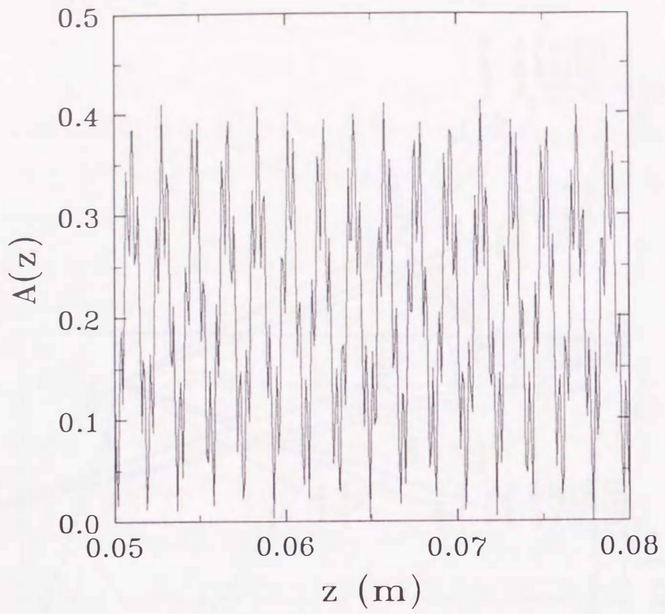

Fig.5-3-3 The analyzing power A(t) plotted as a function of the measuring position z. The velocity of the He beam is assumed to be 10^6m/s (20keV) and the position of the foil is taken as z=0.

5-4 Production of Nuclear Polarized $^3He^+$ Beam

From the result shown in the previous section, we carried out the measurement of the circular polarization degree of 389nm light with a 20keV $^3He^+$ beam produced by a spin polarized electron capture [OH92]. As shown in chapter 2, the relation between the circular polarization degree of the 389nm light $\bar{A}P_N$ and the ^{3}He nuclear polarization P_N is expressed by the following equation,

$$\frac{N_{pol}}{N_{unpol}} = 1 + \bar{A}P_N,$$

where N_{pol} is the photon counting rate for a $^3He^+$ beam formed by an electron capture from a polarized sodium atom, and N_{unpol} is the counting rate for a $^3He^+$ beam formed by an electron capture from a unpolarized sodium atom. For the optical pumping of sodium atoms, a σ_+ circularly polarized light was used.

In Fig.5-4-1 the observed values of $\bar{A}P_N$ using a ^{3}He beam are plotted (closed circles) for two cases; the left one is obtained with σ_+ photon detection and the right one is obtained with σ_- photon detection. The left and right data deviates from each other in the opposite direction with respect to zero. This demonstrates that the 389nm photon has a σ_+ circular polarization. Using the calculated value of $\bar{A}$=0.207 the degree of nuclear polarization is deduced to be P_N=0.018 $\pm$ 0.005.

To ensure that the circular polarization of 389nm photon did not come from the electron polarization but came from the nuclear polarization, the measurement in the same experimental arrangement was carried out for a $^4He^+$ beam formed by a polarized electron capture. An expected value of $\bar{A}P_N$ is zero because the $^4He^+$ ion has no nuclear spin thus no nuclear polarization. The energy of $^4He^+$ ions was chosen to 26.6keV. The corresponding velocity of the $^4He^+$ ions is approximately equal to that of the $^3He^+$ ions with an energy of 20keV. In Fig.5-4-1, the results for $^4He^+$ case are plotted (open circles). The measured $\bar{A}P_N$ values are zero within a statistical uncertainties for both the σ_+ and σ_- photon measurements. From this result, we are definitely convinced that the nuclear polarized $^3He^+$ beam can be obtained by the polarized electron capture method.

The next step is to find the condition for obtaining the maximum nuclear polarization

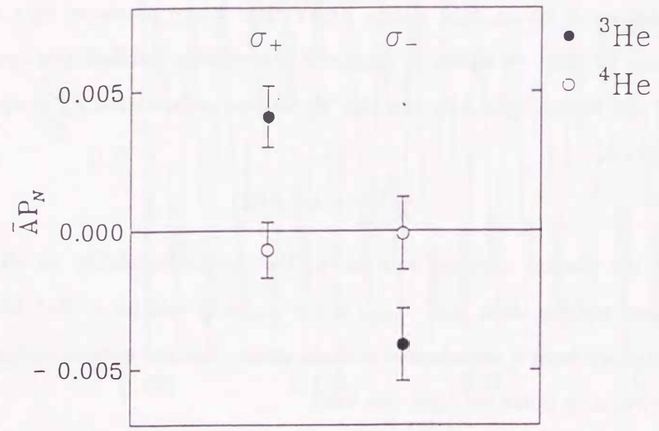

Fig.5-4-1 The observed asymmetry $\bar{A}P_N$ of the 389nm photon with a) a 20keV ^{3}He beam (closed circle) and b) with a 26.6keV ^{4}He beam(open circle).

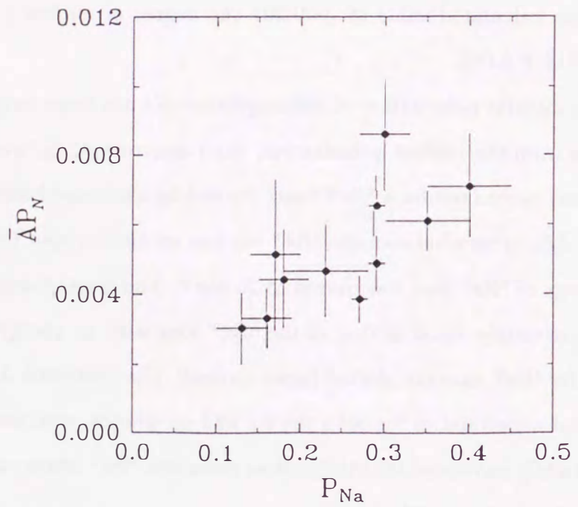

Fig.5-4-2 The observed value of $\bar{A}P_N$ with a 20keV $^3He^+$ beam plotted as a function of the sodium polarization P_{Na}. The new sodium oven with dry-film coating was used.

attainable by this method. The nuclear polarization P_N is expressed as shown in equation (3.3.11),

$$P_N = P_{Na}\ \epsilon_{LS}\ \epsilon_{HF}$$

and the value of $\bar{A}P_N/P_{Na}$ is

$$\bar{A}P_N/P_{Na} = \bar{A}\ \epsilon_{HF}\ \epsilon_{LS}$$

Fig.5-4-2 shows the value of $\bar{A}P_N$ plotted as a function of the sodium polarization P_{Na}. The value of $\bar{A}P_N$ increases as the sodium polarization P_{Na} increases, which shows the sodium polarization is transferred to the ^{3}He nucleus. The largest asymmetry $\bar{A}P_N$ was 0.0086±0.0013 at the sodium polarization of 0.30±0.03 with dry-film coating, and this corresponded to the nuclear polarization of

$$P_N = 0.0415 \pm 0.0061.$$

The nuclear polarization should be proportional to the sodium polarization and the coefficient $\bar{A}P_N/P_{Na}$ should be constant for all data at same incident energy. In Fig.5-4-2 the value of $\bar{A}P_N/P_{Na}$ are rather scattered. So we re-analyze the value of $\bar{A}P_N/P_{Na}$ as a function of the vacuum pressure of the chamber downstream from the sodium cell. Fig.5-4-3 shows the result. One can see an increase of $\bar{A}P_N/P_{Na}$ as the vacuum pressure decreases. This indicates that there is a depolarization process induced by the collisions between ^{3}He ions and residual gases. The collisions between the He^{2+} ion and the unpolarized residual gas result in an unpolarized He^+ ion, and collisions between the polarized He^+ ion and the residual gas atom may induce an excitation of the polarized $^3He^+$ ion or a spin exchange collision with the residual gas and reduce the polarization. The density of residual gas at a pressure of 10^{-6}Torr corresponds to 3×10^{10}atoms/cm^3. The path length between the sodium oven and the foil of the polarimeter is about 1.5m. Thus if the cross section for depolarization process is of the order of 10^{-15}cm^2, the 10% polarization reduction may occur at a pressure of 3×10^{-6}Torr. The value of $\bar{A}P_N/P_{Na}$ at the best vacuum pressure was obtained to be 0.0268 ± 0.0086. Using $\bar{A}$=0.207 and ϵ_{HF}=0.5, the value of ϵ_{LS} is calculated to be

$$\epsilon_{LS} = 0.259 \pm 0.083.$$

If we assume that the electron capture to the 3d state of the He^+ ion is dominant at the incident energy of 20keV as shown in Table 3-3-1, the ϵ_{LS} is expressed in terms of the alignment factor A_0^{col} as, $\epsilon_{LS} = 0.301 + 0.202A_0^{col}$. Using this relation the alignment of the $He^+(3d)$ state A_0^{col} formed by an electron capture from a sodium atom is calculated to be

$$A_0^{col} = -0.21 \pm 0.41.$$

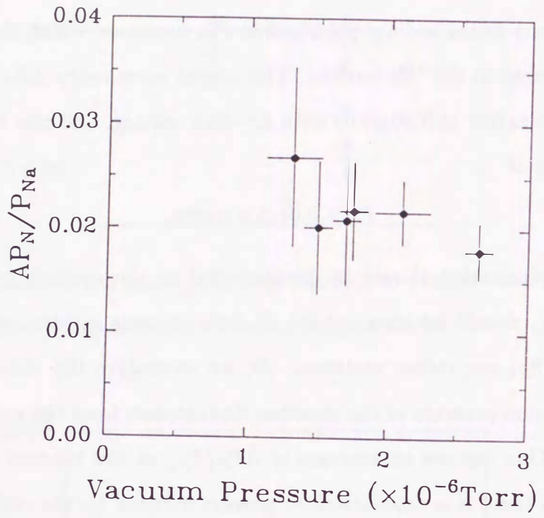

Fig.5-4-3 The value of $\bar{A}P_N/P_{Na}$ plotted as a function of the vacuum pressure of the chamber downstream from the sodium oven.

5-5 Energy Dependence of the Polarization Transfer

The polarization transfer efficiency ϵ_{LS} depends on the alignments of the excited states of the He^+ produced by the reaction $He^{2+} + Na \rightarrow He^+(nlm) + Na^+$, and the alignments may have a dependence on the incident energy of the He^{2+} ion. To know in what energy is the optimum to obtain larger nuclear polarization, we measured the energy dependence of the value of the $\bar{A}P_N/P_{Na}$. The measurement was done at the $^3He^{2+}$ incident energy of 20, 24, and 28keV. The lower limit of this energy comes from a worse beam quality from the ECR ion source, and from a low current after the foil which was used to the normalization of the photon countings. The upper limit of the incident energy comes from the discharge problem of the ECR ion source, and from a small cross section of an electron capture as shown in Fig.3-3-1. The result is shown in Fig.5-5-1. The analyzing power $\bar{A}$ may also vary when the incident beam energy changes. To cancel the energy dependence of $\bar{A}$, we applied a high voltage to the target foil in order to keep the incidence energy of the He^+ ion to the carbon foil constant to be 20keV. The results are shown in Fig.5-5-2. Here the values of $\epsilon_{LS}(E)$ devided by that value with 20keV $^3He^+$ incidence are shown instead of $\bar{A}P_N/P_{Na}$. There appears no drastic change of ϵ_{LS} in an energy region of 20-28keV.

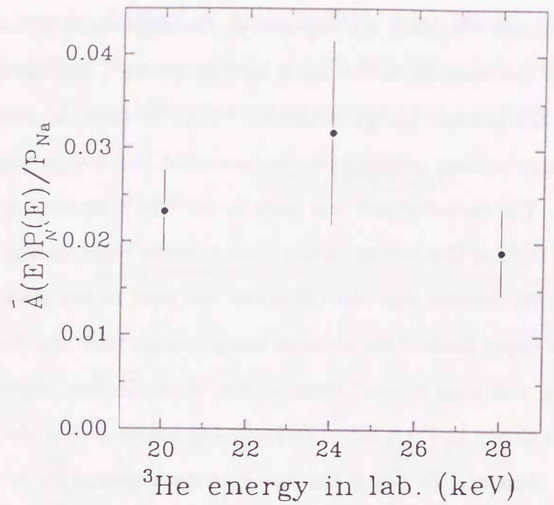

Fig.5-5-1 The value of $\bar{A}(E)P_N(E)/P_{Na}$ plotted as a function of the incident energy of the $^3He^{2+}$ ion in a reaction of $He^{2+} + Na \rightarrow He^+ + Na^+$.

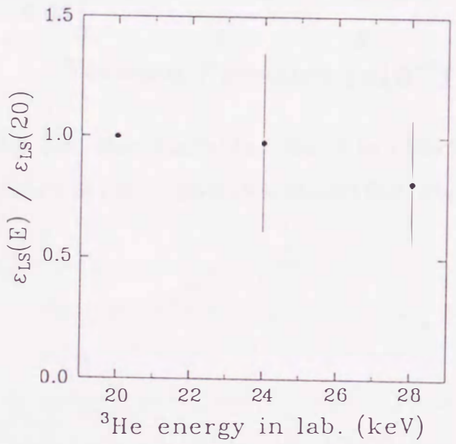

Fig.5-5-2 The values of $\epsilon_{LS}(E)/\epsilon_{LS}(20)$ plotted as a function of the incident $^3He^+$ ion energy. The incident energy to the carbon foil is kept to be 20keV (i.e., $\bar{A}(20keV)$).

6. Future Prospects

6-1 Improvement of the Polarized ^{3}He Ion Source

The quality factor for a polarized ion source Q is characterized by

$$Q = P_N^2 \times I,$$

where P_N is the produced nuclear polarization, and I is the beam intensity. For maximum Q the acquisition time of a polarization sensitive measurement within a given statistical accuracy is minimized. In the following, we consider how to increase the polarization and the beam intensity.

a) Nuclear Polarization

Concerning the nuclear polarization P_N, the expected nuclear polarization of ^{3}He is expressed in the equation (3.3.11), which means that the factors P_{Na}, ϵ_{LS} and ϵ_{HF} should be increased to obtain larger nuclear polarization,.

1) P_{Na}: Electron Polarization of Target Alkali Atom

Large sodium polarization can be expected if a strong light source for the optical pumping is employed. It is reported that a more efficient way is to use potassium or rubidium instead of sodium [YO90]. This is expected from following reasons. (1) At the same vapor density, the velocities of the atoms are slower than that of sodium atoms because the temperatures required to produce the same vapor pressure is lower, and because the masses are larger than sodium. This results in a longer relaxation time. Fig.6-1-1 shows the vapor pressures for alkali atoms plotted as a function of the temperature [WE80]. (2) The photon number of a pumping light in a same wattage is larger than that of the sodium case. (3) A powerful solid laser to pump rubidium and potassium is available, such as Ti Sapphire laser. On the other hand in dye lasers, the power and lasing frequency are influenced by the condition of the dye jet. Using the polarized potassium vapor, the polarization of the electron is expected to be nearly 1.0 at a thickness of a few 10^{13}atoms/cm^2. (4) The cross sections of electron capture process are comparable to that for a sodium atom.

Swenson et al. [SW90] reported that they could obtain a polarized potassium vapor with the polarization of 0.8 at a thickness of 3.2×10^{13}atoms/cm^2 at LAMPF. They used a

TiSaf laser which produced a power of 3.5W at 770nm in an 0.8GHz bandwidth. This bandwidth nearly matched the 1GHz line width of potassium (Hyperfine intervals ν_{HF}=0.46GHz, Doppler width ν_D=0.9GHz at 120°C). The TRIUMF group (Levy et al.) reported that they could obtain a polarized rubidium vapor with the polarization of 1.0 at a thickness of 3.5×10^{13}atoms/cm^2. They used two TiSaf lasers; one had an output of 3.4W in a 2GHz (FWHM) bandwidth, the other produced 5.8W in a 4GHz bandwidth. This light nearly covered the absorption width of rubidium (ν_{HF}=3GHz, ν_D=0.4GHz at 80°C).

2) ϵ_{LS}: depolarization due to fine interactions

If we apply a magnetic field strong enough to decouple the fine interaction, ϵ_{LS} may reach to be near 1.0. As shown in Table 3-3-2, the limitation of the nuclear polarization comes from the strength of the fine interaction of the 2P state of the $^3He^+$ ion, where the required magnetic field is more than 6.4T which is not easily produced. For this reason we tried to optimize the value of ϵ_{LS} by selecting a proper reaction energy. However as shown in previous chapter there was no drastic change in ϵ_{LS} for the incident energy of 20-28keV.

Another way to increase the efficiency of ϵ_{LS} is to use a He^+ (2S) meta-stable ion. As discussed above, the polarization attainable by this method is limited by the fine interaction of the 2P state of the He^+ ion. If we use the 2S state the efficiency ϵ_{LS} may be increased, because the 2S state is populated directly or cascading from excited states without passing through the 2P state. The magnetic field strength to decouple the fine interactions for the 3P, 4D states is about 1.9T, which is not difficult to produce at a laboratory. If we ionize these metastable components, almost all the electron polarization may be transferred to the nucleus by the Sona method. The production rate of the 2S state at an incident of a 20keV ^3He ion is estimated by using the partial cross sections (Table 3-3-1), and the result is shown in Table 6-1-1.

initial state	cross section:σ ($\times10^{-16}$cm^2)	branching to 2s:r	σr ($\times10^{-16}$cm^2)
2S	0.42	1	0.42
3P	10.83	0.12	1.30
4P	10.03	0.12	1.23
4D	13.30	0.03	0.40
total			3.35

Table 6-1-1 The production rate of the 2S state for 20keV $^3He^{2+}$ incident on sodium atom.

The cross section passing through the 2P state is obtained by subtracting the cross section for producing 2S state (3.35×10^{-16}cm^2) from the total cross section (112.14×10^{-16}cm^2) and it is 108.795×10^{-16}cm^2. For the fraction passing the 2P state, the value of ϵ_{LS} is 0.407 (depolarization factor for the transition of 2P to 1S). According to Burcham et al [BU74] the ionization cross section of He^+ to He^{2+} for He^+ (2S) is 100 times larger than He^+ (1S) case. The ionization cross section of He^+ (1S) to He^{2+} is 10^{-16}cm^2 [MA69]. Then the overall nuclear polarization of the $^3He^{2+}$ ion is

$$\epsilon_{LS} = \frac{3.35\times100\times1.0 + 108.79\times1\times0.407}{3.35\times100 + 108.79\times1} = 0.85.$$

3) ϵ_{HF}: Hyperfine Interaction

The polarization transfer efficiency from the electron to the nucleus of the ^3He is 0.5 for the weak field transition. This efficiency can be twiced by employing the Sona method [SO67]. In the Sona method, the ion passes a reversal point of the magnetic field and reaches negative high magnetic field, i.e., the value of x is changed to $-\infty$ in equation (3.3.9) thus the value ϵ_{HF} reaches to be near 1.0.

In Fig.6-1-2 the energy diagram of Zeeman levels is shown for $^3He^+$ ion. We assume that the He^{2+} ions capture the electrons polarized parallel to z axis in a high magnetic field i.e., the produced beam is in the state 1 or 2. Suppose that the particle moves in a region where the magnetic field decreases from a high positive value, changes its direction and reaches a negative high value. We call conventionally "low field" and "high field" as the value of B is much smaller and much larger, respectively, than a critical value B_{hf} defined in equation (3.3.8). If the passage of the magnetic field is adiabatic, then the two states 1,

2 go into the two states 1', 2' at the high negative field. Ionization in this region gives a full polarization transfer from the electron to the nucleus. The necessary condition for this method is described in Appendix. The condition required is possible to be obtained in a reasonable experimental geometry.

b) Beam Intensity

The beam intensity is a second important property of the polarized ion source. We used a 2.45GHz ECR ion source and obtained only a few μA of the $^3He^{2+}$ ion beam. In addition the ion beam transport was not optimized in our present test bench system. But if we employ a new powerful ion source, and improve the beam transportation system, we will be able to obtain more intense currents. Recently a new ECR ion source called Neomafios-10GHz was introduced at the RCNP. The performance was tested at the RCNP and results are tabulated in Table 6-1-2. We could obtain the current of 200 μA for the $^3He^{2+}$ ions. If the cross section of the polarized electron capture is $10^{-14}cm^2$ and the thickness of the polarized atomic target is $3\times10^{13}atoms/cm^2$, the efficiency for polarized electron capture reaches 0.3, thus 60μA of the polarized $^3He^+$ ion will be able to be obtained.

c) Beam Quality

1) Stripping of the electron

After the polarization of the electron is transferred to the nucleus, the added electron becomes a burden when the polarized beam is transported and is accelerated [OH85]. Since the magnetic moment of the electron is much larger than that of the nucleus, the nuclear polarization is reduced through the hyperfine interaction if the electron spin feels perturbed magnetic field. A high charge state is also desired for the acceleration of ^3He in the cyclotron to obtain an energetic beam.

To remove the electron much efficiently, the ion should be once accelerated by a static electric field and then the electron should be removed by a stripper foil or a stripper gas. The equilibrium charge state of He is shown in Fig.6-1-3 [MA68]. The fraction of He^{2+} is 0.3 at the energy of 300keV. In the stripping region a magnetic field should be applied to use the Sona method. A schematic drawing of a stripping process and an injection line to

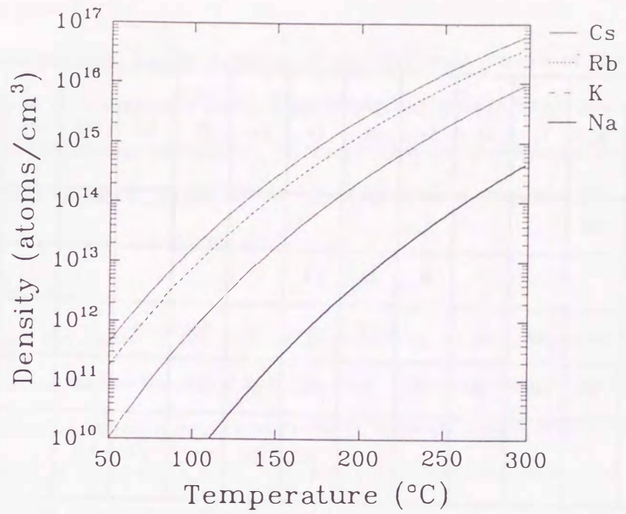

Fig.6-1-1 The vapor pressures for alkali atoms plotted as a function of the temperature [WE80].

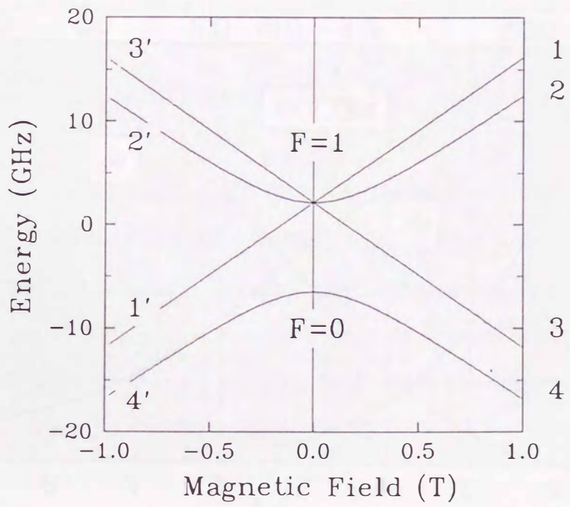

Fig.6-1-2 The energy diagram of Zeeman levels for a $^3He^+$ ion.

Isotope	support gas	1+	2+	3+	4+	5+	6+	7+	8+	9+	10+	11+	12+	13+		
He	He	332	250													
O	O2					43	22	1.4								
Ne	O2		62	50	34		17	5	1.3	.035						
Ar	O2		34	40	33	37	31	26	34	17		2.2				
Ti	O2					7		12	11		6.4	4.5		0.7		ϕ1 rod

Table 6-1-2 The performance of the Neomafios-10GHz ECR ion source at the RCNP.

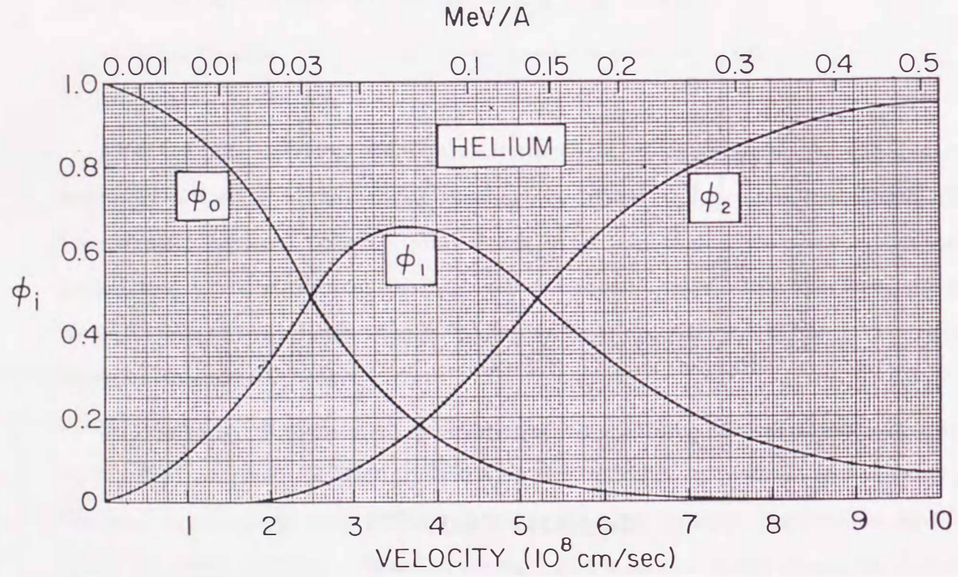

Fig.6-1-3 The equilibrium charge state of He [MA68].

the cyclotron is shown in Fig.6-1-4.

2) Emittance growth

One should mention to the problem of an emittance growth of the beam caused by a charge change in a magnetic field. This emittance growth is caused by an insufficient cancellation of the angular momentum produced by a radial magnetic field. This emittance growth increases as the strength of the magnetic field increases. The evaluation of the emittance growth is given in Appendix.

d) Polarimeter

To monitor the value of the nuclear polarization, various types of a polarimeter are offered in addition to the beam foil spectroscopy. For example a polarimeter based on the left-right asymmetry of recoil deuterons in the d-^{3}He scattering in the ^{3}He energy range from 16.7 to 32.4MeV is reported [KA77]. The analyzing power reaches up to -0.5 at 130° with an incidence of 32.9MeV ^{3}He. This type of experiment will be easily made using the AVF cyclotron facility at the RCNP after an injection and acceleration of a polarized ^{3}He ion beam. The polarimeter based on a nuclear double scattering may be used to confirm the the absolute value of the nuclear polarization determined by the polarimeter based on a Beam Foil Spectroscopy.

To summarize, apparatus required to attain polarized beams with high quality are listed below.

I. $^3He^+$ ion with a polarization of 0.15 and with a current of 60μA

(1) An ECR ion source which produces 200 μA of $^3He^{2+}$ ions.

(2) Two 3W TiSaf lasers pumped by 20W argon ion lasers to polarize rubidium vapor with nearly 100% polarization at a thickness of 3×10^{13}atoms/cm^2.

(3) A solenoidal coil with a magnetic field nearly 1T which should be applied to the region where an electron capture occurs.

Additional apparatus are needed to obtain

II. $^3He^{2+}$ ion with a polarization of 0.30 and with a current of 18 μA

(4) A foil or gas stripper

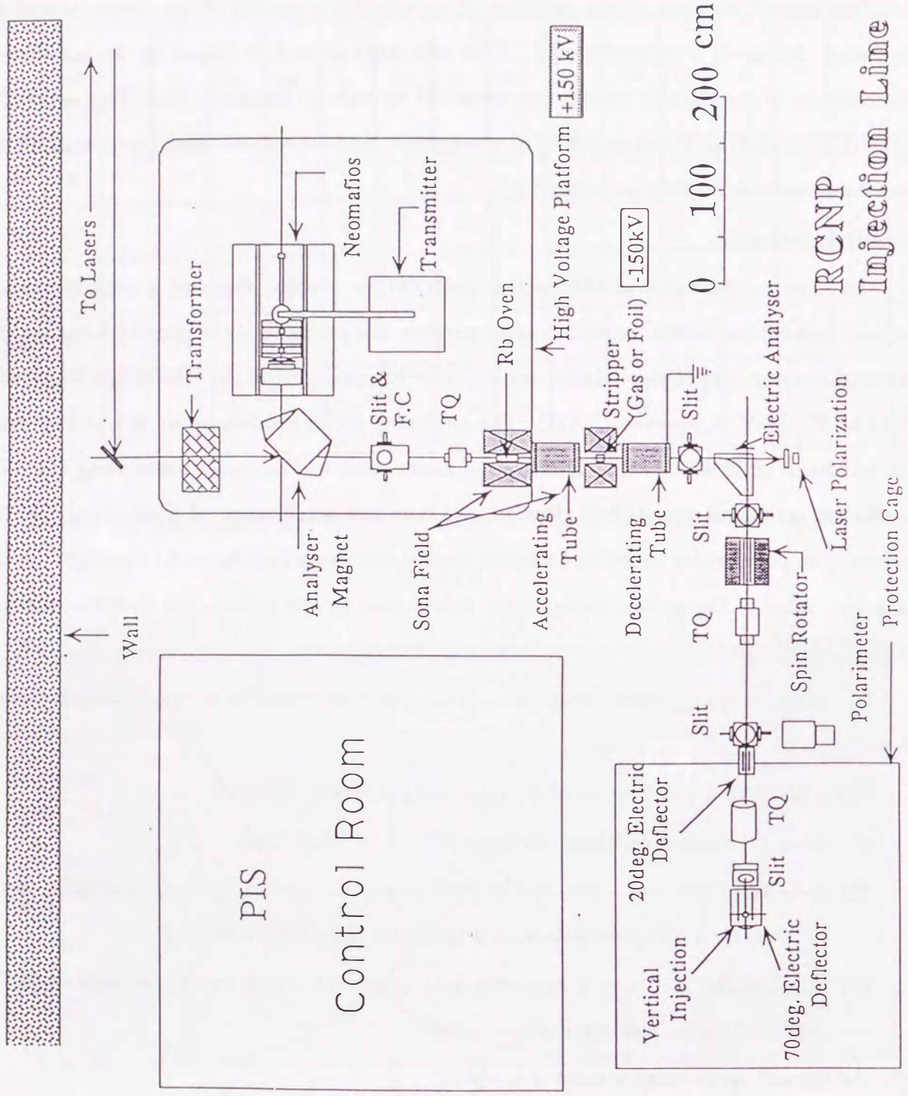

Fig.6-1-4 A schematic drawing of a stripping process and an injection line to the cyclotron.

(5) A solenoidal coil with a strength greater than 0.3T in an opposite direction to the first solenoidal coil. The stripper is equipped in this coil.

(6) Two high voltage suppliers which provide +150kV to the ECR ion source and the first solenoidal coil, and -150kV to the stripper. A very high precision of the order of 10^{-5} is required to the high voltage supplier, because the fluctuation of the accelerating voltage results in a energy spread of the beam.

If the $^3He^+$ (2s) meta-stable state can be utilized,

III. $^3He^{2+}$ ion with a polarization of 0.85 and with a current of 0.6μA

In this case high voltage suppliers (6) are not necessary.

The quality factors for polarized ^{3}He ion sources are tabulated in Table 6-1-3.

Institute	Method	Polarization P	Current I (nA)	Energy E (keV)	P^2I (nA)	Species	Comments
Birmingham	Lamb Shift	0.60	50	29	18	He^{2+}	Acc. 33.3MeV operated till 1985
Laval	Atomic Beam	0.95	100	12	90	He^+	
Rice / Texas A&M	Direct Optical Pumping	0.11	8000	16	97	He^+	Acc. 18.4-49.0MeV operated during the mid 1970s
RCNP	Polarized Electron Capture	0.04	40	20	0.06	He^+	Present Status
		0.30	18000	20	1600	He^{2+}	II Ionization at 300keV
		0.85	600	20	430	He^{2+}	III Ionization of 2S

Fig. 6-1-3 The quality factors P^2I for different types of polarized ^{3}He ion sources.

6-2 Feasibility for polarizing other ions

The polarized electron capture method can be generally applied to other fully stripped ions. The maximum nuclear polarization is limited by an insufficient decoupling of the fine interactions by a magnetic field. The magnetic field to decouple the fine interactions of hydrogenic ion is expressed by

$$B_{fine} \sim C\frac{Z^4}{n^3},$$

where Z is the charge of the ion, n is the principal quantum number of the excited state, and the value of C is approximately 3.2T. Thus the strongest field is needed to decouple the hyperfine interaction of the n=2 state. The value of B_{fine} reaches up to 6.4T for the $^3He^+$ case. As the charge Z increases the larger strength of the magnetic field is required, which is not practically produced.

Here we estimate the nuclear polarization obtainable by the polarized electron capture method in a limit of a weak magnetic field. The most probable state formed by the electron capture is estimated from the matching condition of the ionization potentials of alkali atoms with the energy levels of the hydrogenic ion. Fig.6-2-1 shows the ionization potentials of alkali atoms and energy levels of hydrogenic ions. For example, in case that a proton captures an electron from a sodium atom, the dominant state of the formed hydrogen atom is estimated to be mainly the 2p state, and in case of a capture by He^{2+} ion, the dominant state is estimated to be the 3d state of the He^+ ion, which agrees with more elaborated theoretical calculations. Thus we assume that (1) the hydrogen like ion is formed mainly in the state with a principal number n whose energy level is near the ionization potential of the alkali atom, (2) the dominant orbital state l is $n-1$ because of its statistical weight, and (3) the magnetic field is weak. Under this assumption, the values of ϵ_{LS} is evaluated using the Table 3-3-3. The evaluation of the attainable nuclear polarizations for light heavy ions are given in Table 6-2-1 in case of A_0^{col}=0, i.e., the electron capture cross sections for each magnetic sublevels (l m) are equal.

Here we consider an electron capture from alkali atoms by fully stripped ions. In this case the energy difference is increased as the Z number of the ion is increased, which results

in a polarization loss. But if we can use not fully stripped but rare gas like ion (closed electron shell), the situation may be improved. Because the value Z is replaced by the effective charge $Z*$ which is smaller than Z by the screening effect of electrons, the energy difference is reduced and the field strength to decouple fine interactions may reduced. This topic is one of future subjects.

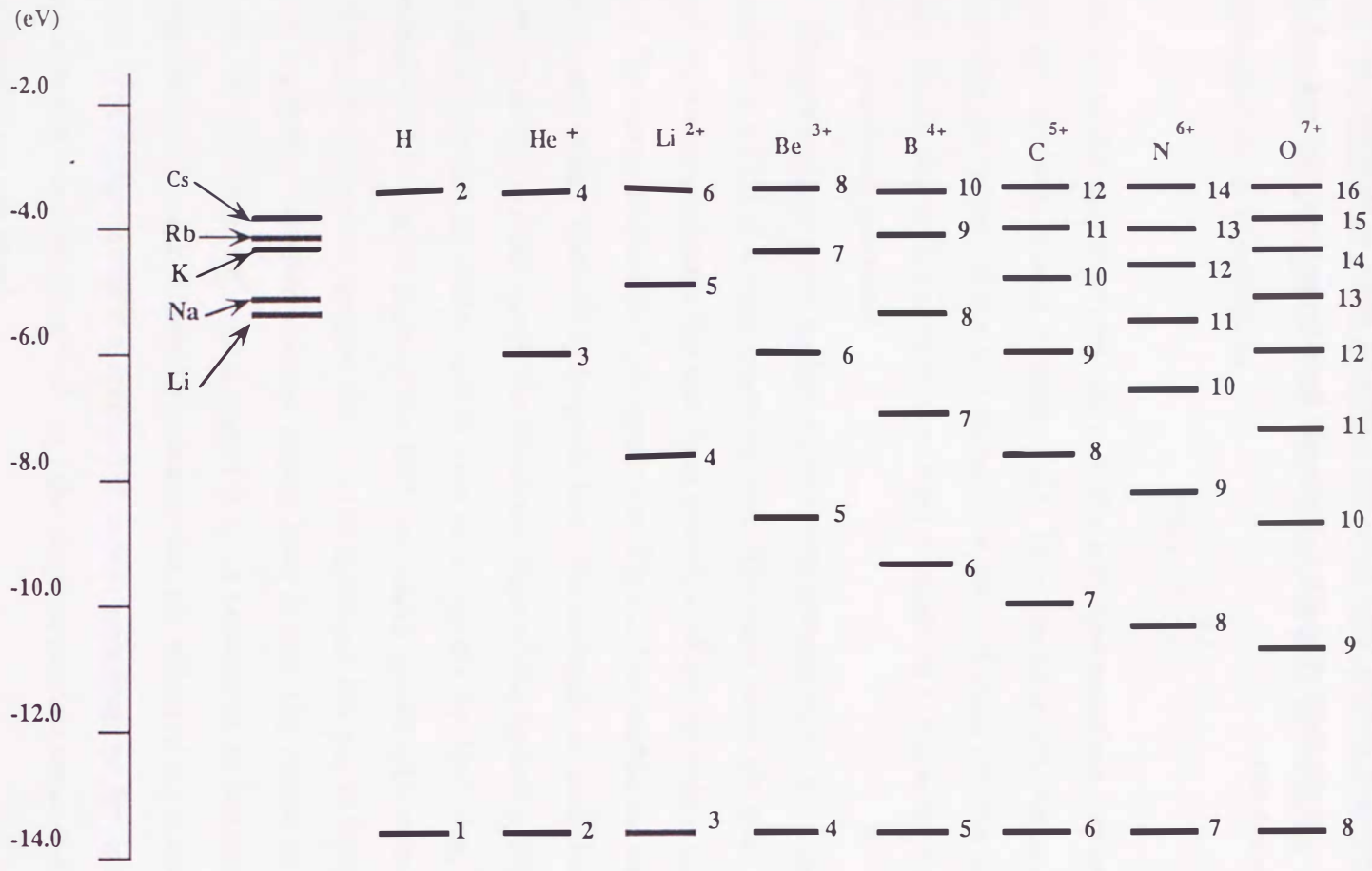

Fig.6-2-1 The ionization potentials of alkali atoms, and energy levels of hydrogenic ions. The small number written on the right side of the energy levels indicates the principal quantum number of the level.

species	I	g_I	abundance (%)	captured channel n	L	ε_{LS}	P_z weak field	Sona	B_{hf} (T)
^{1}H	1/2	+5.58554	99.85	2	1	0.407	0.204	0.407	0.05
^{2}H	1	+0.85741	0.015	2	1	0.407	0.136	0.267	0.01
$^{3}He^{+}$	1/2	-4.25512	8×10^{-4}	3	2	0.301	0.151	0.301	0.30
$^{6}Li^{2+}$	1	+0.82201	7.5	5	4	0.234	0.078	0.156	0.20
$^{7}Li^{2+}$	3/2	+2.17086	92.5	5	4	0.234	0.059	0.118	0.53
$^{9}Be^{3+}$	3/2	-0.78496	100	6	5	0.219	0.055	0.110	0.46
$^{10}B^{4+}$	3	+0.6002	19.9	8	7	0.202	0.029	0.058	0.68
$^{11}B^{4+}$	3/2	+1.79243	80.1	8	7	0.202	0.051	0.102	2.03
$^{13}C^{5+}$	1/2	+1.40478	1.1	10	9	0.192	0.096	0.192	2.76
$^{14}N^{6+}$	1	0.40356	99.63	11	10	0.188	0.063	0.126	1.26
$^{15}N^{6+}$	1/2	-0.5662	0.37	11	10	0.188	0.094	0.188	1.76
$^{17}O^{7+}$	5/2	-0.75748	0.038	13	12	0.183	0.003	0.006	3.52

Table 6-2-1 The expected nuclear polarization produced by the polarized electron capture method under the assumptions that the hydrogen like ion is formed mainly in the state with a principal number n whose energy level is near the ionization potential of the alkali atom, the dominant orbital state l is $n-1$, $A_0^{col}=0$, an electron capture occurs in a low magnetic field.

6-3 Possible Experiments with Polarized ^{3}He Ion Beams at Intermediate Energy

The construction of polarized ^{3}He ion source at RCNP is desired from following reasons. a) No polarized ^{3}He beam is now being accelerated in the world. It was only at the University of Birmingham that data had been accumulated with 33.4MeV [HA81], while at the University of Laval [SL85] and Texas A&M / Rice University [MA85] polarized ^{3}He beams were produced but not used at present. b) At RCNP the available beam energies range from 40 to 540MeV, where experiments have not been done with polarized ^{3}He beam, and have seldom been done even with unpolarized ^{3}He one. c) Data for ^{3}He is indispensable to develop nuclear physics associated with projectile dependence, since data for projectiles of p, n, d, and ^{6,7}Li is being accumulated with high precision at many laboratories in the world.

At the intermediate energy above 100MeV/nucleon, one can distinctly clarify a role of spin in interactions through a folding procedure and a sudden approximation. Firstly each term of effective interactions for ^{3}He-p or ^{3}He-n – spin and isospin terms in central interaction, and spin-orbit, tensor and momentum-dependent terms in noncentral interaction – could be separately obtained in adequate spin observables of ^{3}He induced reactions. Then detailed comparison of effective interactions phenomenologically obtained with interactions for ^{3}He-p or ^{3}He-n folded from effective N-N interaction will provide information on formation of a nucleus. Secondly a sudden approximation well holds, so that polarization observables for nucleon are directly connected to those for ^{3}He. These simple relations will be greatly useful to deduce spin-dependent scattering amplitudes for ^{3}He from those for nucleon.

In elastic scattering, one of a puzzle which has not yet been solved is smallness of a diffuseness parameter ($\sim$ 0.2fm) for the spin-orbit interaction in ^{3}He-nucleus elastic scattering at 33.4MeV. It is different from that in ^{3}H-nucleus at 17MeV. Folding potentials predict the diffuseness parameter of 0.65fm as nucleon and triton. To give a correct answer which leads to the universal potential, fitting procedure at one incident energy is not good enough, and potential search with wider incident energies will be needed. Optical parameters for real and imaginary potentials still have ambiguities in strength as well as in geometry. Measurements and consistent analyses with a wider energy range are essential to untangle ambiguities and

to demonstrate uniqueness and continuity from p, d, to ^{6,7}Li through ^{3}He. Comparisons of phenomenologically obtained potential parameters with parameters obtained by double folding procedure from effective N-N interactions are attractive.

The new combination of polarized ^{3}He beams with high precision magnetic spectrographs RAIDEN and GRAND RAIDEN installed at RCNP will shed light on nuclear structure in nuclear particle spectroscopy as described below.

As for one nucleon transfer, (^{3}He, α) is unique in a sense of I_α=0. One neutron hole state distribution in the residual nucleus can be investigated with less ambiguity compared to that of (p, d) reaction. Since j-dependence by vector polarized ^{3}He beam is established at forward angles [RO85], a hole state distribution with definite spin and parity can be obtained. Energy spectra in ($^3\vec{\text{He}}$, α) is much cleaner and a continuous part is better understood than those in (p, d).

Another uniqueness is (^{3}He, d) in terms of one proton transfer, i.e. a distribution of proton particle state. The j-dependence of ($^3\vec{\text{He}}$, d) helps to obtain a separate distribution for j=$l\pm$1/2 states [RO85]. Two nucleon transfer ($^3\vec{\text{He}}$, n) and ($^3\vec{\text{He}}$, p) are also unique to investigate 2 proton states and deuteron states. The ($^3\vec{\text{He}}$, 2p) channel is useful to identify the states from which sequentially decays with emitting proton after the deuteron transfer. For the ($^3\vec{\text{He}}$, ^{2}He) reaction, determination of p-p final state interaction under the influence of a nuclear field at various incident energy is interesting. Alpha cluster transfer of ($^3\vec{\text{He}}$, ^{7}Be) is an another field to be opened for exploring a distribution of states with 4-hole or n-particle 4-hole configuration.

Charge exchange reaction of ($^3\vec{\text{He}}$, t) is the most expecting one because this reaction plays an important role in selective excitation of Giant Resonances with spin-isospin modes. Problem on quenching of GT-strength for sum rule appeared in (p, n) reaction up to 200MeV has not been solved. One of the reason for quenching is due to Delta excitation. In fact, measurements of (^{3}He, t) above 1.5GeV at Saturne show that Delta excitation is clearly found in the energy spectra for various targets [GA84]. At intermediate energies above 70MeV/nucleon, reaction mechanisms become simple enough to allow one step analysis in

DWBA. Thus, to elucidate the properties of the excitation energy region between normal GT resonances and Delta excitation, systematic studies of energy dependence and consistent analyses from 200MeV to 600MeV are desired with identification of spins for states in residual nucleus by using polarized ^{3}He beam.

Symmetry test experiments are feasible with polarized ^{3}He beam. One of them is on time reversal invariance based on the polarization and analyzing power of inverse reactions. Possible reactions are ^{4}He($^3\vec{\text{H}}$e, p)^{6}Li and ^{6}Li($\vec{p}$, ^{3}He)^{4}He [PO84]. The other symmetry test is on parity violation. For this test the spin direction should be rotated parallel and antiparallel to the beam direction.

If one can regard that two protons in ^{3}He nucleus is unified to make a pair with a spin 0^+, polarized ^{3}He nucleus behaves as a polarized neutron. Scattering between polarized ^{3}He and polarized neutron with various energies can give information on n-n interactions. Any problem related to three bodies will be tackled. For example $^3\vec{\text{H}}\text{e} + ^3\text{He} \rightarrow \alpha + \text{p} + \text{p}$, $^3\vec{\text{H}}\text{e} + ^9\text{Be} \rightarrow \alpha + \alpha + \alpha$, or ^{2}H($^3\vec{\text{H}}$e, ^{3}H)^{2}He will be considered. Even if ^{3}He nucleus is an open system for nucleons, spin dynamics of 3 nucleons may simulate spin dynamics of 3 quarks in a nucleon.

7. Conclusion

In the present work we explored the feasibility of producing a nuclear polarized ion beam by an electron capture from a sodium atom polarized by the optical pumping. We succeeded in production of a nuclear polarized $^3He^+$ ion beam. The nuclear polarization of 0.0415±0.0061 and the ion current of 40nA were obtained under the following conditions; 1) the polarization of sodium atoms was 0.30±0.05, 2) the sodium thickness was 3×10^{13} atoms/cm^2, and 3) the incident energy of $^3He^{2+}$ to the sodium atom was 20keV.

The quality factor of the polarized ion source is expressed by the square of the nuclear polarization times the ion current. To enlarge this value, efforts has been devoted.

A maximum beam current of 6eμA of He^{2+} ions was extracted from the 2.45GHz ECR ion source. The measurement of nuclear polarization of $^3He^+$ beam was carried out using a $^3He^{2+}$ ion beam of $\sim$ 2eμA in the energy range from 16 to 28keV.

To increase the sodium polarization, optical pumping of the sodium atom has been investigated from various points of view; such as a pumping light intensity, an external magnetic field strength, and the thickness of the sodium atoms. In order to minimize the depolarization, various wall materials of the sodium oven, such as copper, pyrex glass and dry-film coated wall were tested. We could obtain the sodium polarization of 0.4 at the sodium thickness of 3×10^{13} atoms/cm^2 with a laser power of 300mW.

To measure the nuclear polarization, a Beam Foil Spectroscopic method was used. A prominent peak with its wavelength of 389nm was observed in the photon spectrum when a polarized ^{3}He passed through a thin carbon foil. This photon peak corresponds to the transition from the 3^3P_J state to the 2^3S_1 state of a neutral He atom. The circular polarization degree of the 389nm photon emitted from a excited ^{3}He atom is measured. It is proportional to the nuclear polarization of ^{3}He, and its coefficient $\bar{A}$ is calculated to be 0.207.

The relation between the nuclear polarization P_N and the sodium polarization P_{Na} is expressed as $P_N = \epsilon_{LS}\epsilon_{HF}P_{Na}$. P_N was observed by the Beam Foil Spectroscopic method, and P_{Na} was observed separately by the Faraday Rotation method. Comparing P_N with P_{Na}, a reduction was observed. The value of ϵ_{HF} is 0.5 for a weak magnetic field transition,

which is our case. This factor can be increased to nearly 1.0 by using the Sona method. The value of ϵ_{LS} was obtained to be 0.259 ± 0.083 at an $^3He^{2+}$ incident energy of 20keV. We searched for the maximum value of ϵ_{LS} by varying an incident energy of the $^3He^{2+}$ ion. The value of ϵ_{LS} did not drastically change in an incident energy range of 20-28keV.

The polarization degree will be increased up to nearly 0.3 by employing highly polarized rubidium atoms and the Sona method. The beam current can be increased by three orders of magnitude (60μA) when we extract 200μA $^3He^{2+}$ ion from a more powerful ECR ion source with an improved ion transport system. The polarized ion should be stripped for minimizing the depolarization during the beam transportation and for obtaining the maximum energy available in the cyclotron.

If a polarized $^3He^+$ beam mentioned above will be attained in the intermediate energy region, a new possibility of developing nuclear physics will be opened. The feasibility for applying this method to polarizing other ions is promising. Nuclear polarization of more than 18% will be expected for ^{13}C and ^{15}N with the Sona method.

Acknowledgment

I thank Professor K. Katori for giving me a chance to join the project of the construction of polarized ^3He ion source, and for helping to overcome difficulties appeared in many places throughout the present work. I thank Professor M. Tanaka who proposed the initial idea of this polarized ion source, has made main contributions in constructing this polarized ion source and guided me to construct it. I express my sincere gratitude to Dr. M. Fujiwara for giving us valuable suggestions and discussions. I thank Professor M. Kondo and Professor H. Ogata to support this project and to give me fruitful advice and encouragement. I acknowledge Professor T. Itahashi for constructing the 2.45GHz ECR ion source and helping us. My doctor thesis is the result of the fruitful collaborative work in developing a polarized ^3He ion source with the above mentioned people. I am thankful to Dr. K. Tamura for discussion on an angular momentum theory. I wish to express appreciation to Professors H. Tawara and H. Kimura for their guidance to atomic collision physics. I thank Mr. K. Abe, Dr. S. Hatori, Dr. K. Shimomura and staffs of the Research Center for Nuclear Physics for their technical supports, advice and encouragement.

A part of this work is supported by the Grant-in-Aid of Japanese Minister of Education.

Appendix

A-1 Description of Polarization

The wave function of the particle with a spin I is expressed in terms of one of the (2I+1) magnetic substates M (-I ≤ M ≤ I) with a certain probability N_M. If N_M differs from the average value $\frac{1}{2I+1}$, the beam is called to have a polarization. The state of a polarized beam can be expressed by a density matrix,

$$\rho = \sum_{I,M} N_M |IM\rangle\langle IM|.$$

The density matrix is usually normalized as

$$tr\ \rho = 1.$$

This density matrix can be expressed using the irreducible tensor representation,

$$\rho = \sum_{KQ} t_{KQ} T(I)_{KQ}.$$

Here $T(I)_{KQ}$ is called the spherical tensor operator with a rank of K. t_{KQ} is called the state multipole and the latter represents the nature of the polarized beam as will be described below.

A general description of an ensemble of particles with a spin I requires tensors up to a rank 2I. There are $(2I+1)^2$ parameters. The definition of the spherical tensor operator $T(I)_{KQ}$ (K≤ 2I) is given as follows,

$$T(I)_{KQ} = \sum_{M'M} (-)^{I-M'}(2K+1)^{1/2} \begin{pmatrix} I & I & K \\ M' & -M & -Q \end{pmatrix} |IM'\rangle\langle IM| \ .$$

And the definition of the state multipole is expressed as,

$$t_{KQ} = \mathrm{tr}\ \rho T(I)_{KQ}$$

For example, we show the tensors with K=0,1 ,2. The polarized beam produced by a polarized ion source has an axial symmetry with respect to the beam axis. So we consider the case

with Q=0. The operator with a rank K=0 is a scalar operator and is proportional to the (2I+1) dimensional unit matrix 1.

$$T(I)_{00} = \frac{1}{(2I+1)^{1/2}} \sum_M |IM\rangle\langle IM|$$
$$= \frac{1}{(2I+1)^{1/2}} 1$$

The state multipole with a rank K=0 is expressed as,

$$t_{00} = \mathrm{tr}\ \rho T_{00} = \frac{1}{\sqrt{2I+1}}$$

State multipoles with a rank K=1 are called a vector polarization. The three vector components $T(I)_{1Q}$ are related to the component of the angular momentum vector I in a spherical description.

$$I_{\pm 1} = \mp \frac{1}{2^{1/2}}(I_x \pm iI_y), \quad I_0 = I_z$$

Using the definition of the spherical tensor we obtain the following relations,

$$\langle IM'|T(I)_{10}|IM\rangle = [\frac{3}{(2I+1)(I+1)I}]^{1/2} M \delta_{M,M'},$$

$$\langle IM'|T(I)_{1\pm 1}|IM\rangle = \mp[\frac{(I \mp M)(I \pm M+1)}{(2I+1)(I+1)I}]^{1/2} (\frac{3}{2})^{1/2} \delta_{M,M'\pm 1}.$$

Thus we obtain

$$T(I)_{1Q} = [\frac{3}{(2I+1)(I+1)I}]^{1/2} I_Q.$$

Similarly the second rank tensors $T(I)_{2Q}$ (K=2) are related to the quadratic combinations of the angular momentum operator,

$$T(I)_{20} = \frac{C}{6^{1/2}}(3I_z^2 - \mathrm{I}^2)$$

$$T(I)_{2\pm 1} = \mp \frac{C}{2}[(I_x I_z + I_z I_x) \pm i(I_y I_z + I_z I_y)]$$

$$T(I)_{2\pm 2} = \frac{C}{2}[I_x^2 - I_y^2 \pm i(I_x I_y + I_y I_x)]$$

$$C = [\frac{30}{(2I+3)(2I+1)I(2I-1)(I+1)}]^{1/2}.$$

Sometimes another expression is used to describe the polarization of the beam. In the Cartesian representation, we get

$$P_z = \frac{\langle I_z \rangle}{I}.$$

Here P_z is a polarization expression in a Cartesian coordinate and this value corresponds to the expectation value of the spin,

$$P_{zz} = \frac{1}{I(2I-1)}\langle 3I_z^2 - \mathrm{I}^2 \rangle.$$

P_{zz} is concerned to the quadratic combination of angular momentum operator.

The relation between the spherical tensor representation and the Cartesian polarization representation is as follows,

$$\sqrt{\frac{I+1}{3I}}\frac{t_{10}}{t_{00}} = P_z$$

$$\sqrt{\frac{(I+1)(2I+3)}{5I(2I-1)}}\frac{t_{20}}{t_{00}} = P_{zz}.$$

For the case of I=1/2, quantum mechanics teaches us that measurements of the component of spin projections of a spin 1/2 particle along a given direction will yield only two answers, $m_I = \pm 1/2$. The polarization t_{10} is defined in terms of the number of particles N_+ and N_-, which have spin projections m_I=+1/2 and m_I=-1/2, respectively:

$$\frac{t_{10}}{t_{00}} = P_z = \frac{N_{+1/2} - N_{-1/2}}{N_{+1/2} + N_{-1/2}} \qquad -1 \le \frac{t_{10}}{t_{00}} \le 1.$$

Particles with I=1/2 such as p, n, t, ^{3}He, ^{13}C, ^{15}N, ^{19}F, $\cdots$ correspond to this case.

For the case of I=1, there is an additional second type of polarization, called a tensor polarization, or an alignment t_{2q}:

$$\sqrt{\frac{2}{3}}\frac{t_{10}}{t_{00}} = P_z = \frac{N_{+1} - N_{-1}}{N_{+1} + N_0 + N_{-1}} \qquad -\sqrt{\frac{3}{2}} \le \frac{t_{10}}{t_{00}} \le \sqrt{\frac{3}{2}}$$

$$\sqrt{2}\frac{t_{20}}{t_{00}} = P_{zz} = \frac{N_{+1} - 2N_0 + N_{-1}}{N_{+1} + N_0 + N_{-1}} \qquad -\sqrt{2} \le \frac{t_{20}}{t_{00}} \le \frac{1}{\sqrt{2}}$$

Particles with I=1 such as d, ^{6}Li, ^{14}N, $\cdots$ corresponds to this case.

It should be noted that the state multipole ${}^J\rho_q^k$ used in section 3-3 and 3-4 is identical in definition to the state multipole $t(J)_{kq}$.

A-2 Faraday Rotation

Faraday rotation effect [MO84] is a rotation of the polarization plane of the linearly polarized light when the light passes through an optical active medium such as a thick sodium vapor. The calculation of the rotation angle is shown below.

In a sodium atom, we consider two levels : the ground state ($3S$) and the first excited state ($3P$). The 3P state of a sodium atom splits into two fine structure levels (J=1/2 and J=3/2). A light corresponding to the transition from the $3S_{1/2}$ to the $3P_{1/2}$ ($3P_{3/2}$) state is called D_1 (D_2) line and its wavelength is 589.593nm (588.996nm). The life time of the 3P state is 16ns. In a magnetic field sufficiently strong to obtain good Zeeman splitting, each state is split into fine structure sublevels which is specified by a quantum number m_j as shown in Fig.A-2-1.

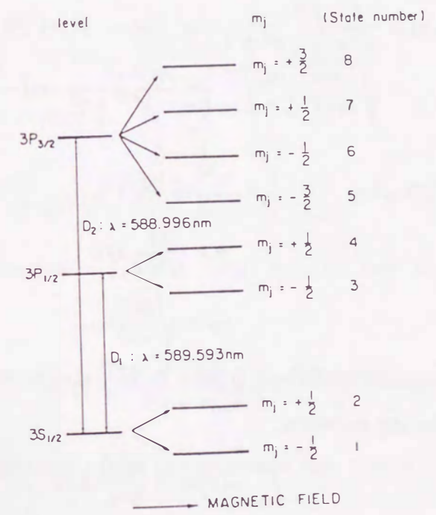

Fig.A-2-1 The Zeeman levels of sodium 3S and 3P states.

Faraday rotation comes from the difference between the refractive indices for left and

right circular polarized light.

$$\begin{aligned}\theta &= \omega\Delta t \\ &= 2\pi\nu(\frac{L}{v_+} - \frac{L}{v_-}) \\ &= \frac{2\pi L}{\lambda}(n_+ - n_-)\end{aligned} \tag{A2.1}$$

where n_+ and n_- are the refractive indices for left and light circular polarized light respectively, λ is the wave-length and L is the length of the media. Refractive indices near a resonance line can be written as follows [ST66],

$$n - 1 = \sum_{ij} \frac{c}{4\pi^2\nu_{ij}\gamma} f(x_{ij}, a) \int_{-\infty}^{\infty} \kappa(\nu) d\nu \tag{A2.2}$$

Here ν_{ij} is the transition frequency between the two levels i and j, and γ is one half of the natural line width;

$$\gamma = \frac{\Delta\nu}{2} = \frac{1}{4\pi\tau},$$

$f(x_{ij}, a)$ is a function representing a Doppler effect in the absorption of light and given as

$$\begin{aligned}f(x_{ij}, a) &= \frac{1}{\sqrt{\pi}a} \int_{-\infty}^{\infty} \frac{y}{y^2+1} \exp(-[\{x_{ij} - y\}/a]^2) dy \\ &= \sqrt{\frac{mc^2}{2\pi kT\nu_{ij}^2}} \frac{a}{\pi} \int_{-\infty}^{\infty} \frac{\nu_{ij} - \nu'}{(\nu_{ij} - \nu')^2 + \gamma^2} \exp(-\frac{mc^2}{2kT}[\frac{\nu_{ij} - \nu'}{\nu'}]^2) d\nu'\end{aligned}$$

where

$$x_{ij} = \frac{\nu_{ij} - \nu}{\gamma},$$

$$a = \frac{2\gamma}{\sqrt{ln2}} \Delta\nu_D$$

$$\nu_D = \sqrt{\frac{2kT}{mc^2}} \nu_{ij},$$

and $\kappa(\nu)$ is an absorption coefficient defined below. $\kappa(\nu)$ is connected with Einstein's coefficient A by the following equation,

$$\int_{-\infty}^{\infty} \kappa(\nu) d\nu = \frac{\lambda_{ij}^2 g_j}{8\pi g_i} A N_i \quad .$$

Here, N_i is the atomic density of the i state, g_i is the statistical weight of i state and λ_{ij} is the wavelength of the transition between level i and j. For non-polarized light, Einstein's coefficient A is related to matrix elements of the electric dipole transition $\langle i|\mathbf{er}|j\rangle$

$$A = \frac{64\pi^4\nu_{ij}^3}{3\pi hc^3} |\langle i|\mathbf{er}|j\rangle|^2.$$

Under the condition that the state i has an angular momentum J' and the state j has an angular momentum J, the dipole moment is expressed using Wigner-Eckart theorem as,

$$\begin{aligned}\sum_{JJ'mm'} |\langle i(J'm')|\mathbf{er}|j(Jm)\rangle|^2 &= |\langle J'||\mathbf{er}||J\rangle|^2 \sum_{JJ'mm'} (-)^{J'-m'} \begin{pmatrix} J' & K & J \\ -m' & Q & m \end{pmatrix} \\ &= |\langle J'||\mathbf{er}||J\rangle|^2 \sum_{JJ'mm'} \beta_{JJ'}^{mm'}.\end{aligned}$$

This results in

$$\int_{-\infty}^{\infty} \kappa(\nu) d\nu = \frac{\lambda_{ij}^2 g_j}{8\pi g_i} N_i \frac{1}{\tau} \sum_{JJ'mm'} \beta_{JJ'}^{mm'}$$

If the polarization of the state i is P, the population of m (P_m) is expressed as,

$$P_{m=+1/2} = \frac{1}{2}(1 + P)$$

$$P_{m=-1/2} = \frac{1}{2}(1 - P)$$

Then

$$\int_{-\infty}^{\infty} \kappa(\nu) d\nu = \frac{\lambda_{ij}^2 g_j}{8\pi g_i} N_i \frac{1}{\tau} \sum_{JJ'mm'} g_i P_m \beta_{JJ'}^{mm'}$$

So equation (A2.2) can be written as

$$n - 1 = \sum_{ij} \frac{c}{4\pi^2\nu_{ij}\gamma} f(x_{ij}, a) \frac{\lambda_{ij}^2 g_j}{8\pi g_i} N_i \frac{1}{\tau} \sum_{JJ'mm'} g_i P_m \beta_{JJ'}^{mm'}$$

The next step is an evaluation of $f(x_{ij}, a)$. This function can be expressed by a series expansion as,

$$f(x_{ij}, a) = \frac{x_{ij}}{1 + x_{ij}^2} \{1 - a^2 \frac{3 - x_{ij}^2}{2(1 + x_{ij})^2} + a^4 \frac{3}{4} \frac{5 - 10x_{ij}^2 + x_{ij}^4}{4(1 + x_{ij})^2} + \cdots\}$$

If the wavelength of the light is far from the resonance line, that is $\sqrt{1 + x_{ij}^2} \gg a$, neglecting the above second order term,

$$f(x_{ij}, a) \approx \frac{x_{ij}}{1 + x_{ij}^2}$$

So we get

$$n - 1 = \frac{g_j c N_i \lambda_{ij}^2}{8\pi^2\nu_{ij}} \frac{x_{ij}}{1 + x_{ij}^2} \sum_{JJ'mm'} P_m \beta_{JJ'}^{mm'}$$

For the D_1 and D_2 resonance of a sodium atom in a high magnetic field (strong enough to decouple the hyperfine interactions, >1kG), we can get n^+ for left circular light and n^- for right circular light:

$$\begin{aligned} n_+ - 1 = \frac{g_{3p} c N_0}{8\pi^2} \Big[& \frac{\lambda_{14}^2 x_{14}}{\nu_{14}(1+x_{14}^2)} \frac{1}{2}(1-P)\frac{1}{3} \\ & + \frac{\lambda_{17}^2 x_{17}}{\nu_{17}(1+x_{17}^2)} \frac{1}{2}(1-P)\frac{1}{6} \\ & + \frac{\lambda_{28}^2 x_{28}}{\nu_{28}(1+x_{28}^2)} \frac{1}{2}(1+P)\frac{1}{2} \Big] \end{aligned}$$

$$\begin{aligned} n_- - 1 = \frac{g_{3p} c N_0}{8\pi^2} \Big[& \frac{\lambda_{23}^2 x_{23}}{\nu_{23}(1+x_{23}^2)} \frac{1}{2}(1+P)\frac{1}{3} \\ & + \frac{\lambda_{26}^2 x_{26}}{\nu_{26}(1+x_{26}^2)} \frac{1}{2}(1+P)\frac{1}{6} \\ & + \frac{\lambda_{15}^2 x_{15}}{\nu_{15}(1+x_{15}^2)} \frac{1}{2}(1-P)\frac{1}{2} \Big] \end{aligned} .$$

The Faraday rotation angle θ for the electron spin polarized sodium atoms can be derived as

$$\theta = \frac{2\pi L}{\lambda}(n_+ - n_-) = (\theta_0 + P\theta_p) N_0 L,$$

where

$$\begin{aligned} \theta_0 = \frac{g_{3p} c}{8\pi\lambda} \Big[& \frac{\lambda_{14}^2 x_{14}}{\nu_{14}(1+x_{14}^2)} \frac{1}{2}\frac{1}{3} - \frac{\lambda_{23}^2 x_{23}}{\nu_{23}(1+x_{23}^2)} \frac{1}{2}\frac{1}{3} \\ & + \frac{\lambda_{17}^2 x_{17}}{\nu_{17}(1+x_{17}^2)} \frac{1}{2}\frac{1}{6} - \frac{\lambda_{26}^2 x_{26}}{\nu_{26}(1+x_{26}^2)} \frac{1}{2}\frac{1}{6} \\ & + \frac{\lambda_{28}^2 x_{28}}{\nu_{28}(1+x_{28}^2)} \frac{1}{2}\frac{1}{2} - \frac{\lambda_{15}^2 x_{15}}{\nu_{15}(1+x_{15}^2)} \frac{1}{2}\frac{1}{2} \Big] \end{aligned}$$

$$\begin{aligned} \theta_p = \frac{g_{3p} c}{8\pi\lambda} \Big[& \frac{\lambda_{14}^2 x_{14}}{\nu_{14}(1+x_{14}^2)} \frac{1}{2}\frac{1}{3} + \frac{\lambda_{23}^2 x_{23}}{\nu_{23}(1+x_{23}^2)} \frac{1}{2}\frac{1}{3} \\ & + \frac{\lambda_{17}^2 x_{17}}{\nu_{17}(1+x_{17}^2)} \frac{1}{2}\frac{1}{6} + \frac{\lambda_{26}^2 x_{26}}{\nu_{26}(1+x_{26}^2)} \frac{1}{2}\frac{1}{6} \\ & - \frac{\lambda_{28}^2 x_{28}}{\nu_{28}(1+x_{28}^2)} \frac{1}{2}\frac{1}{2} - \frac{\lambda_{15}^2 x_{15}}{\nu_{15}(1+x_{15}^2)} \frac{1}{2}\frac{1}{2} \Big] \end{aligned} .$$

Then the polarization P can be obtained from the rotation angle θ,

$$P = \frac{\theta - \theta_0 N_0 L}{\theta_p N_0 L}.$$

The calculation, for example, shows that

$$\theta_0 = 0.8°,$$

$$\theta_p = 32°,$$

at the sodium thickness of 3×10^{13}atoms/cm^2 and the magnetic field of 3kGauss. The calculated θ_0 and θ_p is shown in Fig.3-2-3 as a function of the wavelength of the light.

A-3 Calculation of ϵ_{LS}

We show the calculation of ϵ_{LS} for the case that the polarized electron is captured in an L=1 state and the state decays to an L=0 state. We choose the quantization axis as the ion beam propagation axis. Because of the axial symmetry, the multipoles with q≠0 vanish. The electron spin is also along the beam propagation axis in our case. ${}^{S}\rho_0^1$ is expressed by using the Cartesian polarization P_e of the electron as,

$$\frac{{}^{S}\rho^1{}_0}{{}^{S}\rho_0^0} = P_e.$$

There are two state multipoles of initial state, J=L+1/2 and J=L-1/2. Here we have J=1/2 and J=3/2. The state multipoles J of initial state are constructed by the state multipole L and the state multipole S as,

$$\begin{aligned}
{}^{J=1/2}\rho_0^1 = -2\Bigg[3\begin{pmatrix}0 & 1 & 1\\ 0 & 0 & 0\end{pmatrix}\begin{Bmatrix}1 & 1/2 & 1/2\\ 1 & 1/2 & 1/2\\ 0 & 1 & 1\end{Bmatrix}{}^{L=1}\rho_0^{0\,S=1/2}\rho_0^1 \\
+3\sqrt{5}\begin{pmatrix}2 & 1 & 1\\ 0 & 0 & 0\end{pmatrix}\begin{Bmatrix}1 & 1/2 & 1/2\\ 1 & 1/2 & 1/2\\ 2 & 1 & 1\end{Bmatrix}{}^{L=1}\rho_0^{2\,S=1/2}\rho_0^1\Bigg] \\
{}^{J=1/2}\rho_0^0 = 2\begin{Bmatrix}1 & 1/2 & 1/2\\ 1 & 1/2 & 1/2\\ 0 & 0 & 0\end{Bmatrix}{}^{L=1}\rho_0^{0\,S=1/2}\rho_0^0 \\
{}^{J=3/2}\rho_0^1 = -4\Bigg[3\begin{pmatrix}0 & 1 & 1\\ 0 & 0 & 0\end{pmatrix}\begin{Bmatrix}1 & 1/2 & 3/2\\ 1 & 1/2 & 3/2\\ 0 & 1 & 1\end{Bmatrix}{}^{L=1}\rho_0^{0\,S=1/2}\rho_0^1 \\
+3\sqrt{5}\begin{pmatrix}2 & 1 & 1\\ 0 & 0 & 0\end{pmatrix}\begin{Bmatrix}1 & 1/2 & 3/2\\ 1 & 1/2 & 3/2\\ 2 & 1 & 1\end{Bmatrix}{}^{L=1}\rho_0^{2\,S=1/2}\rho_0^1\Bigg] \\
{}^{J=3/2}\rho_0^0 = 4\begin{Bmatrix}1 & 1/2 & 3/2\\ 1 & 1/2 & 3/2\\ 0 & 0 & 0\end{Bmatrix}{}^{L=1}\rho_0^{0\,S=1/2}\rho_0^0 .
\end{aligned}$$

Then the state multipoles of the ground state ${}^{J}\rho(g.s.)$ are given by

$${}^{J=1/2}\rho_0^1(g.s.) = C[B(1,1/2,1/2)^{J=1/2}\rho_0^1(0) + B(1,1/2,3/2)^{J=3/2}\rho_0^1(0)]$$

$${}^{J=1/2}\rho_0^0(g.s.) = C[B(0,1/2,1/2)^{J=1/2}\rho_0^0(0) + B(0,1/2,3/2)^{J=3/2}\rho_0^0(0)].$$

The electron spin polarization of the ground state ion $P_e(g.s.)$ is given by

$$\begin{aligned}
P_e(g.s.) &= {}^{S}\rho_0^1(g.s.)/{}^{S}\rho_0^0(g.s.) = {}^{J}\rho_0^1(g.s.)/{}^{J}\rho_0^0(g.s.) \\
&= (0.407 + 0.210\frac{{}^{L}\rho_0^2(0)}{{}^{L}\rho_0^0(0)})\frac{{}^{S}\rho_0^1(0)}{{}^{S}\rho_0^0(0)} \\
&= (0.407 + 0.296A_0^{col})\frac{{}^{S}\rho_0^1(0)}{{}^{S}\rho_0^0(0)}
\end{aligned}$$

Thus,

$$P_e(g.s.) = \epsilon_{LS}P_e(0),$$

where ϵ_{LS} is defined by

$$\epsilon_{LS} = \frac{P_e(g.s.)}{P_e(0)} = 0.407 + 0.296A_0^{col} \qquad (L=1)$$

For the case of L=1 the value of A_0^{col} can take

$$-1 \le A_0^{col} \le \frac{1}{2} \qquad (L=1).$$

If the excited states are equally populated $\sigma(m_L) = \frac{1}{2L+1}\sigma$, there is no alignment $A_0^{col} = 0$ and the value of ϵ_{LS} is 0.407. If the excited states are formed in $m_L = 0$ state only, the alignment factor $A_0^{col} = -1$ and the value of ϵ_{LS} is 0.111.

A-4 Sona method

As described in section 6-1, the electron polarization can be transferred to the ^{3}He nucleus by using the Sona method [SO67]. Here we show details of the Sona method and a required condition to apply it to the polarized ^{3}He ion beam with 20keV energy.

In Fig.6-1-2 the energy diagram of the Zeeman levels of a $^3He^+$ ion is shown. We assume that the produced beam is in the state 1 or 2 in a high magnetic field. It enters then a region where the strength of the magnetic field B is decreasing with keeping the direction parallel to the beam direction. Suppose that the particle moves in a region where the magnetic field decreases from a high positive value, changes its direction and finally reaches a negative high value. If the passage in the magnetic field is adiabatic, the particle wave function is sticking on the energy line of Fig.6-1-2, and the two states 1, 2 go into the two states 1', 2' at the high negative field. Ionization in this region gives a full polarization transfer from the electron to the nucleus. The adiabaticity is fulfilled under the following condition as shown in section 3-3,

$$T \gg \frac{1}{a}$$

$$T = \frac{B_{hf}}{\frac{dB}{dt}} = \frac{B_{hf}}{v_z \frac{dB}{dz}},$$

$$B_{hf} = \frac{a}{g_I \mu_N - g_J \mu_e}$$

where T is the time needed to change the magnetic field strength from B_{hf} to zero, a is the hyperfine interval, and v_z is the velocity of the ion beam.

We have to take into account the finite beam cross section, and therefore the presence of the transverse component B_r of the field B near B=0. The value of B_r is related to the gradient of the parallel component of B via the Maxwell equations divB=0, rotB=0. At low fields the He^+ ion behaves like a particle having the magnetic moment of the spin F=1. And the coupled electron and nuclear spin F rotates around the magnetic field direction with the Larmor frequency. A particle traveling off-axis never sees a field going exactly to zero, but feels the field which changes continuously its direction of 180°. If the frequency of the field reversal ω_B is much smaller than the Larmor frequency ω_L of the lowest field, the spin

direction is kept during the field reversal ("sudden" crossing) and high nuclear polarization is expected. The value of B_r at a distance r from the axis is given by,

$$div\mathrm{B} = 0,$$

$$\frac{1}{r}\frac{d}{dr}(rB_r) + \frac{dB_z}{dz} = 0,$$

$$B_r = -\frac{r}{2}\frac{dB_z}{dz} = -\frac{r}{2}\dot{B}_z.$$

The corresponding angular velocity of the precession is,

$$\omega_L = \frac{g\mu_e B_r}{\hbar}.$$

The angular velocity of the rotation of the B direction as seen by a particle traveling with the velocity v and at a distance r from the axis is,

$$\omega_B = 2\frac{v}{r}.$$

Here the factor of 2 comes from that the direction of the magnetic field changes twice during the rotation of 2π. The requirement for sudden crossing is

$$\omega_L \ll \omega_B.$$

We can rewrite this requirement as

$$\dot{B}_z r^2 \ll \frac{4\hbar v}{g\mu_e}.$$

Another constraint comes from the residual magnetic field in the region of the zero crossing point, which comes from a slight misalignment and from an external magnetic fields like a terrestrial one. This magnetic field is equivalent to a lateral displacement of zero crossing point at a distance $r_{res} = \frac{2B_r}{\dot{B}_z}$. This in turn requires

$$\dot{B}_z r_{res}^2 \ll \frac{4\hbar v}{g\mu_e}$$

$$\frac{4B_r^2}{\dot{B}_z} \ll \frac{4\hbar v}{g\mu_e}.$$

For 20keV $^3He^+$ ion, using the values of $v = 10^6$m/s, μ_e=9.27×10^{-24}J/T, $g = 2$. $\hbar$=1.05×10^{-34}Js. we finally obtain

$$\frac{4B_r^2}{1.1 \times 10^{-5} Tm} \ll \dot{B}_z \ll \frac{1.1 \times 10^{-5} Tm}{r^2}.$$

These conditions are satisfied for r<0.5cm, $\frac{dB_z}{dz}$=2Gauss/cm, B_r < 0.5Gauss, which are available with a reasonable geometry. The condition of the adiabaticity $\frac{dB_z}{dz} \leq 10^5$ Gauss/cm is also fulfilled by the above values.

A-5 Emittance Degradation Effects associated with Charge Transfer in a Magnetic Field

The effect on beam emittance which results from charge transfer collisions within a magnetic field is discussed. Consider a particle with a charge q which travels with velocity v_z parallel to the axis of a solenoidal coil at radius R. And the particle captures an electron when the particle reaches the point $z = Z$ in the solenoid. For simplicity, we assume v_z is large compared to any additional velocity components which are acquired as the particle leaves the field region. Therefore we consider the orbit in the solenoid to be straight line for the purpose of estimating the velocity change. Fig.A-5-1 shows a schematic diagram of this process. The force on the particle is given by the Lorentz force:

$$\mathrm{F} = m\dot{\mathrm{v}} = q\mathrm{v} \times \mathrm{B},$$

where m is the particle mass, B is the magnetic field vector, and v is the particle velocity. The motion of the particle in a θ direction in a cylindrical frame is expressed as,

$$m\frac{d}{dt}(R^2\frac{d\theta}{dt}) = -qeR(B_z\frac{dr}{dt} - B_r\frac{dz}{dt}).$$

This indicates the change of an angular momentum of the particle is expressed as

$$d(mR^2\frac{d\theta}{dt}) = -qeR(B_z dr - B_r dz).$$

When the particle changes its position by dz and dr, the particle crosses a magnetic flux $d\Phi$

$$d\Phi = 2\pi R(B_z dr - B_r dz).$$

Then the particle gains an angular momentum

$$d(mR^2\frac{d\theta}{dt}) = -\frac{qe}{2\pi}d\Phi.$$

When the particle captures an electron at a position $z = Z$, the gained angular momentum L is obtained by integrating the above equation,

$$\begin{aligned} L &= -\int_{-\infty}^{Z} \frac{qe}{2\pi}d\Phi - \int_{Z}^{\infty} \frac{(q-1)e}{2\pi}d\Phi \\ &= -\frac{1}{2}eR^2B_z(Z). \end{aligned}$$

This shows a rotational velocity v_θ is added to the particle

$$v_\theta = \frac{L}{mR} = -\frac{1}{2}\frac{\epsilon}{m} RB_z(Z).$$

The important measure of the beam quality is the transverse beam emittance. This is commonly defined as the $x - x'$ or the $y - y'$ phase space area which the beam occupies with its velocity v_z, where $x' = \frac{v_x}{v_z}$ and $y' = \frac{v_y}{v_z}$.

The effect of this rotational velocity on the beam emittance is evaluated as follows. For a perfectly parallel cylindrical beam with radius R, the $x - x'$ coordinates all lie on a heavy line shown in Fig.A-5-2(b). If a rotational velocity is added, we may represent the velocity field schematically as in Fig.A-5-2(c). If we consider the particles in the beam which lie at radius R, the corresponding $x - x'$ coordinates fall on the ellipse shown in Fig.A-5-2(d). Particles which lie at smaller radii have $x - x'$ coordinates which lie on smaller ellipse; hence, the ellipse shown is the boundary of the emittance diagram. Arguments for the $y - y'$ phase space are identical.

The quantity of interest is therefore the effective transverse emittance η:

$$\eta = \pi v_\theta(max)R(max)/v_z = \pi eB_z R(max)^2/(2mv_z),$$

where $R(max)$ is the radius of the beam envelope at the axial position $z = Z$. In the case for a electron capture of a 20keV He^{2+} ion, the value of η is obtained to be $\eta = 39\ \pi$ mm mrad assuming $R(max)$=3mm, and B_z=0.3T. Since this value is smaller than the acceptance of a cyclotron whose value is around 200 π mm mrad. But if the field is increased 10 times higher, the emittance growth exceeds the acceptance, which results in a intensity reduction.

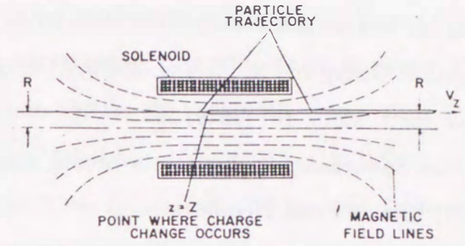

Fig.A-5-1 Schematic diagram showing charge transfer in a solenoidal magnetic field. The charge state of the particle changes from q to $(q - 1)$ at a position of z=Z.

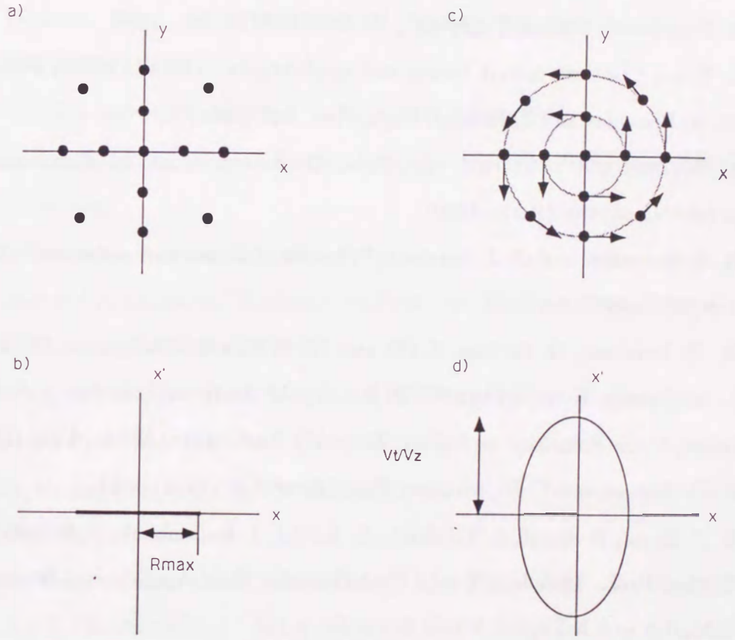

Fig.A-5-2 (a) Distribution of particles for a parallel beam; (b) Emittance diagram for a parallel beam with radius $R(max)$; (c) Schematic diagram of the transverse velocity field characterizing a beam of radius $R(max)$ after angular momentum has been acquired; (d) Emittance diagram for a beam of radius $R(max)$ after angular momentum has been acquired.

References

[AL90] J. G. Alessi, B. Devito, A. Hershcovitch, A. Kponou, and C. R. Meitzler, Proc. Int. Workshop on Polarized Ion Sources and Polarized Gas Jets. KEK, (1990) 93

[AN77] H. J. Andrä, H. J. Pöhn, A. Gaupp and R. Fröhing, Z. Phys. A281 (1977) 15

[AN79] L. W. Andrerson, Nucl. Instr. Meth. 167 (1979) 363

[AN79II] H. J. Andrä, "Fast Beam Spectroscopy", Progress in Atomic Spectroscopy. ed. Hanle and Kleinpoppen (1977) Plenum Press, New York

[AB58] A. Abragam and J. M. Winter, Phys. Rev. Lett. 1 (1958) 374

[BA75] S. Baschkin and J. O. Stoner,Jr., "Atomic Energy Levels and Grotorian Diagrams" vol I, North Holland Publishing Company (1975) proton

[BE65] R. Bernheim, "Optical Pumping", W..BENJAMIN, Inc. 1965

[BL81] K. Blum, "Density matrix theory and applications", (1981) Plenum Press, New York

[BO66] M. A. Bouchiat and J. Brossel, Phys. Rev. 147 (1966) 41

[BO90] A. Boudard and Y. Terrien, eds., Proc. 7th Intern. Conf. on Polarization phenomena in nuclear physics (Paris, 1990)

[BR83] B. H. Bransden and C. J. Joachain, "Physics of atoms and molecules" (1983) Longman Scientific and Technical

[BU74] W. E. Burcham, O. Karban, S. Oh and W. B. Powell, Nucl. Instr. Meth. 116 (1974) 1

[BU91] L. Buchmann, K. Jayamana, C. D. P. Levy, M. McDonald, R. Ruegg, P. W. Schmor, A. Belov, V. G. Polushkin and A. N. Zelenskii, Nucl. Instr. Meth. A306 (1991) 413

[DU85] R. D. Dubois and L. H. Toburen, Phys. Rev. A31 (1985) 3603

[EH89] H. P. Ehret, R. Ernst, L. Friedrich, E. Huttel, J. Kaltenbeak, F. Schulz, L. Wiss and P. Ziegler, Proc. 12th Int. Conf. Cyclotron and their Applications,Berlin (1989) ed. by B.Martin and K.Ziegler, World Scientific, p.194

[FA73] U. Fano and J. H. Macek, Rev. Mod. Phys. 45 (1973) 553

[GA84] C. Gaarde, J. Physique coll C4, 45 (1984) C4-405

[GE91] R. Geller, Z. Phys. D 21 (1991) S117-121

[HA67] W. Haeberli, Annu. Rev. Nucl. Sci. 17 (1967) 373

[HA72] W. Happer, Rev. Mod. Phys. 44 (1972) 169

[HA81] W. C. Hardy, R. G. Green, G. W. Guest, O. Karban, W. B. Powell and S. Roman,"Polarization Phenomena in Nuclear Physics-1980" AIP Conference Proceedings No.69 (1981) 913

[HA82] W. Haeberli, M. D. Baker, C. A. Gossett, D. G. Mavis, P. A. Quin, J. Sowinski and T. Wise, Nucl. Instr. Meth. 196 (1982) 319

[JA87] H. Jänsch et al., Nucl. Instr. Meth. A254 (1987) 7

[JO89] Y. Jongen and C. M. Lyneis, "The Physics and Technology of Ion Sources", ed. I. G. Brown, Wiley, New York, (1989) 207

[KA77] O. Karban, C. O. Blyth, Y. W. Lui and S. Roman, Nucl. Instr. Meth. 141 (1977) 387

[LE88] C. D. P. Levy, P. W. Schmor and W. M. Law, J. Appl. Phys. 63 (1988) 4819

[LE90] J. L. Lemaire, Proc. Int. Workshop on Polarized Ion Sources and Polarized Gas Jets,KEK (1990) 116

[LI91] Chia-Jung Liu and R. W. Dunford, J. Phys. B24 (1991) 2059

[MA68] J. B. Marion and F. C. Young, "Nuclear Reaction Analysis" (1968) North Holland Publishing Company

[MA69] V. Malaviya et al., J. Phys. B2 (1969) 843

[MA85] D. P. May and S. D. Baker,"Workshop on Polarized ^{3}He Beams and Targets" AIP Conference Proceedings No.131 (1985) 1

[ME60] A. Messiah, "Mecanique Quantique" Tome II (1960) 642 Dunod, Paris

[MO29] N. F. Mott, Proc. Soc. (London) A124 (1929) 425

[MO84] Y. Mori, K. Ikegami, A. Takagi, S. Fukumoto and W. D. Cornelius, Nucl. Instr. Meth. 220 (1984) 264

[MO89] Y. Mori, Proc. of Int. Conf. "High Energy Spin Physics" ed. K.J.Heller AIP Conf. Proc. No187 (1989) 1200

[OH69] G. G. Ohlsen, J. L. McKibben, R. R. Stevens,Jr. and G. P. Lawrence, Nucl. Instr. Meth. 73 (1969) 45

[OH85] S. Oh, "Workshop on Polarized ^{3}He Beams and Targets" AIP Conference Proceedings No.131 (1985) 29

[OH92] T. Ohshima, K. Abe, K. Katori, M. Fujiwara, T. Itahashi, H. Ogata, M. Kondo and M. Tanaka, Phys. Lett. B275 (1992) 163

[OM83] K. Omidvar, Atomic Data and Nuclear Data Tables 28 (1983) 1

[PE58] I. C. Percival and M. J. Seaton, Phil. Trans. R. Soc. A251 (1958) 113

[PO84] J. Pouliot et al., J. Physique 45 (1984) p.71 and references there in.

[RO85] S. Roman, "Workshop on Polarized ^{3}He Beams and Targets" ed. R. W. Dunford and F. P. Calaprice, AIP Conf. Proc. 131 (1985) p. 196

[SC81] P. Schmelzbach, W. Grüebler, V. König and B. Jenny, Nucl. Instr. Meth. 186 (1981) 655

[CL84] T. B. Clegg, "Polarized Proton Ion Source" ed. G. Roy and P. Schmor, TRIUMF Vancouver, 1983, AIP Conf. Proc. No117 (1984) p.63

[SC91] P. W. Schmor et al., Proc. IEEE Particle Accelerator Conf., San Francisco, 1991 to be published

[SC92] P. Schiemenz, Rev. Sci. Instr 63 (1992) 2519

[SH87] R. Shingal, C. J. Noble and B. H. Bransden, J. Phys. B19 (1987) 793

[SI74] M. Simonius, Polarization Nucl. Physics, Springer (1974)

[SL85] R. J. Slobodrian, C. Rioux, J. Giroux and R. Roy, "Workshop on Polarized ^{3}He Beams and Targets" AIP Conference Proceedings No.131 (1985) 8

[SO67] P. G. Sona, Energia nucleare 14 (1967) 295

[ST66] F. Strumia, Nuovo Cimento 44B (1966) 387

[ST81] E. Steffen, Nucl. Instr. Meth. 184 (1981) 173

[SW88] D. R. Swenson and L. W. Anderson, Nucl. Instr. Meth. B29 (1988) 627

[SW90] D. R. Swenson, D. Tupa, O. B. Van Dyck, T. J. Rosson and R. Y. York, Proc. Int. Workshop on Polarized Ion Sources and Polarized Gas Jets, KEK, (1990) p.187

[TA85] M. Tanaka, Polarized Heavy Ion Source using Optical Pumping and Charge Exchange -Hispaniola Project- , (1985) unpublished

[TA90] M. Tanaka, T. Ohshima, K. Katori, M. Fujiwara, T. Itahashi, H. Ogata and M. Kondo, Phys. Rev. A41 (1990) 1496

[TA91] M. Tanaka, T. Ohshima, K. Abe, K. Katori, M. Fujiwara, T. Itahashi, H. Ogata and M. Kondo, Nucl. Instr. Meth. A302 (1991) 460

[TI73] K.Tillmann, H. J. Andrä and W. Wittmann, Phys. Rev. Lett. 29 (1973) 155

[TH87] C. E. Theodosius, Atomic Data and Nuclear Data tables 36 (1987) 97

[TU86] D. Tupa, L. W. Anderson, D. L. Huber and J. E. Lawler, Phys. Rev. A33 (1986) 1045

[VA92] W. Vanderpoorten, J. Wouters, P. Demoor, P. Schuurmans, N. Severijns and L. Vanneste, Rev. Sci. Instr. 63 (1992) 2636

[WA90] Y. Wakuta, Proc. China-Japan Joint Symp. on Accelerator for Nucl. Sci. and their Applications (1990) 98

[WE80] R. C. Weast, "Handbook of Chemistry and Physics" 61st ed., CRC Press Inc. (1980) D-218

[WI79] G. J. Witteveen, Nucl. Instr. Meth. 158 (1979) 57

[YO90] R. L. York, Proc. Int. Workshop on Polarized Ion Sources and Polarized Gas Jets, KEK, (1990) 142

[ZA57] E. K. Zavoiskii, JETP 5 (1957) 378

[ZE90] A. N. Zelenskii, S. A. Kohanovskii, V. G. Polushkin and K. N. Vishnevskii, Proc. Int. Workshop on Polarized Ion Sources and Polarized Gas Jets, KEK, (1990) 154